REDUCED ORDER MODELLING AND CONTROL USING ADVANCED TECHNIQUES

Thesis

Submitted for the award of

DOCTOR OF PHILOSOPHY

by

Ruchika Mehta

(Regd. No.-951404002)

Under the supervision of

Dr. Sunil K. Singla
Associate Professor
TIET, Patiala

Dr. Swati Sondhi
Assistant Professor
TIET, Patiala

THAPAR INSTITUTE
OF ENGINEERING & TECHNOLOGY
(Deemed to be University)

Department of Electrical and Instrumentation Engineering

THAPAR INSTITUTE OF ENGINEERING AND TECHNOLOGY, PATIALA

(Declared as Deemed-to-be-University u/s 3 of the UGC Act., 1956)

Punjab (INDIA)-147004

NOVEMBER, 2020

Dedicated to my family

Declaration

The matter presented in this thesis has not been submitted elsewhere for the award of any other degree in India or Abroad.

I, hereby declare the work presented in the thesis entitled **Reduced Order Modelling and Control Using Advanced Techniques**, in partial fulfilment of the requirements for the award of the degree of Doctor of Philosophy and submitted to the Department of Electrical & Instrumentation Engineering, Thapar Institute of Engineering & Technology, Patiala, Punjab, is an authentic record of my own work carried out under the supervision **Dr. Sunil Kumar Singla and Dr. Swati Sondhi.**

Date:

Ruchika Mehta
Candidate

This is to certify that the above statement made by the candidate is correct to the best of our knowledge.

Date:

Dr. Sunil Kumar Singla
(Associate Professor)

Dr. Swati Sondhi
(Assistant Professor)

Acknowledgement

Achievement of goal is feasible with strong determination and guidance. The only way to success and knowledge is constant efforts with zeal and passion. In this journey, the nature plays its role by providing sources and limelight to show the right way. I would like to thank those persons who helped me to achieve my goals.

First of all, I would like to express my deep gratitude to my thesis supervisor Dr. Sunil Kumar Singla. This work could not have been possible without his faith, motivation, patient guidance and every time support. Success can never be attained without proper guidance and I am glad to receive perfect guidance from him. I am truly very fortunate to have the opportunity to work with him. I found his guidance to be extremely valuable. I am thankful to him that he had full confidence in my ability. Much of this work has not been completed without his vision and encouragement.

I would like to express my warm and sincere gratitude to my thesis co-supervisor Dr. Swati Sondhi. She always supported me through the work by motivating me from time to time. It would have been very difficult for me to come out with results without her valuable suggestions. She is like an ocean of knowledge and ideas from where I got inspiration to work and attain the clues for my assignments. I may fall short of words to thank my mentors, as they gave me wealth of knowledge beyond my expectations.

I would like to thank Ministry of Electronics and Information Technology (MeitY), New Delhi and Dr. Prakash Gopalan, Director TIET, Patiala for providing research facilities. I express my sincere thanks to Dr. R. S. Kaler, Head of the Department, and the members of my doctoral committee for providing continuous motivation and encouragement throughout the research work.

I would like to thank my mother Mrs. Sunita Mehta for standing by me throughout the ups and downs of life. She had been the primary reason behind the completion of this thesis. A huge thanks and life-long gratitude to my father Mr. Rakesh Kumar for his love and affection. I feel fortunate that I spent the golden years of life with him. I hope he was here to see me achieve my goals. A very special thanks to my brother and sister Mr. Nishant and Ms. Surbhi for always being supportive morally and emotionally. I express a deep gratitude towards them for their love and affection towards me.

I would also like to thank my husband Mr. Deepak Lamba for his unending support, motivation and encouragement for achieving my aim. A big thanks to him for always enlightening a ray of inspiration in me for completion of this thesis. The biggest supporter in completion of this work are my kids Agrima and Aadit. Also, I would like to thank my in-laws for their support and encouragement.

I would like to extend a mighty thanks to my fellow researchers Rohit, Sharad for always being an excellent support to me. A huge thanks to all my friends for standing by always, for motivating me every time, for encouraging me during every stage of research, for being there for me morally and emotionally throughout the journey.

Although I have tried to express my gratitude to every person who contributed in this work directly or indirectly, there may still be someone hiding behind the veils of my forgetful part of memory. Last but not the least, I would like to thank all such souls.

Ruchika Mehta

ABSTRACT

In the present day of automated world, control system has become a very imminent research area. System modelling, stability testing, and controller design are the major aspects that have to be considered to obtain the desired control in the real-world applications. The control algorithms formulated using fix values of the system parameters, reveal an assured level of robustness, however, if the parameter values of the system go ahead a certain limit due to some external disturbance or some abnormal system behavior, the nominal controllers (i.e., controllers devised using fix parameter values) may at times become unsuccessful to stabilize the system or to maintain the system output at the required level. Fractional order control systems have emanated as a new control strategy in the recent literature which provides robust performance over conventional control techniques. Although a lot of research is being carried out in direction of using fractional calculus in system modelling and designing efficient control strategies for fractional controller design, however, still there is scope of development in this area. The available techniques are mathematically complex and have limited applicability. Hence in this work, an attempt has been made to carry out fractional system modelling and formulate simpler and robust controller design strategies.

The analysis of any dynamical system requires a mathematical model. The real time behavior can be much easily approximated with the fractional modelling for large and complex systems. Hence, fractional order modelling of a liquid-liquid heat exchanger system has been carried out using various optimization techniques. The system has been modelled in fractional first and second order templates with time delay. Promising results have been achieved and obtained results demonstrate that the second order estimated models better fit the original data than the first order models.

Higher order dynamics prove mathematically complex due to which controller design becomes a cumbersome task. Reduced order helps in simplifying the mathematical design procedure but it has to preserve the system's prime characteristics at the same time. The reduced order modelling of a Pressurized Heavy Water Reactor (PHWR) of the sixth order has been carried out using Balanced Truncation technique. The reduced order model has been obtained by curtailing the states analogous to the smaller Hankel Singular Values (HSVs). This technique gave pronounced results to reduce the unstable sixth order PHWR system to a lower third order system while maintaining

the dominant characteristics of the higher order original system. This stride helped to concoct a controller for the higher order system with lesser intricacy.

The fractional order PID controller has been designed for the higher (sixth) order model of the Pressurized Heavy Water Reactor using corresponding reduced (third) order model and stability boundary locus technique with specific gain-phase margin. The simulation results reveal that the proposed FOPID controller (designed with the reduced order model) works very well on the original higher order PHWR system. The existing controllers gave unstable results when applied to original higher order system whereas the proposed FOPID controller gave a stable response. Moreover, it has also been observed that the integer order PID controller has a higher settling time in comparison to the proposed FOPID controller. A reduction of almost 40% in the settling time has been obtained for all the operating conditions of PHWR with the proposed controller.

Further, the new interval fractional order PID (INFOPID) controllers have been designed for perturbed PHWR and two area interconnected power system applications. The proposed controllers have been designed taking into account the parametric variations because most of the available controllers face performance precincts while working in an uncertain or dynamic environment. The fractional controller design has been carried out for the perturbed PHWR fractional order system using Stability Boundary Locus technique and Edge theorem. The proposed INFOPID controller has been designed for eight nuclear reactor models considering eight interval conditions (±50% variations in system parameters) for each reactor model of the PHWR. The performance of the proposed controller has been evaluated using different error criterion by comparing its performance with the existing methods. As observed from comparison, the proposed INFOPID controller provides the best performance under the given perturbed conditions as well as the varying step back operating conditions and is hence much more robust than the nominal controllers. Moreover, the proposed controller has a faster set point tracking ability as compared to existing controllers under different step back conditions.

Similarly, the fractional controller design has been carried out using Kharitonov's theorem and Stability boundary locus technique for frequency control in a perturbed two area interconnected power system. The analysis of the designed controller has been performed by changing system parameters such as governor constant, turbine time constant and step load perturbation (magnitude and location). Further, the performance of the controller has also been monitored under the effect

of nonlinearities like Generation Rate Constraint (GRC) and Governor Dead Band (GDB). The simulation results show that proposed controller is capable of providing better performance under the given perturbed conditions than the nominal controllers.

Therefore, the key objective of designing robust controllers capable of delivering improved performance under unsure operating conditions has been successfully achieved.

CONTENTS

Declaration i

Acknowledgment ii

Abstract iv

List of Figures ix

List of Tables xi

1. INTRODUCTION 1

1.1 Preamble 1

1.2 Objectives of the Thesis 2

1.3 Contributions in the Thesis 3

1.4 Organization of the Thesis 4

2. IMPORTANCE OF FRACTIONAL CALCULUS AND STABILITY TESTING 6

2.1 Fractional Calculus 6

2.2 Importance of Fractional Calculus 8

2.2.1 Modelling Perspective 8

2.2.2 Control Perspective 11

2.3 Stability Testing of Fractional Order Systems 15

2.3.1 Stability Testing of Fractional Order Linear Systems 15

2.3.2 Stability Testing of Fractional Order Interval Systems 17

3. FRACTIONAL SYSTEM MODELLING USING OPTIMIZATION TECHNIQUES 20

3.1 Introduction 20

3.2 Fractional Order Modelling of Liquid-Liquid Heat Exchanger Using Various Optimization Techniques 23

3.2.1 Dynamics of Heat Exchanger 24

3.2.2 Model Structure and Performance Measures 25

3.2.3 Modelling Procedure 26

3.2.4 Results 32

3.2.5 Comparative Performance Analysis 35

4. MODEL ORDER REDUCTION 38

4.1 Introduction to Model Order Reduction 38

4.2 Balanced Truncation Method 40

4.3 Reduced Order Modelling for PHWR System 42
5. CONTROLLER DESIGN AND STABILITY ANALYSIS 54
5.1 Introduction 54
5.2 Fractional Order Controller Design for PHWR System 55
5.2.1 Mathematical Modelling of PHWR System 55
5.2.2 Proposed INFOPID Controller Design for Power Control in Perturbed PHWR System 58
5.2.3 Proposed FOPID Controller for Power Control in PHWR using ROM 79
5.3 Fractional Order Controller Design for Load Frequency Control in Perturbed Two Area Interconnected Power System 89
5.3.1 Mathematical Modelling of LFC 90
5.3.2 Proposed INFOPID controller Design for LFC in Perturbed Two Area Interconnected Power System 93
5.3.3 Stability Analysis 98
5.3.4 Simulation Results 99
5.3.5 Performance Analysis 106
6. CONCLUSION AND FUTURE SCOPE 110
List of Publications 112
References 113

LIST OF FIGURES

Figure Name	P. No.
Figure 2.1 Heat flowing through a thermocouple	8
Figure 2.2 Effect of integrator and differentiators	13
Figure 2.3 Effects of cascading fractional integrators and differentiators with first order system	14
Figure 3.1 Modelling procedure for system modelling of liquid-liquid heat exchanger	26
Figure 3.2 General steps in an optimization algorithm procedure	27
Figure 3.3 Experimental data for LLHE system	32
Figure 3.4 Results of system modelling of heat exchanger in fractional first order and second order model	34
Figure 3.5 Step response of identified fractional FOPTD models	35
Figure 3.6 Step response of identified fractional SOPTD models	35
Figure 4.1 Hankel Singular Values	47
Figure 4.2 Step response and expended view of original and reduced P_{100}^{30} models	48
Figure 4.3 Step response and expended view of original and reduced P_{90}^{30} models	49
Figure 4.4 Step response and expended view of original and reduced P_{80}^{30} models	50
Figure 4.5 Step response and expended view of original and reduced P_{70}^{30} models	51
Figure 5.1 Closed loop control system	58
Figure 5.2 Stability regions for edge transfer functions	65
Figure 5.3 Global stability region for all the 8 transfer functions	65
Figure 5.4 Zoomed view of global stability region of all the 8 transfer functions	65
Figure 5.5 Response of various controllers to different interval conditions of P_{100}^{30}	72
Figure 5.6 Response of various controllers to different step back conditions	75
Figure 5.7 Feedback control system	79

Figure 5.8 Performance of different controllers for P_{100}^{30} 85

Figure 5.9 Performance of different controllers for P_{90}^{30} 87

Figure 5.10 Performance of different controllers for P_{80}^{30} 87

Figure 5.11 Performance of different controllers for P_{70}^{30} 88

Figure 5.12 Block diagram of two area interconnected power system 91

Figure 5.13 Stability region for area 1 and area 2 97

Figure 5.14 Performance of various controllers under nominal conditions 100

Figure 5.15 Performance of various controllers for area 1 and area 2 with parametric uncertainty 103

Figure 5.16 Performance of various controllers for area 1 and area 2 with GRC under nominal conditions 104

Figure 5.17 Performance of various controllers for area 1 and area 2 with GDB under nominal conditions 104

Figure 5.18 Performance of various controllers for area 1 and area 2 with GRC and parametric uncertainty 105

Figure 5.19 Performance of various controllers for area 1 and area 2 with GDB and parametric uncertainty 106

LIST OF TABLES

Table Name	P. No.
Table 3.1 Estimated parameters for fractional FOPTD model	33
Table 3.2 Estimated parameters for fractional SOPTD model	33
Table 3.3 Model validation of the obtained fractional models using performance indices	36
Table 3.4 Performance of various optimization algorithms	36
Table 4.1 Transfer function models of the PHWR plant at different power levels	44
Table 4.2 Reduced order models of P_{100}^{30}	48
Table 4.3 Poles of different transfer function of P_{100}^{30}	48
Table 4.4 Reduced order models of P_{90}^{30}	52
Table 4.5 Poles of different transfer functions of P_{90}^{30}	52
Table 4.6 Reduced order models of P_{80}^{30}	50
Table 4.7 Poles of different transfer functions of P_{80}^{30}	52
Table 4.8 Reduced order models of P_{70}^{30}	52
Table 4.9 Poles of different transfer functions of P_{70}^{30}	53
Table 5.1 FO models of the PHWR for various operating conditions	57
Table 5.2 Transfer function for the interval model of P_{100}^{30} PHWR	59
Table 5.3: Roots of characteristic polynomial $P(s)$	66
Table 5.4 Comparison of performance of various controllers under interval conditions	76
Table 5.5 Performance comparison under different step back conditions	77
Table 5.6: Roots of characteristic polynomial $P_1(s)$	84
Table 5.7 Integral error measures for P_{100}^{30}operating condition of PHWR	86
Table 5.8 Integral error measures of various controllers for P_{90}^{30} operating condition	87
Table 5.9 Integral error measures of various controllers for P_{80}^{30} operating condition	88

Table 5.10 Integral error measures of various controllers for P_{70}^{30} operating condition 88

Table 5.11 Nomenclature of power systems components 91

Table 5.12 Two-area interconnected system parameters 92

Table 5.13 Roots of characteristic polynomial $H(s)$ 99

Table 5.14 Performance analysis of various controllers under nominal conditions 107

Table 5.15 Performance analysis of various controllers under different parameter changes 107

Table 5.16 Performance analysis of various controllers under nominal conditions with GRC 108

Table 5.17 Performance analysis of various controllers with GRC under different parameter changes 108

Table 5.18 Performance analysis of various controllers under nominal conditions with GDB 108

Table 5.19 Performance analysis of various controllers with GDB under different parameter changes 108

CHAPTER 1

INTRODUCTION

1.1 Preamble

Autonetics and control has evolved as an appropriate important facet of engineering in the present technologically modernized world. Control engineering is a multidisciplinary field built on the basics of linear system study, feedback principle and also integrates the philosophies of network theory and transmission. Therefore, control engineering is evenly relevant to all the engineering disciplines like image processing, robotics, signal processing etc. So, the robust control strategies that can provide accurate performance is the need of the hour.

The main aspects when dealing with controller design of any large complex systems are mathematical complexity and varying operating conditions. The higher order mathematical models lead to increase in mathematical complexity while designing a controller. However, if the controller is designed by decreasing the order of the original higher order system, the complexity can be decreased to a large extent. The tool used to reduce the mathematical complexity is called reduced order modelling. This helps in reducing the order of original higher order system to lesser order while making sure that the dominant characteristics of the original system are maintained. Thus, reduced order modeling can be used as a technique for controller design decreasing the mathematical complexity of the overall system.

Presently, there are numerous control design techniques existing in literature like Ziegler Nichols, Internal model control, LQR etc. [1], [2]. However, these controller design techniques suffer from various performance limitations when applied in real time. The actuality behind this is that the operating conditions are never ideal when working in real time. This is another main aspect to be kept in mind while designing a controller. In the real time working environment, the parametric uncertainty and external disturbances are the issues of concern which affect the controller performance. Most of the prevalent controller design techniques face a limitation in providing accurate performance under such conditions. Hence, there is a need to devise some control methodology that can work well even under real time operating conditions. A new branch called

the fractional order (FO) control system has emerged in control system area in latest years to cope-up with the increased complexity of real time systems.

FO control systems came up with the advent of fractional calculus. The mathematics which deals with the derivatives and integrals of random non-integer order is generally known as the fractional calculus. Several well-known mathematicians like L'hospital, Euler, Riemann, etc., engineers and inventors like Heaviside, Caputo, have aided thoughtfully to this appealing branch of mathematics [3]. In current years, the differential equations involving fractional derivatives and integrals (FDEs) have found increasing contribution in the modelling of real-time systems and control theory [4], [5]. This has proved a great milestone in control system area. The systems modelled using FO have been found to be much closer to real time behavior of large complex systems. When these real time physical systems are modelled, they may lead to higher order system. Analyzing this real time higher order system and its control may prove more difficult. The controllers designed using the notion of FO control has been found to behave robustly and accurately as compared to the existing controllers. These controllers provide reduced steady state errors, improved disturbance rejection capability and better stability. Existing controller design techniques for fractional systems are mathematically very complex and lengthy. Most of the techniques are not generally applicable, rather applicable to specific types of systems.

1.2 Objectives of the Thesis

In this thesis, fractional order (FO) has been used for system modeling and controller design. Also, the reduced order modelling (ROM) has been employed in the design of FO controllers. The objectives of the Ph.D. research work titled "Reduced Order Modelling and Control Using Advanced Techniques" are:

i) To model complex systems using advanced techniques

ii) To reduce the order of the model of complex systems

iii) To design a controller for the reduced order model

iv) To analyze the stability and performance of the control system designed

1.3 Contributions in the Thesis

In order to fulfil the objectives, the work has been carried out in the field of FO system modelling, reduced order modelling for controller design, FO controller design techniques and stability analysis of FO systems. The brief description of the contributions in the thesis are as follows:

i) The performance analysis of any dynamic system essentially requires a precise mathematical modelling. The real time behavior of any practical system can be captured more closely by developing its fractional order model. The analytical methods of modeling are widely used and most precise methods. However, these methods are mathematically very complex and lengthy. So, to overcome the drawback of analytical modeling, in this present work, various nature inspired optimization algorithms have been explored for fractional order modelling of a liquid-liquid heat exchanger system. The performance of different optimization algorithms has been quantified and compared. The system has been modelled in fractional first and second order templates with time delay. The obtained results demonstrate the applicability of nature inspired algorithms in fractional order system modeling. The second order models have been seen to better fit the original data than the first order models.

ii) Majority of physical processes result in high dimensional models. The analysis of such higher order models is a cumbersome task, so it is very important to estimate its lower order model. The estimated lower order model must approximate the higher order model with highest possible accuracy, while retaining the significant (weighty) characteristics of the original system. Here, the reduced order modelling of a Pressurized Heavy Water Reactor (PHWR) has been carried out using Balanced Truncation technique. This technique gave pronounced results to reduce the unstable sixth order PHWR system to a lower third order system. The reduction in the order of the system will simplify the controller design.

iii) The FO controllers are one of the best-known controllers for handling uncertainty, and disturbed operating conditions in real time environment. However, the controller design using higher order model is a protracted task. Hence, to overcome this downside, it is required to develop such controller which can be designed using lower order system model and performs well even with its higher order model. In this research work, a FOPID controller has been designed for the higher (sixth) order model of the Pressurized Heavy Water Reactor using

corresponding reduced (third) order model along with stability boundary locus technique with specific gain-phase margin. The designed controller works very well and resulted in a stable response even when applied on the original higher order system with a significant reduction in settling time.

iv) Majority of the existing controller design techniques fail to provide satisfactory performance under parametric variations and external disturbances. The new interval fractional order PID (INFOPID) controllers have been proposed for perturbed PHWR and two area interconnected power system applications. The fractional controller design has been carried out for the perturbed PHWR fractional order system using Stability Boundary Locus technique and Edge theorem. The proposed INFOPID controller has been designed for eight nuclear reactor models considering eight interval conditions (±50% variations in system parameters) for each reactor model of the PHWR. The proposed INFOPID controller provides the faster set point tracking ability even under the given perturbed conditions as well as the varying step back operating conditions.

v) Further, the fractional controller has been designed using Kharitonov's theorem and Stability boundary locus technique for frequency control in a perturbed two area interconnected power system. The performance of designed controller has been evaluated for parametric variations as well as under the effect of nonlinearities. The proposed controller can provide better performance under the given perturbed conditions than the nominal controllers.

1.4 Organization of the Thesis

In Chapter 2, the importance of FO control has been illustrated with respect to three main aspects of control system i.e., modelling, stability analysis and controller design. Firstly, the importance of fractional calculus from system modelling and control perspectives have been illustrated [6]. It is shown that the naturally occurring phenomena in the real world can be better modelled using fractional calculus operators. Moving further, the basic concepts involved in the stability testing of fractional linear as well as interval systems have been explained [7]–[9]. According to existing literature, a Kharitonov theorem for stability analysis of FO interval systems was proposed in 2002 [10]. However, applicability of this technique was limited only to a specific class of systems, i.e. commensurate fractional order systems (FOS). In 2009, an Edge theorem based technique was

suggested by Tan [11] which could be applied to all classes of FO interval systems. The details of these methods and the contributions made by other researchers in this area have also been discussed in this chapter.

In Chapter 3, a comparative analysis of the FO modelling techniques for a liquid-liquid heat exchanger (LLHE) system has been carried out. Various optimization techniques have been employed for FO system modelling using input-output dataset. It has been found that the second order fractional templates are more suitable than the first order fractional templates for this application.

Chapter 4 describes technique for decreasing the mathematical complexity of complex higher order system. In this chapter, Balanced Truncation method [12] has been utilized to reduce the order of a sixth order Pressurized Heavy Water Reactor (PHWR) to third order. This reduced model has been used in Chapter 5 for designing the controller for the original system that is higher order and it has been seen that the controller designed using reduced order works equally well on the original higher order system. This reduces the mathematical complexity to a great extent. All the related work carried out by various researchers in this direction has been discussed in this chapter.

Further, Chapter 5 deals with the FO controller design techniques for the linear as well as interval systems. Firstly, the controller design techniques that are presented in literature have been discussed [13]–[20]. Further, two different systems have been considered for illustrating the FO controller design techniques. The controller design has been carried out for power control in perturbed PHWR using Edge theorem and Stability boundary locus technique; and Load Frequency Control (LFC) in perturbed two area interconnected power system using Kharitonov theorem and Stability boundary locus method. Also, the controller design for power control in PHWR has been carried out using the concept of reduced order modelling. The proposed techniques have been explained step by step in detail and the simulation outcomes prove the superiority of the suggested controllers in contrast with the existing ones.

CHAPTER 2

IMPORTANCE OF FRACTIONAL CALCULUS AND STABILITY TESTING

2.1 Fractional Calculus

The academicians and researchers working in numerous fields of science and engineering come across calculus operators like $\frac{d}{dt}, \frac{d^2}{dt^2}, \frac{d^3}{dt^3}$ etc. The thought that why the order of calculus operator should always be an integer value, not any real number gave birth to an entirely new branch of mathematics called fractional calculus. This area of fractional calculus remained limited for a long time, although this concept is almost as old as the conventional calculus. Obtaining the mathematical definitions of the fractional operators was a very challenging task for the researchers of mathematics. However, systematic approach towards this area of research was started by researchers like Liouville (1832), Holmgren (1864), Riemann (1953) etc. in the early 19th century [6]. The applicability of fractional calculus gained popularity in science and engineering once the basic meanings of the fractional differential and integral operators were obtained. The mathematical definition of fractional derivative and integral operators has been given by different approaches. Riemann-Liouville (RL) and Grunwald-Letnikov (GL) definitions are the two most commonly used definitions [21]. RL definition represents the FO integral as:

$$ {}_aD_t^{-\alpha} f(t) = \frac{1}{\Gamma(-\alpha)} \int_a^t \frac{f(\tau)}{(t-\tau)^{\alpha+1}} d(\tau) \tag{2.1} $$

while the FO derivative is given as:

$$ {}_aD_t^{\alpha} f(t) = \frac{1}{\Gamma(n-\alpha)} \frac{d^n}{dt^n} \int_a^t \frac{f(\tau)}{(t-\tau)^{\alpha-n+1}} d(\tau) \tag{2.2} $$

where, $\Gamma(x)$ is the gamma function, a and $t$are the limits and α ($(n-1) < \alpha < n, \alpha > 0$ and $\alpha \in R$) is the order of the performed operation. The GL approach definition is given in Eq. (2.3) [21].

$$ {}_aD_t^{\alpha} f(t) = \lim_{h \to 0} \frac{1}{h^{\alpha}} \sum_{j=0}^{\left[\frac{t-a}{h}\right]} (-1)^j \binom{\alpha}{j} f(t - jh) \tag{2.3} $$

where, $\left[\frac{t-a}{h}\right]$ denotes the integer part of $\frac{t-a}{h}$, a and t are the limits and the binomial coefficients are,

$$ \binom{\alpha}{j} = \frac{\alpha!}{j!\,(\alpha - j)!} = \frac{\Gamma(\alpha + 1)}{\Gamma(j + 1)\Gamma(\alpha - j + 1)} \tag{2.4} $$

The above mentioned calculus definitions were further used to formulate fractional models and FO controllers.

The three most important aspects in the area of control system are modelling, stability analysis and controller design. The beginning of fractional calculus has brought massive improvement in all these three areas of control theory. This chapter demonstrates a brief overview about the basic theories of FO control systems from modelling, stability analysis and control action perspectives. The modelling of real time physical systems could be carried out more accurately after the development of fractional calculus operators. It was observed that for large and complex systems, the real time behavior can be much easily approximated with the fractional modelling [22]. However, when fractional modelling gained popularity, it became necessary to examine the stability of such FOS. The development of Matignon's theorem provided a strong base to solve this potential problem in 1996 [7], [23]. Further, with the advent of the FOPID controller in 1999 [24], it was found that these controllers gave better performance and disturbance rejection competence than the conventional controllers. The enhanced performance of these controllers have been appreciated in various areas like process control [25]–[29], secure communication and multimedia security [30], [31], robotics [32]–[35], power electronics [36]–[40] , LFC [41]–[44] etc. The importance of fractional control from modelling and control perspectives has been illustrated in Section 2.2. The basic concepts concerned with the stability testing of FOS have been discussed in Section 2.3.

2.2 Importance of Fractional Calculus

2.2.1 Modelling Perspective

FO control is a new control strategy that has gained popularity in the recent times. It is well known to have better system modelling capacity as well as better controlling ability. A considerable research is going on in this area and control engineers are continuously working in the direction of making fractional control easily applicable to various engineering applications.

Along with this, researchers in field of process control, biological systems, electrochemistry etc. usually perform experiments in frequency domain to obtain equivalent electrical circuits which reflect the dynamic demeanor of the system under study. In such areas, it is observed that for common elements such as R, L and C, system behaviors are far from expected ones. Such systems are modelled using FO mathematical models and are designed using FO circuits.

In order to understand the occurrence of FO behavior in nature, let us consider an example of relationship between temperature and heat flux for a semi-infinite conductor. This relationship can be studied by taking a thermocouple into consideration. It is a device consisting of a pair of unlike metals with a shared junction point. These wires are insulated and long enough to be looked upon as 'semi-infinite' heat conductors. The heat flow is amount of heat relocated per unit area per unit time from the surface or to the surface [21].

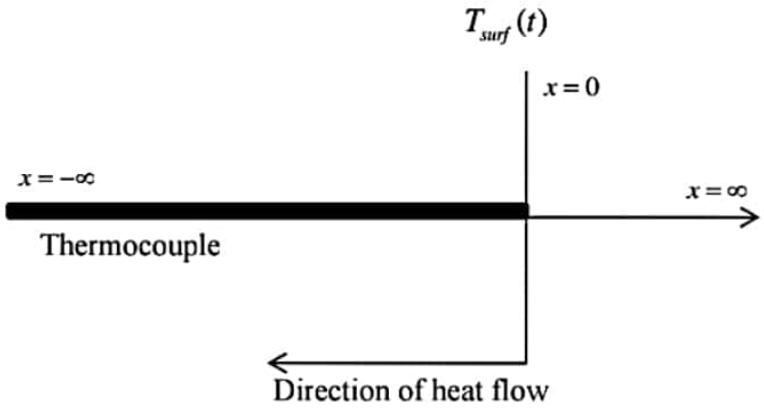

Figure 2.1 Heat flowing through a thermocouple

In Figure 2.1, the coordinate $x = 0$ is called the furnace wall, $T_{surf}(t)$ denotes the temperature at the furnace wall while T_0 is the initial temperature i.e. at $t = 0$. A function T is chosen that denotes

the temperature at coordinate x. The function T changes with time as the heat spreads all through the space. It assists to quantify the change in T. The principle property of the heat equation suggests that the peak value of T is either earlier in time in the region of concern or on its edges.

The Fourier's law and law of conservation of energy are used to derive the heat equation. According to Fourier's law, the rate of flow of heat energy through a surface is proportionate to the negative temperature gradient across the surface and is given by,

$$q = -k\frac{\partial T}{\partial x} \tag{2.5}$$

Where $\frac{T}{x}$ is the temperature gradient, k is proportional constant and$q$ denotes the rate of flow of energy through the surface.

The variation in internal energy per unit volume in the material ΔQ is proportional to difference in temperature ΔT, when no work is done in changing the temperature i.e. no displacement is caused.

$$\Delta Q = c\rho\Delta T \tag{2.6}$$

where c and ρ are the specific heat capacity and mass density of the material, respectively. At absolute zero temperature, zero energy is considered. Therefore, Eq. (2.6) becomes

$$Q = c\rho T \tag{2.7}$$

The increase in internal energy in small spatial region $x - \Delta x \leq \xi \leq x + \Delta x$ of the material, over the time period$t - \Delta t \leq \tau \leq t + \Delta t$ with change in temperature is given by

$$c\rho \int_{x-\Delta x}^{x+\Delta x} [T(\xi, t+\Delta t) - T(\xi, t-\Delta t)]\, d\xi = c\rho \int_{t-\Delta t}^{t+\Delta t} \int_{x-\Delta x}^{x+\Delta x} \frac{\partial T}{\partial \tau} d\xi d\tau \tag{2.8}$$

When no work is done, the change in internal energy in the spatial interval $[x - \Delta x, x + \Delta x]$ is compensated by the flux of heat across the boundaries.

Applying the Fourier's law (2.5) to the interval $x - \Delta x \leq \xi \leq x + \Delta x$ and $t - \Delta t \leq \tau \leq t + \Delta t$

$$k \int_{t-\Delta t}^{t+\Delta t} \left[\frac{\partial T}{\partial x}(x + \Delta x, \tau) - \frac{\partial T}{\partial x}(x - \Delta x, \tau)\right] d\tau = k \int_{t-\Delta t}^{t+\Delta t} \int_{x-\Delta x}^{x+\Delta x} \frac{\partial^2 T}{\partial \xi^2} d\xi d\tau \tag{2.9}$$

As stated by law of conservation of energy, the difference between change in internal energy and the heat flux across the boundaries is zero. Hence, subtracting Eq. (2.9) from Eq. (2.8), the following equation is obtained

$$\int_{t-\Delta t}^{t+\Delta t}\int_{x-\Delta x}^{x+\Delta x}\left[c\rho T_t - kT_{\xi\xi}\right]d\xi d\tau = 0 \Rightarrow c\rho T_t - kT_{xx} = 0 \tag{2.10}$$

Therefore

$$T_t = \frac{k}{c\rho}T_{xx} \tag{2.11}$$

or

$$\frac{\partial T}{\partial t} = \frac{k}{c\rho}\left(\frac{\partial^2 T}{\partial x^2}\right) \tag{2.12}$$

or

$$c\rho\frac{\partial T}{\partial t} = k\left(\frac{\partial^2 T}{\partial x^2}\right) \tag{2.13}$$

Eq (2.13) obtained above is called heat equation. Now a function is assumed

$$u(t,x) = T(t,x) - T_0 \tag{2.14}$$

Substituting Eq. (2.14) in Eq. (2.13), we get

$$c\rho\frac{\partial u}{\partial t} = k\frac{\partial^2 u}{\partial x^2} \tag{2.15}$$

where $t > 0, -\infty < x < 0, u(0,x) = 0,\ u(t,0) = T_{surf}(t) - T_0$ and $\left|\lim_{x\to-\infty} u(t,x)\right| < \infty$, After taking Laplace transform we get,

$$c\rho sU(s,x) = k\frac{\partial^2 U(s,x)}{\partial x^2} \Rightarrow \frac{\partial^2 U(s,x)}{\partial x^2} - \frac{c\rho s}{k}U(s,x) = 0 \tag{2.16}$$

The bounded solution for $x \to -\infty$

$$U(s,x) = U(s,0)\,exp\left(^{x}\sqrt{\frac{sc\rho}{k}}\right) \tag{2.17}$$

Differentiating

$$\frac{dU(s,x)}{dx} = U(s,0)\sqrt{\frac{sc\rho}{k}}exp\left(^{x}\sqrt{\frac{sc\rho}{k}}\right), \text{ at } x = 0 \tag{2.18}$$

$$\frac{1}{\sqrt{s}}\frac{d}{dx}U(s,0) = \sqrt{\frac{c\rho}{k}}U(s,0) \tag{2.19}$$

Taking inverse laplace,

$$\frac{d^{-\frac{1}{2}}}{dt^{-\frac{1}{2}}}\frac{\partial u(t,0)}{\partial x} = \sqrt{\frac{c\rho}{k}}u(t,0),\ \frac{\partial u(t,0)}{\partial x} = \sqrt{\frac{c\rho}{k}}\frac{d^{\frac{1}{2}}}{dt^{\frac{1}{2}}}u(t,0) \tag{2.20}$$

Returning from $u(t,0)$ to $T(t,x)$

$$k\frac{\partial T(t,0)}{\partial x} = \sqrt{c\rho k}\frac{d^{\frac{1}{2}}}{dt^{\frac{1}{2}}}\left(T_{surf}\{t\} - T_0\right) \tag{2.21}$$

The term $k\frac{\partial T(t,0)}{\partial x} = Q(t)$ is called heat flux, flowing through the thermocouple wire at the interface of the furnace wall and point of contact.

Therefore, the heat flux expression is,

$$Q(t) = \sqrt{c\rho k}\frac{d^{\frac{1}{2}}}{dt^{\frac{1}{2}}}\left(T_{surf}\{t\} - T_0\right) = \frac{k}{\sqrt{\frac{k}{c\rho}}}\frac{d^{\frac{1}{2}}}{dt^{\frac{1}{2}}}\left(T_{surf}\{t\} - T_0\right) \tag{2.22}$$

This can be expressed in the form of fractional operator as

$$Q(t) = \frac{k}{\sqrt{\alpha}}\,{}_{\alpha}D_t^{\frac{1}{2}}T_b(t) \tag{2.23}$$

where,

$$T_b(t) = \left(T_{surf}\{t\} - T_0\right) \text{ and } \alpha = \frac{k}{c\rho} \tag{2.24}$$

Thus, from the example explained above, it can be seen that the real life phenomenon when modelled mathematically (Eq. 2.23), give rise to expressions involving FO calculus operators. In order to work with such kind of systems, it is very important to have some means to deal with such mathematical equations. The development of fractional calculus operators has proved very useful in the mathematical modelling of such real time physical systems. Hence, it can be seen that the FO calculus has great importance in modelling aspect of control system.

2.2.2 Control Perspective

Conventionally *P*, *I*, and *D* control actions are available. They can be used individually or in combination such as PI, PD or PID. The effects of each of these control actions are discussed below:

i) The speed of response increases and steady state error and relative stability decreases when proportional action is used.

ii) The relative stability and noise sensitivity increase with derivative action.

iii) Steady state error and relative stability can be reduced by integral action.

The increased relative stability and sensitivity to high frequency noise, i.e. the effect of derivative (s) action can be incorporated by $\pi/2$ phase lead and slope of 20/dB sec respectively, in the frequency response. Similarly, by the infinite gain at zero frequency and the $\pi/2$ phase lag respectively, the elimination of steady state error and the decreased relative stability can be observed in case of integral control (1/s). To make this strategy more powerful and flexible to satisfy desired performance specifications, the control action of the form s^n or $1/s^n, n \in R^+$can be incorporated. This helps in achieving better compromise between positive and negative effects of control action. Figure 2.2(a) and Figure 2.2(b) show the Bode plot of the integrators and differentiators of various orders, respectively.

It can be interpreted from Figure 2.2 that adding the integrators and differentiators of FO provide intermediate control action that seems more attractive. Figure 2.2(a) shows the Bode plot of integrators of orders 0.5, 1, 1.5 and 2 and it can be observed that Bode diagram of integrator of order 1.5 lies between that of order 1 and 2. Similarly, the Bode plots of differentiators of different orders are shown in Figure 2.2(b).

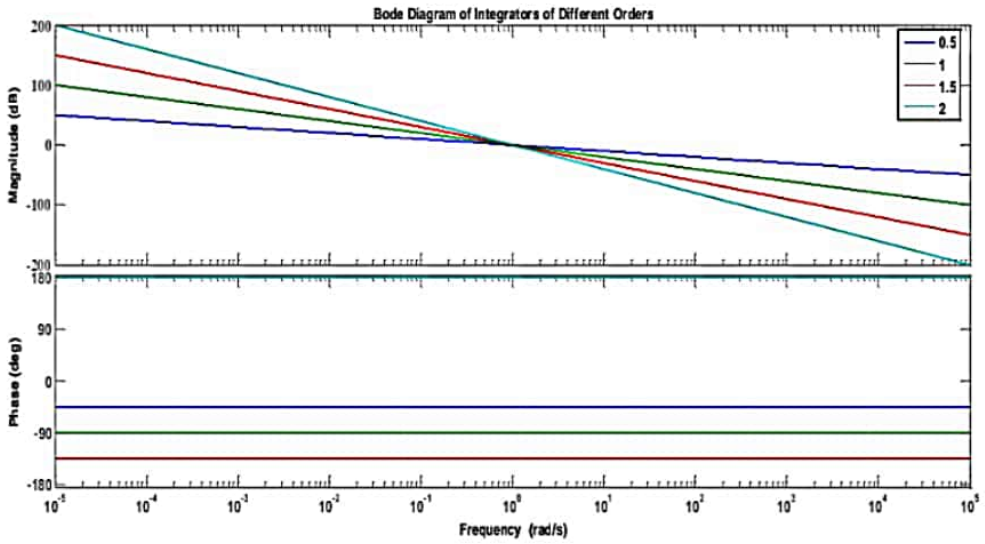

(a) Integrators

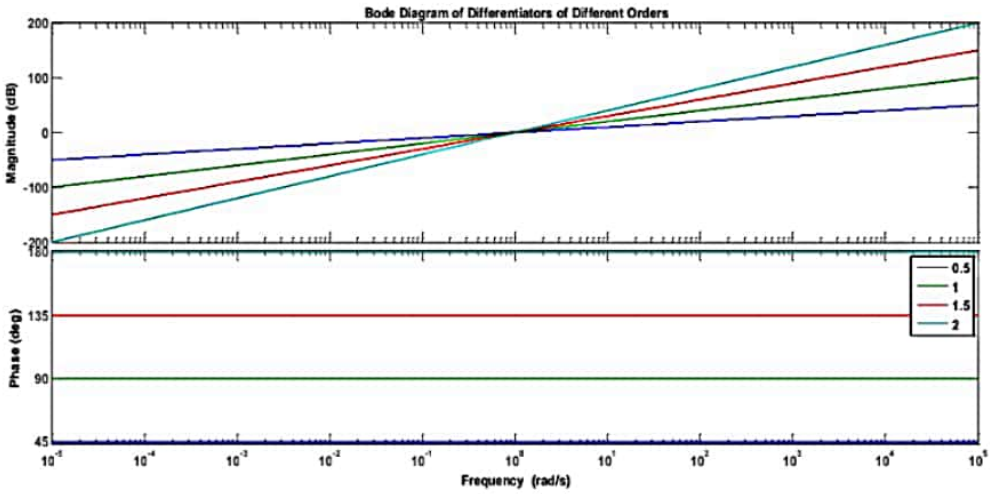

(b) Differentiators

Figure 2.2 Effect of integrator and differentiators

In addition, the effect of FO integrator and differentiator on first order system is displayed in Figure 2.3(a) and Figure 2.3(b) respectively. The following first order system is considered to see the effects of cascading FO integrator and differentiator of varying orders.

$$G(s) = \frac{1}{s+1} \tag{2.25}$$

Cascading an integrator of order 0.5, the system becomes

$$G(s) = \frac{1}{s^{0.5}}\left(\frac{1}{s+1}\right) \tag{2.26}$$

Cascading an integrator of order 1, the system becomes

$$G(s) = \frac{1}{s^{1}}\left(\frac{1}{s+1}\right) \tag{2.27}$$

Cascading a differentiator of order 0.5, the system becomes

$$G(s) = s^{0.5}\left(\frac{1}{s+1}\right) \tag{2.28}$$

Cascading a differentiator of order 1, the system becomes

$$G(s) = s^{1}\left(\frac{1}{s+1}\right) \tag{2.29}$$

Figure 2.3(a) and Figure 2.3(b) show the effect of cascading integrator and differentiator of order 0.5 and 1 respectively to the first order system considered above using Bode plot.

It can be again observed from Figure 2.3 that the effect of FO operators on the system is intermediate in comparison to the integer order ones. This means that incorporating the fractional operators in the system function can provide better and accurate control than the integer order systems [11]. Hence, it can be concluded that FO operators are playing a very vital role for the researchers working in control engineering community from the control action perspective.

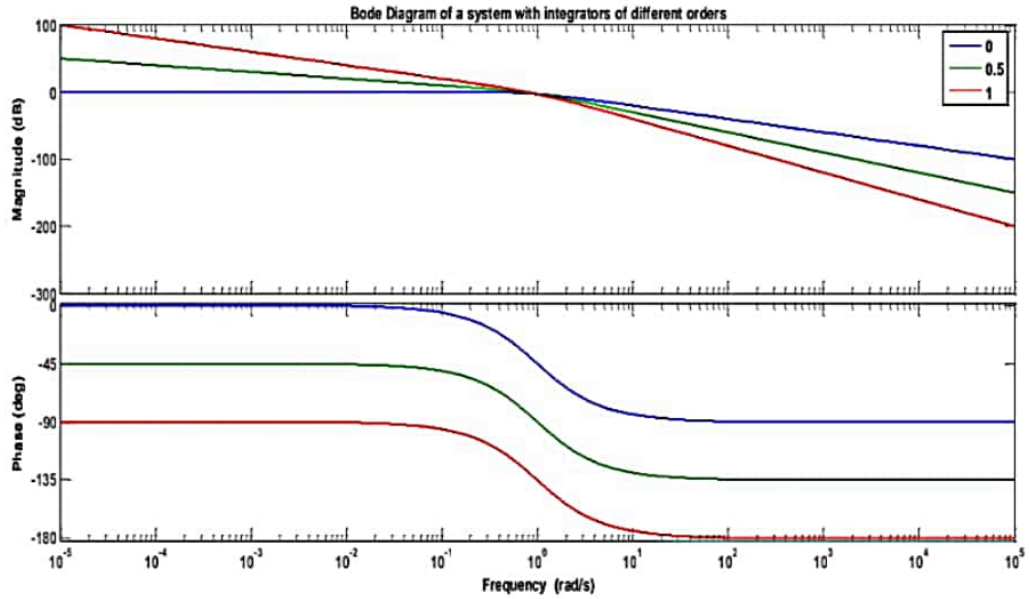

(a) Integrators

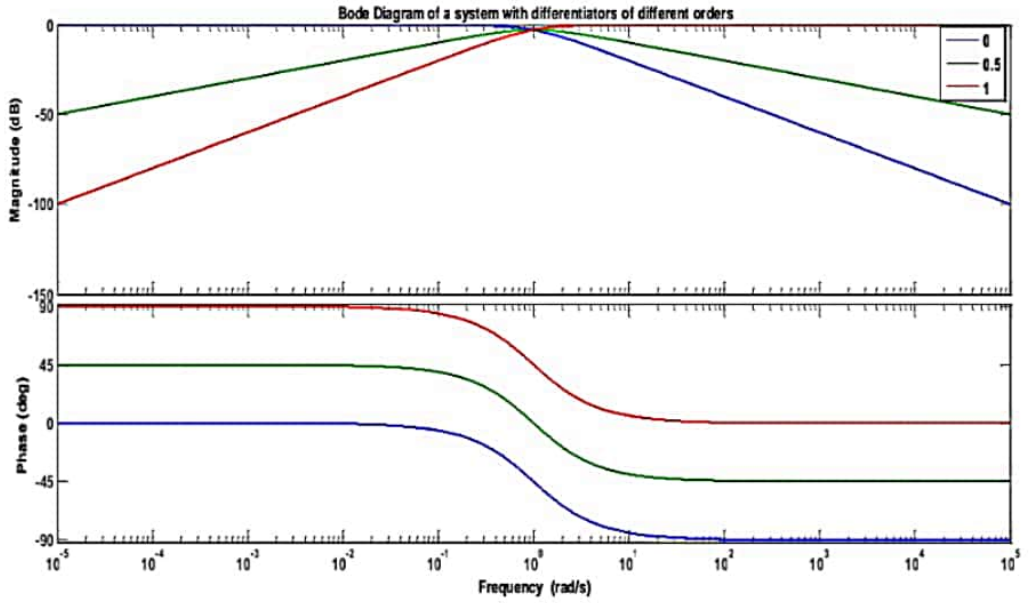

(b) Differentiators

Figure 2.3 Effects of cascading fractional integrators and differentiators with first order system

2.3 Stability Testing of Fractional Order Systems

The classical stability testing approaches like Routh Hurwitz criteria cannot be straightforwardly applied for stability analysis of FOS, as fractional polynomial is a multi-valued function. Riemann surfaces deal with the stability of such FO polynomials. A Riemann surface is a surface like arrangement that covers the complex plane with many sheet like structures having intricate interconnections [45]. A FO polynomial is converted to an integer plane, i.e. w plane by making a substitution $w = s^{\frac{1}{v}}, v \in N$ and s denotes a complex number. Out of the v generated Riemann sheets, the physically realizable values are carried by the first sheet whereas remaining sheets carry the repeated values. Matignon's theorem is an important concept that was proposed in 1996 [7] and provided the base of stability testing of the FOS.

Matignon theorem states that a commensurate-order system represented by

$$G(s) = K\frac{\sum_{k=0}^{m} b_k (s^\alpha)^k}{\sum_{k=0}^{n} a_k (s^\alpha)^k} = K\frac{U(s^\alpha)}{V(s^\alpha)}, n \geq m, \alpha \in R^+, k, n, m \in N, K \in R \tag{2.30}$$

is stable in the case that

$$|arg(\lambda_i)| > \alpha\frac{\pi}{2} \text{ for all } i \tag{2.31}$$

Here, λ_i is the i^{th} root of the polynomial $P(s^\alpha)$. This theorem helps in finding the stability relationship between s plane and roots of the fractional polynomial in w plane. The w plane polynomial is of integer order and it is easy to obtain the roots of this polynomial. Therefore, the FO polynomials are first converted to integer order by substituting $w = s^q, q \in R^+, 0 < q < 2$ i.e. transferred from s plane to w plane for stability testing. The stability condition is checked by using the roots of w plane with the help of the above theorem.

2.3.1 Stability Testing of Fractional Order Linear Systems

The generalized LTI FO system can be characterized by following dynamic equation

$$q(s) = p_n s^{\alpha_n} + p_{n-1} s^{\alpha_{n-1}} + \ldots\ldots + p_1 s^{\alpha_1} + p_0 s^{\alpha_0} \equiv \sum_{j=0}^{n} p_j s^{\alpha_j} = 0 \tag{2.32}$$

The equation (2.32) can also be expressed as

$$\sum_{j=0}^{n} p_j s^{\frac{u_j}{v_j}} = 0 \text{ where } \alpha_j = \frac{u_j}{v_j}, j = 0,1,\ldots\ldots,n \tag{2.33}$$

The transformation of the above equation in the w -plane can be represented as

$$\sum_{j=0}^{n} p_j w^{x_j} = 0, \tag{2.34}$$

with $w = s^{\frac{l}{m}}$, where $\frac{u_j}{v_j} \times \frac{m}{l} = x_j, j = 0,1,\ldots\ldots,n$ is any integer and m is the LCM of v_j. The steps followed for stability test of the above system are [5]:

1. The roots of Eq. (2.34) are calculated and then their absolute phase $|\phi_w|$.

2. The physically realizable roots are obtained by checking that which roots lie in the region $|\phi_w| < \frac{\pi}{m}$. The roots which are physically realizable in the primary sheet of $w$plane are the analogous roots in s plane. The region $|\phi_w| > \frac{\pi}{m}$ doesn't contain physically realizable roots and are hence not considered.

3. Then, the stability condition (as obtained from Matignon's theorem) is checked. The requirement for stability is $\frac{\pi}{2m} < |\phi_w| < \frac{\pi}{m}$.

The above prerequisite for stability corresponds that if all the physically realizable roots, as obtained from Step 2 lie in the left half of s plane, then the polynomial is stable. System is unstable in nature if any of these physically realizable roots doesn't satisfy the condition $|arg\, \phi_w| > (\pi/2m)$.The right half plane roots produce instability in the system and follow the condition $|arg\, \phi_w| < (\pi/2m)$. The system is marginally stable if the physically realizable roots of the polynomial satisfy the condition $|arg\, \phi_w| = (\pi/2m)$. The roots of this oscillatory system lie on the imaginary axis in the s plane.

The technique discussed above proves very helpful in analyzing the stability of FOS. But, when real time systems are considered, the parameters do not persist fixed and fluctuate according to the operational conditions and environmental circumstances. So, parametric uncertainty becomes a major issue when practical real time systems are considered. The FO interval mathematical models give a closer representation of the dynamic behavior of large intricate practical systems. In such type of systems, the coefficients in the transfer function do not have the fixed values. These coefficients have a range of values. The stability testing techniques for fractional interval systems is explained in the next part.

2.3.2 Stability Testing of Fractional Order Interval Systems

In recent years, testing the stability of Fractional Order Interval Systems (FOIS) has been a potential research area. The remarkable growth in this direction was noticed in 2002 when Kharitonov based technique was proposed by Petras *et al.* for stability testing of FOIS[10]. This technique could be applied only to a certain class of FOIS, i.e. commensurate FOS. Many researchers have been engaged since then in the area of developing competent techniques for stability analysis of FOS [9], [46]–[50]. In [51] and [52], necessary and sufficient conditions for stability of uncertain FOIS are introduced in terms of Linear Matrix Inequalities. An approach presented in [53] relied on finding the system having same stability properties as those of the FOS which could be analyzed as an ordinary linear system and is easy to understand than the FOS under consideration. But this technique could examine the stability of FOS with order between 1 and 2. In [54], LMI based conditions for stability analysis of fractional commensurate order $(0 < \alpha < 2)$ systems has been proposed.

Tan *et al.* made a significant contribution by suggesting a stability analysis technique which was applicable to all classes of FOS [11]. This technique was based on calculating $2^{(n+1)}$ polynomials for (n+1) uncertain parameters in the FOS. If the number of uncertain parameters increases, the calculations become lengthy as the number of the edge polynomials to be calculated increases in this technique. Further, it was proposed in [9] that only the outer edge polynomials are sufficient for stability analysis of FOIS. But, this approach was suited only to commensurate order systems. In method suggested in [55], the stability of FOIS could be tested using $n2^{n-1}$edges that were formed using scan sampling method.

A probabilistic stability analysis technique was proposed in [56] that calculates the stability distribution according to the FO and is capable of finding the FO interval that makes the system stable robustly. This method is also applicable to robustly stabilize commensurate order systems. The Edge theorem is not able to handle FOS with general interval uncertainties, i.e. the uncertainty exists both in coefficients and order of the FOS. A necessary and sufficient condition to test the stability of such systems has been proposed in [57]. Although a lot of literature is available on stability analysis of FOIS however, the two most well-known techniques are discussed below in detail. These are Kharitonov's theorem and Edge theorem for stability testing of fractional as well as integer order interval systems.

2.3.2.1 Kharitonov's theorem

The commensurate order fractional system is represented by the characteristic polynomial

$$G(s) = d_n s^{\alpha_n} + \ldots\ldots + d_1 s^{\alpha_1} + d_0 s^{\alpha_0} = 0 \tag{2.35}$$

Where, $\alpha_l > \alpha_m > 0$ for $l > m, l = 0,1,2,\ldots\ldots,n$ and $d_l \in \left[\underline{d_l}, \overline{d_l}\right]$ are the interval parameter.

The above FO interval system with commensurate order α can be checked for stability using Kharitonov theorem using the following steps [10]:

1. The FOIS system $G(s)$ is transformed to $T(\varsigma)$, using the transformation $s^{\alpha} \to \varsigma, \alpha \in R^{+}$.
2. The interval polynomial is obtained and is defined as $T(\varsigma, d) = \sum_{l=0}^{n} \left[\underline{d_l}, \overline{d_l}\right] \varsigma^l$
3. The four Kharitonov polynomials are constructed for the interval polynomial $T(\varsigma, d)$

$$\begin{aligned}
T^{--}(\varsigma) &= \underline{d_0} + \underline{d_1}\varsigma + \overline{d_2}\varsigma^2 + \overline{d_3}\varsigma^3 + \underline{d_4}\varsigma^4 + \underline{d_5}\varsigma^5 + \ldots\ldots \\
T^{-+}(\varsigma) &= \underline{d_0} + \overline{d_1}\varsigma + \overline{d_2}\varsigma^2 + \underline{d_3}\varsigma^3 + \underline{d_4}\varsigma^4 + \overline{d_5}\varsigma^5 + \ldots\ldots \\
T^{+-}(\varsigma) &= \overline{d_0} + \underline{d_1}\varsigma + \underline{d_2}\varsigma^2 + \overline{d_3}\varsigma^3 + \overline{d_4}\varsigma^4 + \underline{d_5}\varsigma^5 + \ldots\ldots \\
T^{++}(\varsigma) &= \overline{d_0} + \overline{d_1}\varsigma + \underline{d_2}\varsigma^2 + \underline{d_3}\varsigma^3 + \overline{d_4}\varsigma^4 + \overline{d_5}\varsigma^5 + \ldots\ldots..
\end{aligned} \tag{2.36}$$

4. Check whether all the four Kharitinov polynomials satisfy the Routh stability condition or not.

The FOIS system $G(s)$ is stable within the parameter variations $d_l \in \left[\underline{d_l}, \overline{d_l}\right]$ if all the four Kharitinov polynomials satisfy the stability condition independently.

2.3.2.2 Edge theorem

The applicability of Kharitonov Theorem described above is limited only to commensurate order FOIS. Tan proposed the edge theorem to evaluate the stability of FOIS in 2009 [11]. This stability testing technique can be applied to all the classes of FOIS. In this analytical technique, 2^n polynomials are required for testing the stability of polynomial having n uncertain parameters. Consider a FO interval polynomial family represented by

$$G(s) = d_n s^{\alpha_n} + \ldots\ldots + d_1 s^{\alpha_1} + d_0 s^{\alpha_0} = 0 \tag{2.37}$$

Where, $\alpha_l > \alpha_m > 0$ for $l > m, l = 0,1,2,\ldots\ldots,n$ and $d_l \in \left[\underline{d_l}, \overline{d_l}\right]$ are the interval parameter The 2^{n+1} edge polynomials for $G(s)$ can be written as:

$$
\begin{aligned}
v_1(s) &= \underline{d_0}s^{\alpha_0} + \underline{d_1}s^{\alpha_1} + \underline{d_2}s^{\alpha_2} + \ldots + \underline{d_n}s^{\alpha_n} \\
v_2(s) &= \overline{d_0}s^{\alpha_0} + \underline{d_1}s^{\alpha_1} + \underline{d_2}s^{\alpha_2} + \ldots + \underline{d_n}s^{\alpha_n} \\
v_3(s) &= \underline{d_0}s^{\alpha_0} + \overline{d_1}s^{\alpha_1} + \underline{d_2}s^{\alpha_2} + \ldots + \underline{d_n}s^{\alpha_n} \\
&\cdot \\
v_{2^{n+1}}(s) &= \overline{d_0}s^{\alpha_0} + \overline{d_1}s^{\alpha_1} + \overline{d_2}s^{\alpha_2} + \ldots + \overline{d_n}s^{\alpha_n}
\end{aligned}
\tag{2.38}
$$

All these edge polynomials are individually tested for stability using technique discussed in Section 2.3.1. If all these polynomials satisfy the stability criteria as described for the linear systems, then the original family of polynomials $G(s)$ is stable under all possible given perturbed conditions. The above mentioned stability testing techniques have been used while designing FO controllers for various applications illustrated in Chapter 5. Using Kharitinov's and Edge theorem at the time of controller design helps in incorporating stability in the system at the design stage itself. This helps in making the system more robust and improve the controller performance.

Summary

The present chapter explains the significance of fractional calculus from system modelling and control perspective. It is observed from the study that the fractional calculus helps in obtaining mathematical model that are closer to the real time dynamics of the physical systems. Also, the fractional calculus has made controllers more flexible and accurate by making it possible to introduce intermediate corrections in the controlled system. Since this new form of mathematical modelling also requires new methods for stability testing therefore, the stability testing techniques that can be applied to linear as well as interval FOS have also been explained.

CHAPTER 3

FRACTIONAL SYSTEM MODELLING USING OPTIMIZATION TECHNIQUES

3.1 Introduction

The depiction of the vital characteristics of a system which presents information of that particular system in a usable form is called mathematical modelling. The most difficult task is to develop an accurate mathematical model of a process for the reason such as different input and output constraints, associated non-linearities, various uncertainties in the system etc. [58]. Accurate control demands an operative mathematical illustration of the plant with an acceptable certainty.

The determination of the dynamic attributes of the mechanism using the experimentally collected input-output data set is referred to as system modelling [59]. System modelling can be categorized as 'grey box modelling', 'white box modelling', and 'black box modelling'. In white and grey box modelling, all the parameters (example, a RC circuit) or some of the parameters are known in advance. But, in black box modelling, none of the parameters are preliminarily known. In this case, the dynamics of the process has to be depicted from the experimentally collected input-output dataset. In this, the model structure has to be assumed which can be linear or nonlinear. Linear models are more frequently used due to their simplicity, and also for the reason that they allow for easy and systematic examination of the properties of the resulting model [60]. However, real systems are non-linear to some extent, and arises a need for development of more advanced models.

When talking about FO models, it is difficult to find an exact model for a given system from the input-output data as it requires

(a) The number of fractional operators to be chosen
(b) The fractional powers
(c) The coefficients of operators

The FO transfer functions cannot be easily handled by classical identification methods. FO modelling has been used in various applications like biomedical to model the dielectric responses

of amorphous biological samples, for dissimilar redundant actuating system used in large passenger aircraft, in Polymer Electrolyte Membrane Fuel Cell systems, heat exchangers etc. [61]–[69]. In [65], the parameters and order of a variable order system have been identified using an adaptive order/parameter identification method. In [68], identification of diffusion parameters of electrochemical cell has been done in time domain and validated in frequency domain using Electrochemical Impedance Spectroscopy (EIS) measurements. In [67], the integer order has been approximated to find the parameters of FO model and a state space framework was conferred for employing output-error identification algorithm.

Valerio *et al.* [70] provided a methodology how Levy's method and its variants using frequency domain data can be utilized to find a fractional model. A frequency domain method has been employed in [71]. The Levenberg-Marquardt optimization is used with non-linear programming and sensitivity functions to find the fractional models of an electrical network. In [72], experiment design methodology has been used for system identification of fractional transfer function of first kind and further in [73], the same design methodology has been applied to deal with system identification of FO models of second kind . The frequency domain approach has been used to calculate any one of the assumed unknown parameters. A state space commensurate FO model with input time delay was obtained by Li *et al.* [74] by employing differential algorithm and frequency domain based subspace identification algorithm.

In [75], identification of MIMO FO commensurate LTI systems have been carried out from uniformly sampled input-output data. Fractional Laguerre generating functions have been utilized to find the missing data and the continuous-time FO system's parameters have been identified by employing the multivariable output error state space (MOESP) method. In the field of non-linear modelling, block oriented approach is very attractive due to its ease. Block oriented models are interconnections of LTI blocks and static nonlinear blocks. An example of block-oriented model is Wiener- Hammerstein (W-H) system. In [76], a subspace based method has been used to identify W-H system. The state space model has been attained from the input-output data by means of Orthogonal Projection (ORT) subspace identification technique and separable least squares. In [60], [77] fractional approach has been employed to generate the initial estimates for the W-H model.

The introduction of time domain fractional system identification led to two main types of models called equation-error and output-error models and have been detailed by Malti *et al.* [78]. The former method helps in estimating the model parameters using least squares keeping the differentiation order fixed, while in the latter method, both can be estimated using non-linear programming increasing the complexity of the calculation procedure. In [79], a continuous time FO system has been identified using operational matrices. The algebraic equations for this system are formed using operational matrices. The system parameters are estimated using multi-dimensional optimization technique. The same technique was applied to FO time delay systems to estimate the time delay and differentiation orders by Tang *et al.* [80].

Another time domain based identification method using input-output data was presented in [81]. The FO linear system was formed into set of algebraic equations with the help of Haar wavelet operational matrices. The parameters were identified by minimizing the errors between output of the actual and identified FO system. The same technique was used by Kothari *et al.* in [82] to model fractional order time delay systems. In [83] , time domain identification of FO system has been carried out by recursive least square and recursive instrumental variable methods. Again in [84], recursive least square method has been used for identification and modulating function has been used for pre-processing of system equations, as differentiation of all kinds of orders of input and output signals cannot be handled by direct identification methods. In [85], the model parameters and fractional (or integer) orders in linear fractional models have been predicted from the input-output data using convolution of the known signals. Further, an optimal input design technique was introduced for continuous system identification using fractional models. An optimal input spectrum has been synthesized for both continuous time LTI systems and FOS [86].

In [87], the parameters have been identified for a FO linear system via modified fractional-order gradient method when the output signal is corrupted by noise and outliers. Here, the outlier detection is basically a matrix decomposition problem based on nuclear norm method. Optimization techniques have also been employed for fractional system identification. In [88], a hybrid transfer function of integer and FO have been chosen for improving the identification accuracy of some typical thermal processes. PSO has been employed to estimate the order and coefficients of this chosen hybrid template.

In the present work, a liquid-liquid heat exchanger (LLHE) system has been considered for FO modelling using various optimization techniques. The applicability and performance of various nature inspired optimization algorithms have been estimated for fractional order system identification. The system identification can be achieved with any one of the compared algorithms. The present research work explored the performance of various algorithms for a particular system, when input and output information of the system is available. The performance of any optimization algorithm is highly dependent on the algorithm tuning parameters and system available information. Hence, it is necessary to explore all possible algorithms for a given problem and opt for the best performing algorithm. A comparative analysis of performance of various nature inspired optimization techniques has been discussed in the subsequent sections.

3.2 Fractional Order Modelling of Liquid-Liquid Heat Exchanger Using Various Optimization Techniques

Heat exchangers are used for transferring the heat amongst two or more media, at different temperature and in thermal contact. The heat is transferred without transferring the fluid that transports the heat. The basis of the classification of heat exchangers is the transfer processes involved, construction features, degree of periphery compactness, tally of fluids, flow arrangements, and mechanisms involved in heat transfer [89]. Various researchers have carried out mathematical modelling of different types of heat exchangers. A theoretic model for the coil heat exchanger has been established by N.A. Khan [90]. A lot of assumptions have been considered in the heat transfer process and the relative error between the estimated model and the actual experimental data does not exceed 10%. The heat transfer model for Compact air-air heat exchanger (CAAHXs) has been presented in [91]. However, it has to be applied only in the dry air and steady state. Gao *et al.* [92] used the mathematical model to analyze the transient problems which were present in cross flow heat exchangers. Tiwari *et al.* [93] carried out numerical simulations of various types of nano-fluids streaming in a plate heat exchanger using FLUNET.

Many evolutionary algorithms have also been employed to carry out system modelling. Zambrano *et al.* [94] used WH-EA to look for the Best Linear Approximation (BLA) to cater with the process static non-linearity. Different optimization algorithms like GA, hybrid algorithm using GA and PSO, bee algorithm, improved harmony search, imperialistic competitive algorithm have been used for optimization of plate-fin heat exchangers [95]–[99]. The system parameters modelling in

continuous space using ant system algorithm was proposed by Lei et al. [100]. Neural network approach has been employed by Bittanti *et al.* in [101]. Sahoo *et al.* [89] utilized Pseudo Random Binary Signal (PRBS) as input to find 'Auto Regressive–Moving-Average model with eXogenous inputs' (ARMAX) model of the heat exchanger. The tubular heat exchanger has been represented by Hammerstein model and Nonlinear Auto Regressive with eXogeneous inputs (NARX) model in [102]. The least squares support vector machine-based algorithms have been employed for modelling. Gupta *et al.* [58] employed the prediction error estimation method to model the parameters of liquid-liquid heat exchanger system. Deng *et al.* [103] used improved PSO for system modelling which provided better results than Basic PSO and GA. Jing Yong Lv [104] estimated the parameters of an induction motor using modified artificial fish swarm algorithm. In [105], the authors estimated the forward and inverse dynamic behaviors of a magneto-rheological (MR) damper by applying Takagi–Sugeno (T–S) fuzzy model. Li *et al.* [63] used Simulated Annealing Optimization Algorithm for fractional system modelling of shell and tubular heat exchanger and it has been found that as compared to integer order counterpart , FO models represent the system more accurately. Wang *et al.* [106] proposed an online parameter estimation method for the fractional equivalent circuit model of lithium ion batteries.

Different nature inspired metaheuristic algorithms namely PSO, BAT, CuSA , FFA, CrSA , SA, and MFO have been employed for system modelling of various systems [103], [107]–[113]. These techniques have been opted for the FO mathematical modelling of liquid – liquid heat exchanger because these techniques are easy to implement with low computational complexity. Moreover, their performance for FO system modelling has not been explored yet.

3.2.1 Dynamics of Heat Exchanger

The dynamic equations for the fluid-fluid heat exchanger can be written as [114]

$$\frac{dT_{co}}{dt} = \frac{2}{M_c}\left[F_c(T_{ci} - T_{co}) + \left(\frac{UA\Delta T_{1m}}{C_{pc}}\right)\right] \tag{3.1}$$

$$\frac{dT_{po}}{dt} = \frac{2}{M_p}\left[F_p(T_{pi} - T_{po}) - \left(\frac{UA\Delta T_{1m}}{C_{pp}}\right)\right] \tag{3.2}$$

In the above equations, the log mean temperature difference is designated by ΔT_{1m}, and controlled variable outlet process fluid temperature is designated by T_{po}. The manipulated and disturbance variable are the heating fluid flow rate (F_c) and the process fluid flow rate (F_p) respectively. In the

model described in Eq. (3.1) and (3.2), when the fluid in the heat exchanger is liquid, the dynamics of the tube wall can be neglected. It is also assumed that the tube wall is having negligible heat capacity in comparison to hot fluid and cold fluid.

3.2.2 Model Structure and Performance Measures

The various parameters of model structure have to be estimated so as to obtain best fit using I/O data gathered from an experimental set-up. Choosing an optimum model structure is critical because system dynamics may not be expressed adequately with a lower order model; and model uncertainties may be added if a higher model order is chosen.

Here, two different fractional order model have been estimated by applying individual optimization algorithm and quality of both type of models has been quantified using multiple performance index. The system has been modelled as 'Fractional First Order Plus Time Delay' and 'Fractional Second Order Plus Time Delay' models given by Eq. (3.3) and (3.4).

$$G_{FFOPTD} = \frac{Ke^{-Ls}}{1 + T_1 s^{\beta_1}} \tag{3.3}$$

$$G_{FSOPTD} = \frac{(Ks^{\alpha} + 1)e^{-Ls}}{1 + T_1 s^{\beta_1} + T_2 s^{\beta_2}} \tag{3.4}$$

Here, K is system gain, L is the time delay, α and β are the fractional powers of the numerator and denominator respectively.

An index used to evaluate the superiority of estimated model is called goodness-of-fit (FIT). The root mean square error (RMSE) between estimated and actual output can also be considered as one of the measures of accuracy. These are calculated using Eq. (3.5) and (3.6).

$$FIT = 100\left(1 - \frac{\sqrt{\sum_{k=1}^{N}(O_a(k) - O_e(k))^2}}{\sqrt{\sum_{k=1}^{N}(O_a(k) - \overline{O_a}(k))^2}}\right) \tag{3.5}$$

$$RMSE = \left(\sqrt{\frac{\sum_{k=1}^{N}(O_a(k) - O_e(k))^2}{N}}\right) \tag{3.6}$$

Here, $O_a(k)$ is the measured output and $O_e(k)$ is the predicted output. The higher the goodness of-fit, more is the accuracy of estimation.

3.2.3 Modelling Procedure

The structure of the model has been assumed and the parameters of the model are estimated using the modelling procedure. Figure 3.1 depicts the block diagram representation of the modelling procedure for the LLHE. It utilizes the temporal input output dataset of heat exchanger and optimization algorithm with RMSE as fitness function to identify the model parameters. A pre-defined FO template of model has been embedded with the optimization algorithm. Number of unknown parameters in model template is considered as the order of the optimization problem. Here, various nature inspired optimization algorithms have been used to estimate the parameters of the model structure. The aim is to carry global search and utilize enhanced modelling capabilities of these algorithms to solve large problems in a faster way [110]. The algorithms such as PSO, BAT, CuSA, FFA, CrSA, SA, and MFO have been employed for system modelling. All of the above mentioned optimization algorithms follow a general structure to find the optimized solution of any given problem; though their governing equations differ.

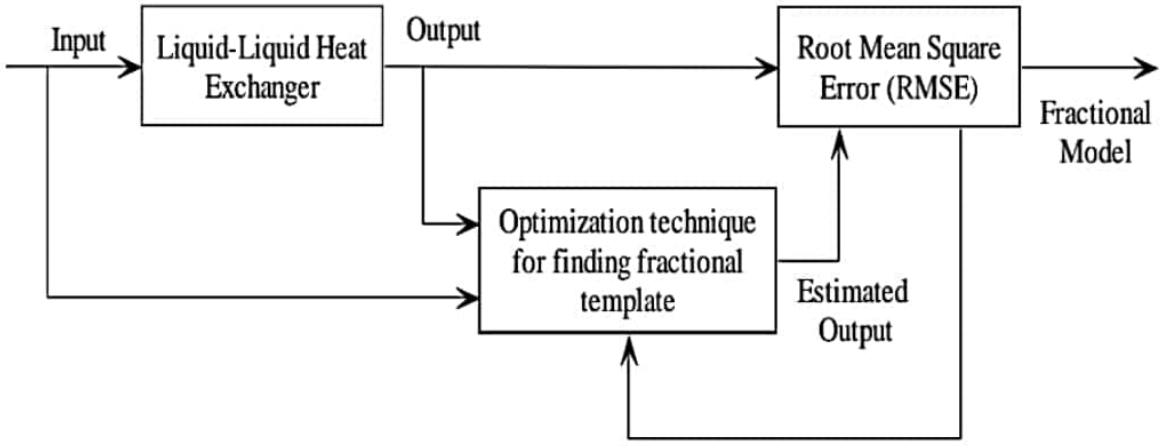

Figure 3.1 Modelling procedure for system modelling of liquid-liquid heat exchanger

Figure 3.2 shows the general steps involved in finding the optimum solution using nature inspired optimization algorithm. The optimization algorithm works iteratively. In each iteration, new model parameters are identified using global as well as local search agent information. Further, the fitness function (RMSE) is estimated for new model parameters. Depending upon the current iteration RMSE and previous best RMSE, the global and local best solution are assigned. The aforementioned steps are repeated for each iteration until the stopping criteria is not achieved.

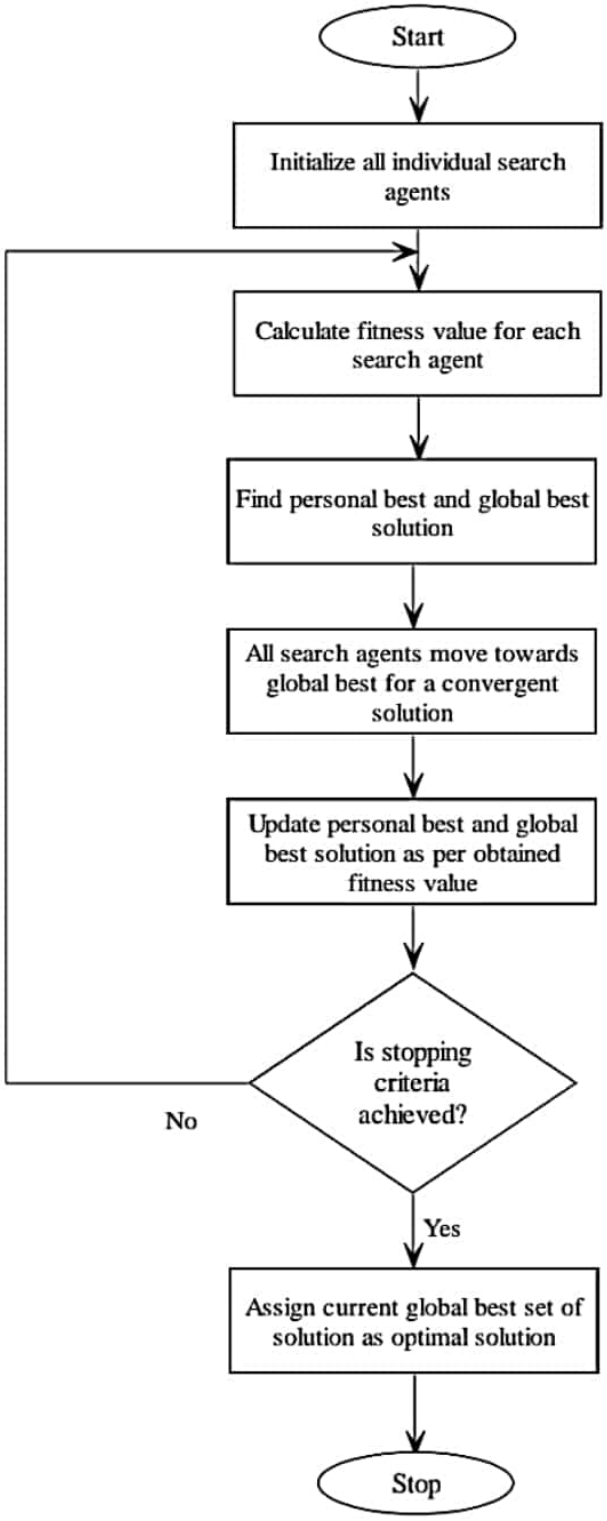

Figure 3.2 General steps in an optimization algorithm procedure

The optimization algorithms that have been used for the present work are descripted below.

i) Particle Swarm Optimization (PSO)

PSO is a nature influenced strategy dependent on the aggregate conduct in decentralized, self-composed swarm knowledge. A swarm is comprised of a populace of straightforward operators connecting locally with each other and furthermore with their condition. Neighbourhood cooperation of operators result to the rise of an ideal worldwide conduct. The PSO calculation comprises of only three stages: assessing the wellness of every molecule, refreshing individual and worldwide bests lastly, refreshing speed and location of every molecule. These means are rehashed as far as any halting condition is confronted. Each particle's velocity and position are updated according to Eq. (3.7) and (3.8) [115]:

$$v_i(n+1) = wv_i(n) + c_1r_1[p_i(n) - x_i(n)] + c_2r_2[g(n) - x_i(n)] \quad (3.7)$$

$$x_i(n+1) = x_i(n) + v_i(n+1) \quad (3.8)$$

where i, w, c_1 and c_2 represent the particle index, inertial coefficient, and the acceleration coefficients $(0 \leq c_1, c_2 \leq 2)$ respectively. r_1 and r_2 denote the random values $(0 \leq r_1, r_2 \leq 1)$ regenerated with each update of velocity.

$x_i(n), v_i(n), p_i(n)$ are particle's position, velocity, and individual best solution at n^{th} iteration and $g(n)$ represent the swarm's superlative solution at n^{th} iteration.

ii) BAT Algorithm

This calculation does the pursuit procedure utilizing counterfeit bats as search operators impersonating the common conduct of genuine bats. Bats as a rule use echolocation to discover nourishment. During nourishment search, each bat conveys short pulsations, in any case, when they experience nourishment, their pulsations convey rates increment and the recurrence goes up. The increment in recurrence implies recurrence tuning, which abbreviates the echolocations' time and boosts the position certainty.

A bat flies randomly at position x_i with a velocity v_i for a frequency interval $[f_{\min}, f_{\max}]$ fluctuating its emission level $r \in [0,1]$ and loudness A_0 to hunt for prey, relying on the proximity of their aim. Their frequency, velocity and position update in each iteration are given by eqns. (3.9)-(3.11) [116].

$$f_i = f_{min} + (f_{max} - f_{min})\varepsilon \quad (3.9)$$

$$v_i^{t+1} = v_i^t + (x_i^t - x^\dagger)f_i \quad (3.10)$$

$$x_i^{t+1} = x_i^t + v_i^{t+1} \quad (3.11)$$

where ε is a random number obtained from a uniform distribution, and the current paramount solution obtained so far during iterative procedure is represented by $x^\dagger$.

iii) Cuckoo Search Algorithm (CuSA)

Cuckoo search is a macrocosm-roused meta-heuristic calculation dependent on the offspring parasitism of a couple of cuckoo categories. The cuckoo search pursues three fundamental advances:

- Each cuckoo lays each egg in turn, and puts it in discretionary nominated native place;
- The culminating living places with top notch eggs will be extended to the following ages;
- The statics of manageable host native places is fixed, and the ovum lie down by a cuckoo is found by the owner feathered living being with a likelihood [0,1]

Each egg in a home serves as a competitor arrangement. The objective of CuSA is to produce the new and conceivably better arrangements that will supplant the more terrible arrangements in the present home populace. The nature of arrangements is assessed with the wellness capacity of the issue to be comprehended.

The position update is given by Eq. (3.12)

$$x_i^{t+1} = x_i^t + \alpha L(st, \lambda) \text{ where } L(st, \lambda) = \lambda\Gamma(\lambda)\frac{sin\left(\frac{\pi\lambda}{2}\right)}{\pi}\frac{1}{st^{1+\lambda}}, st >> st_0 > 0 \quad (3.12)$$

where $L(st, \lambda)$ denotes the characteristic scale and $\alpha > 0$ denotes a scaling factor of the step size.

iv) Firefly Algorithm (FFA)

The Firefly Algorithm relies upon the ideal conduct of the glaring characteristics of fireflies. In context on computation improvement, it watches these rules:

- One firefly is fascinated to various fireflies paying little personality to their sex.

- Attractiveness is proportionate to their illuminance, as such for any two gleaming fireflies; the less splendid one will move towards the more marvellous one. The intrigue is comparing to the quality and both of them decay as their separation increases.
- Brightness or light intensity of a firefly is resolved by the estimation of fitness ability to be enhanced or optimized.

Eq.(3.13) demonstrates the displacement of a firefly i attracted to another more attractive (brighter) firefly j [116].

$$x_i = x_i + \beta_0 e^{-\gamma r_{ij}^2}(x_j - x_i) + \alpha \in_i \tag{3.13}$$

where $r_{ij} = \|x_i - x_j\|_2$ denotes the separation between two fireflies i and j at x_i and x_j or the $l_2 - norm$, $\in_i$is the vector of random variables.

v) Crow Search Algorithm (CrSA)

CrSA relies upon the knowledgeable attitude of crows. CrSA is a commonality collect framework which endeavours to figure on this theory that crows reserve their abundant sustenance in veil places and recover it when the sustenance is required.

It is presumed that there is a d-dimensional condition including different crows. The amount of crows (crowd size) is N and the status of crow $i$at iteration $iter$ in the interest space is stated by a vector $x^{i,iter}(i = 1,2 \ldots N; iter = 1,2 \ldots\ldots iter_{max})$ where $x^{i,iter} = [x_1^{i,iter}, x_2^{i,iter} \ldots\ldots x_d^{i,iter}]$ and $iter_{max}$ represents utmost count of iterations. Each crow has a memory where-in the circumstance of its disguising spot is recollected. At iteration $iter$, the status of hiding spot of crow i is showed up by $m^{i,iter}$. This is the best status that crow i has procured till now. Undoubtedly, in memory of each crow, the status of its best experience has been held. Crows move around and explore for better sustenance sources. Consider that at cycle $iter$, crow j needs to visit its hiding spot, $m^{i,iter}$ and using Eq. (3.14) crow $i$seeks after crow j to approach to trail the veiling spot [111].

$$x^{i,iter+1} = x^{i,iter} + r_i \times fl^{i,iter} \times (m^{i,iter} - x^{i,iter}) \tag{3.14}$$

where, r_i is random number generated between 0 and 1 and flight dimension of crow i at iteration $iter$ is given by $fl^{i,iter}$.

vi) Simulated Annealing (SA)

The key belief of SA algorithm is to use arbitrary exploration in terms of a Markov chain, which reforms the objective function by acquiring favorable alternatives, but also preserving some alternations that are not classical sometimes. To minimize the objective function f in a particular problem, only those modifications are acknowledged that diminish the value of the objective function; however, some variations that enhance f will also be approved with a probability p. It is determined by Eq. (3.15) and (3.16) [117].

$$p = exp\left[\frac{-\Delta E}{k_B T}\right] \tag{3.15}$$

$$\Delta E = \gamma \Delta f \tag{3.16}$$

where k_B, T and ΔE are the Boltzmann's constant, temperature for controlling the annealing process and the change of the energy level, respectively and γ is a real constant.

Hence, using Eqns. (3.15) and (3.16) the probability p can be defined as in Eq. (3.17)

$$p(\Delta f, T) = e^{\frac{-\Delta f}{T}} \tag{3.17}$$

Usually, the move is accepted or rejected depending on a random number r which is used as a threshold. Thus, if calculated probability is greater than the random number, only then the move is allowed.

vii) Moth Fly Algorithm (MFO)

Moths are creepy crawlies; they have extraordinary development system at night. They fly around evening time by keeping a fixed point concerning the moon. This strategy is useful for roving in a straightforward path particularly when the luminous origin is at far off. At the point, when the luminous origin is close, moths glide spirally about it and in the long run unite toward it after only a couple of upgrades.

The moths are genuine pursuit specialists that act around the inquiry space, while flames are the prime state of moths that have been attained until now. Accordingly, flames can be investigated as banners that are expelled by moths when looking through the inquiry zone. Thusly, every moth enquires near the vicinity of the flame and amends itself in each iteration in order to find superior solution. As such, a moth always retain its best position. In this manner, the logarithmic spiral

function is picked as the fundamental mechanism for refreshing state of every moth with regard to the flame.

The updation of position of each moth with respect to a flame is given by Eq. (3.18) [118].

$$M_i = D_i e^{bt} cos(2\pi t) + F_j \tag{3.18}$$

where D_i represents the distance between i^{th}moth and j^{th}flame, the shape of logarithmic spiral is designated by a constant b, and t is a random number between [-1,1].

3.2.4 Results

Simulation results for the parametric modelling of LLHE system have been illustrated in the current section. Figure 3.3 represents the experimental data for the LLHE system [58]. The data set comprises of 5000 samples and the sampling frequency the data set is sampled at 600Hz. The input information/signal given to the system visually resembles a Pseudo Random Binary Sequence (PRBS) signal.

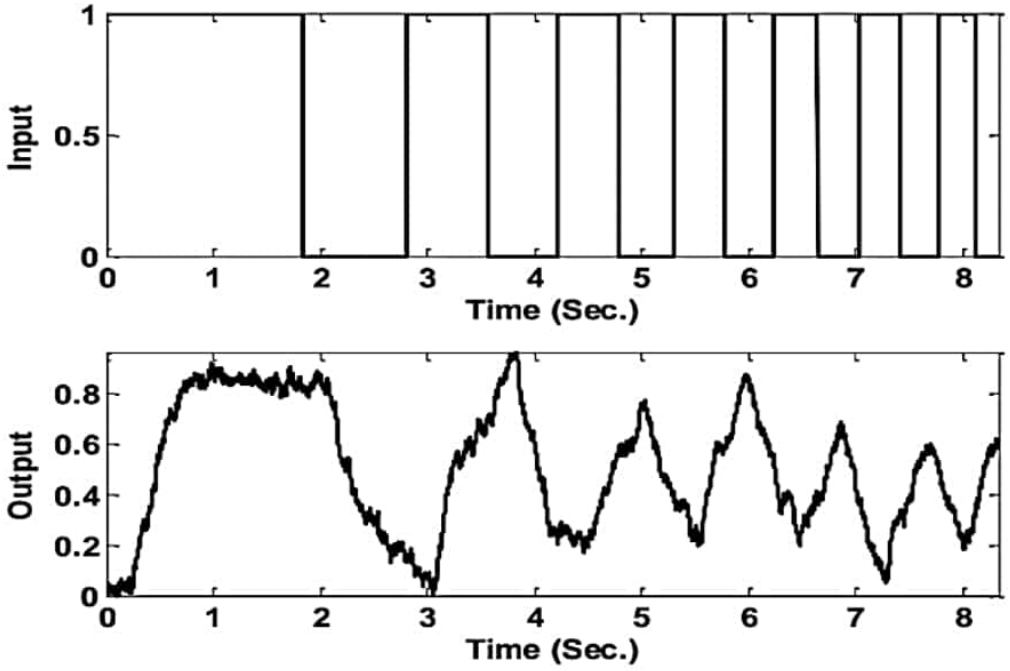

Figure 3.3 Experimental data for LLHE system [58]

Numerous nature inspired metaheuristic algorithms have been used with RMSE as a fitness function for modelling this system. The parameters have been estimated in fractional FOPTD and SOPTD templates. Table 3.1 and Table 3.2 show the estimated parameters for fractional FOPTD and SOPTD templates, respectively.

Now, to validate the results obtained, the same input has been applied to the estimated model (parameters shown in Table 3.1 & Table 3.2) and the output has been obtained. Figure 3.4 illustrates the actual output and estimated output using various optimization techniques for the fractional FOPTD and SOPTD systems.

Table 3.1 Estimated parameters for fractional FOPTD model

	K	T_1	β_1	L
PSO	-63.8073	-100	0.178449	0.371296
MFO	-57.8963	-90.8353	0.17826	0.370256
CuSA	0.902717	0.315962	1.013776	0.252484
BAT	12.28711	16.58494	0.150914	0.481767
SA	55.03104	84.5118	0.184502	0.368708
FFA	-61.8012	-65.8307	0.170421	0.303465
CrSA	-63.8073	-100	0.178449	0.370031

Table 3.2 Estimated parameters for fractional SOPTD model

	K	T_1	β_1	T_2	β_2	α	L
PSO	-100	-100	2	-42.0114	1.204402	1.532714	0.312994
MFO	-90.369	-100	0	-31.2803	1.013776	0	0.252667
CuSA	-63.4063	-74.1992	0.887758	-19.2888	1.957302	0.858482	0.243758
BAT	-46.5289	1.569929	1.698533	-99.7133	1.544645	1.232855	0.511603
SA	248.8798	78.26868	1.26947	289.5022	0.206561	0.182967	0.243359
FFA	-91.3667	-83.6367	0.386877	-43.1538	1.281736	0.444614	0.274962
CrSA	-86.7643	-28.0175	1.225951	-98.922	0.17642	0.162094	0.247956

The output has been first estimated for fractional FOPTD model and it has been observed that the Cuckoo Search Algorithm shows the best fit out of all the other optimization algorithms. Next, the output has been estimated for fractional SOPTD model. Here, BAT Algorithm has been seen to give the least fit to the actual data, whereas all the other optimization algorithms have been seen to respond very well and the estimated data for the fractional SOPTD identified system fit the

actual data for the heat exchanger system very well. Overall, it can be said that the fractional SOPTD model seems to better fit the actual output in comparison to the fractional FOPTD model.

Figure 3.5 and Figure 3.6 show the step response of the identified fractional FOPTD and SOPTD systems for the LLHE system. The step responses of identified models are inline with the performance of respective optimization algorithms (Table 3.3 and Table 3.4). It has been observed from step response that for FOPTD template, only CuSA algorithm provides satisfactory (stable) response as compared to other algorithms. However, for SOPTD template, BAT and PSO algorithm fails to provide satisfactory response as compared to other algorithms. So, it has been concluded that for input-output dataset of liquid-liquid heat exchanger, SOPTD template has proved to be more suitable than FOPTD models for FO modelling of the system using considered optimization techniques.

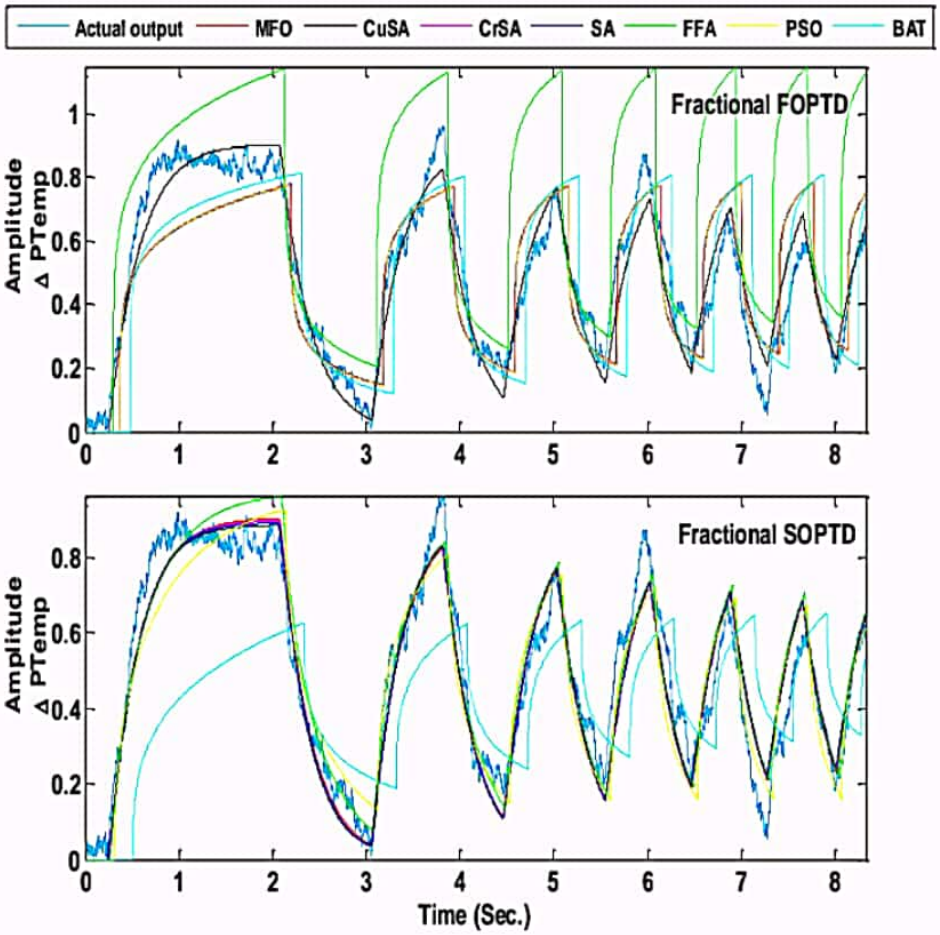

Figure 3.4 Results of system modelling of heat exchanger in fractional first order and second order model

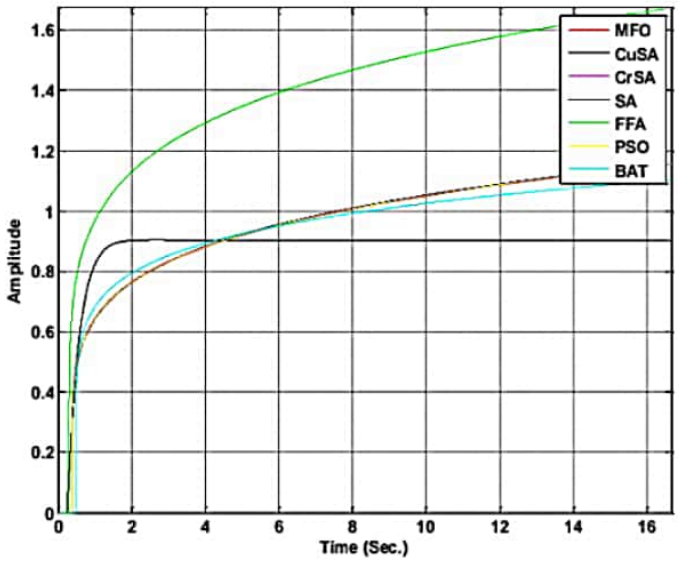

Figure 3.5 Step response of identified fractional FOPTD models

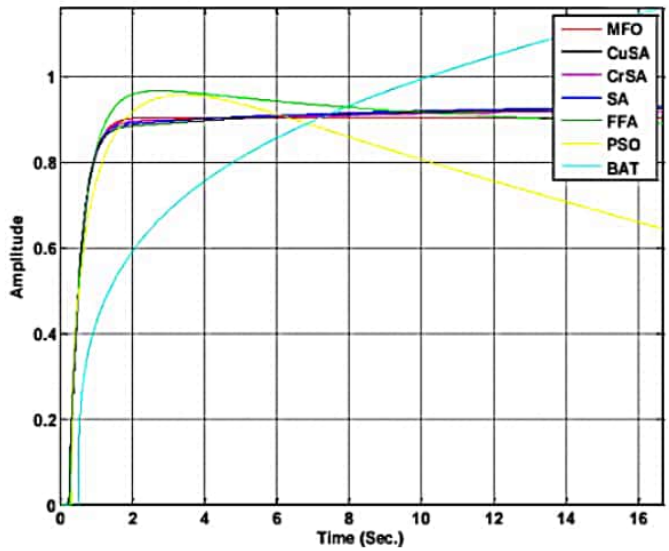

Figure 3.6 Step response of identified fractional SOPTD models

3.2.5 Comparative Performance Analysis

Next, the performance of the optimization algorithms used for FO modelling has been analyzed quantitatively. Table 3.3 presents the quantitative results of model validation of the obtained fractional models using performance indices (RMSE and % FIT). Out of all the considered optimization algorithms, Cuckoo search Algorithm provides the best performance (0.0056 RMSE and 70.368 % FIT) when fractional FOPTD model is considered. Whereas, it can be seen that the Firefly Algorithm does not provide the satisfactory performance (0.094 RMSE and -21.61% FIT)

i.e. this algorithm is not at all able to fit the actual data for identifying the system in fractional FOPTD model. It has also been observed that only the BAT algorithm is not able to give good results (0.0528 RMSE and 9.11 %FIT) when fractional SOPTD template is considered. All the other algorithms considered for modelling of SOPTD template have been seen to provide a good fit to the actual output.

Table 3.3 Model validation of the obtained fractional models using performance indices

	Fractional FOPTD		Fractional SOPTD	
Algorithms	RMSE	% FIT	RMSE	% FIT
PSO	0.01797217	47.013186	0.0079535	64.7509074
MFO	0.01797670	47.006508	0.0056203	70.3687551
CuSA	0.00562036	70.368755	0.0055706	70.5000455
BAT	0.03017223	31.345147	0.0528718	9.11764077
SA	0.01787527	47.156221	0.0055798	70.4756704
FFA	0.09467582	-21.61497	0.0065687	67.9661944
CrSA	0.01797217	47.013186	0.0055861	70.4590630

Table 3.4 shows the performance of different optimization algorithms on the basis of fitness, computation cost and algorithm run time. The number of times the fitness function is evaluated is precisely associated to the computational cost of algorithm.

Table 3.4 Performance of various optimization algorithms

Fractional FOPTD				
Optimization Algorithms	Fitness Max	Fitness Min	No. of Evaluation	Run Time (seconds)
PSO	0.0708	0.017972172	34	643.91
MFO	0.0643	0.017976703	38	720.68
CuSA	0.0541	0.005620368	516	19701.64
BAT	0.0427	0.030172233	16962	2971.75
SA	67.0161	0.017875274	14211	2795.17
FFA	0.125	0.094675824	44	844.74
CrSA	0.0673	0.017972172	66	259.27

Fractional SOPTD				
Optimization Algorithms	Fitness Max	Fitness Min	No. of Evaluation	Run Time (seconds)
PSO	0.027	0.007953547	141	3009.24
MFO	0.752	0.005620368	38	810.12
CuSA	0.0265	0.005570673	676	29042.71
BAT	0.0647	0.052871808	23171	5264.96
SA	981000	0.005579883	49623	12761.00
FFA	0.1289	0.00656874	426	9254.62
CrSA	0.1169	0.005586162	485	2092.90

It can be observed from Table 3.4 that PSO, FFA and MFO algorithms reach their convergence in very less number of iterations for fractional FOPTD template but do not provide satisfactory performance in terms of achieving minimum fitness. Also, from fractional SOPTD models, it can be seen that MFO, SA, CrSA and CuSA algorithm provide minimum fitness but MFO algorithm is able to converge to the global optimal solution in minimum number of iterations.

Thus, from the comparative analysis carried above for the FO system modelling of the LLHE using various optimization techniques, it has been monitored that the fractional second order template provides a better fit to the actual output than the fractional first order template. Out of the chosen optimization algorithms, all the algorithms except the BAT algorithm are able to estimate the parameters of the identified fractional SOPTD model. Therefore, it has been proved that the optimization algorithms can be used as an efficient tool in FO system modelling.

Summary:

This chapter explored optimization techniques as a tool for FO system modelling of a LLHE system. The results present a quantitative comparison of performance of seven well-known nature inspired optimization algorithms for FO modelling of liquid - liquid heat exchanger system by using its input output dataset. It can be concluded from encouraging results obtained from optimization algorithms that it can be useful and efficient tool for system modelling using input output dataset.

CHAPTER 4

MODEL ORDER REDUCTION

4.1 Introduction to Model Order Reduction

Most of the engineering applications are determined by mathematical models. The most crucial and vital step for analysis of any dynamical system and its control is mathematical modelling. The differential equations developed from the physical laws depict the mathematical model. Most of the physical processes result in high dimensional models. It is very important to estimate the lower order model that approximate the higher order model with highest possible accuracy. Therefore, this area of control theory deals with the study of properties of high dimensional system for reducing their complexity, while retaining the significant (weighty) characteristics of the original system. It becomes easy to interpret the physical attributes of this lower order system model than the complex system. Moreover, the controller design for these lower order systems is much easier than the corresponding higher order systems.

The classical model reduction methods in frequency domain use the theory of mathematical approximation. In Pade approximation method, the initial coefficients of Laurent series expansion on the basis of frequency responses of original and reduced model are matched to find the parameters of reduced model [119] . The idea of Pade approximation has been extended from single point to multiple points ($s = 0$ and about points along the imaginary axis $s = jw$) [120], [121]. These multiple points can even be the mixture of real, complex and purely imaginary points [122], [123]. Many authors have used the idea of time moment matching technique or a hybrid of Markov parameters and time moment; clustering and time moment; Big Bang Crunch Optimization with time moment [124]–[127]. Another interesting polynomial approximation method used in order reduction doesn't use any eigen values or vectors and contain most of the useful information in first few terms. This is continued fraction expansion or Cauer form [128]. Routh Hurwitz method has been utilized by many authors [129]–[132]. In [129]–[131], the applicability of this method to discrete time systems has been illustrated. In [132], the technique has been used for linear multivariable systems. Even, the Routh approximation techniques have been put forth in model reduction of the interval systems [133], [134]. All these methods like

continued fraction, Pade approximation, modified Cauer continued fraction have been combined with differentiation method [135], [136] and extended to multivariable and interval systems [137]–[139]. Another important method called stability equation method has also been combined with Pade approximation, continued fraction expansion, error minimization etc. [140]–[142]. Stability equation method has also been combined with optimization techniques like big-bang crunch, GA, PSO, Fire-fly etc. for reduction of higher order systems [143]–[146].

Sinha *et al.* [147] proposed another mathematically simple method called clustering approach. This technique preserves the stability in the reduced model if the original higher order system (HOS) is stable. This technique is even applicable to unstable systems. In [148], the clustering based reduction approach has been utilized to design a 2 DOF controller for LFC. Another class of model reduction includes evolutionary algorithms such as PSO, GA, Big-bang crunch, Harmony search, DE etc. to find the reduced model by minimization of cost function which may be ISE, IAE, ITAE etc. [149]–[153].

The state space original models have been utilized in time domain methods for model reduction to derive a model with less state variables. This requires the information of eigen values or vectors of original higher order system. The basic idea in reducing the model order is to retain the large time-constant in the reduced order model (ROM) and discard the lower one. The first reduction approach, i.e. modal analysis using state space model was given by Davison [154]. In [155], a mixed method utilizing dominant eigen value and integral square criteria method has been suggested for reduced order modeling. Many error minimization methods also used the notion of dominant pole retention [156], [157]. In these methods, the dominance in the pole is considered by taking the poles nearest to *jw* axis, i.e. with large time constant. In optimization based techniques for MOR, the error function between the response of original model and ROM is optimally minimized, with no constraint on location of eigen values [153].

Testing the stability and designing the controller are the two most significant constituents for scheming an efficient control system and to have an exact model that nearly delineates the real time dynamic performance of the plant is critical.

Even though, several controller design methods are demonstrated in the recent research works. But, the design of the controller involving the MOR techniques don't work equally good in most

of the control design techniques. If the controller is designed utilizing the concept of MOR, it is essential that it should work satisfactorily on its corresponding higher order original system. The parametric unpredictability and external perturbation are the most crucial things that the controller is required to handle in almost all real time intricate systems. The control methods framed for original higher order system are mathematically very complex; however, if the order of the system is reduced, similar performance can be achieved through simpler mathematical procedures. Moreover, it is important that the controller designed should be able to tackle the disturbances, track the set point, stabilize the higher order complex systems and at the same time should be computationally simple.

Many more methods have been reported in literature such as Balanced truncation, krylov method, singular value decomposition, modal analysis, Hankel norm approximation etc. [158]. The balanced truncation method is a well-known and simple method suggested by Moore [159] as it maintains the important modes of the original system. The high frequency modes contribute very less to the system dynamics and are therefore, truncated. The method is based on determining a coordinate system for a reduced order state space model in a manner that the observability and controllability gramians for HOS are diagonal and equal. These Gramians are solutions of dual Lyapunov equations. This method is able to preserve the stability in the ROM. Balanced Truncation has been applied in [160] to heat conduction distribution and wind farms linearized model [161]. The method is applicable to unstable systems, as well [12], [158], [162], [163]. Therefore, this technique has been considered for reduction of unstable PHWR system.

Through this technique, an attempt has been made to obtain ROM for the PHWR system. The MOR approach has been used for the ease of controller synthesis for the higher order system. This approach involves modelling of PHWR as a model of third order and second order respectively. In Chapter 5, these reduced order models are used to design an FOPID controller for the Reactor Regulating System of the PHWR. The controller design has been carried out using the Stability Boundary locus with specific gain-phase margin [164].

4.2 Balanced Truncation Method

This section presents a descriptive idea of the MOR technique used to reduce the order of higher order PHWR.

Consider the transfer function matrix $G(s) = C(sI - A)^{-1}B + D$ and the associated standard realization of a linear time invariant (LTI) dynamical system as [12]:

$$\begin{aligned} \dot{x}(t) &= Ax(t) + Bu(t) \\ y(t) &= Cx(t) + Du(t) \end{aligned} \tag{4.1}$$

Here, $x \in R^n, u \in R^m, y \in R^r$ represent the states, inputs and outputs of the system, respectively. Also, it is assumed that (A, B) is stabilizable and (C, A) is detectable. The MOR using balanced truncation is done by following steps:

Step 1: Decompose the transfer function matrix $G(s)$ additively as

$$G(s) = G_S(s) + G_U(s) \tag{4.2}$$

where $G_s(s)$ is the stable part and $G_U(s)$ is the unstable part of the transfer function.

Step 2: Find a reduced-order model $G_{RS}(s)$ of the stable part $G_S(s)$

Convert the transfer function of the stable part of the original model ($G_S(s)$) to state space form as A_S, B_S, C_S, D_S.Compute the controllability and observability Gramians, C_G and O_G by solving, respectively, the Lyapunov equations [12]:

$$\begin{aligned} A_S C_G + C_G {A_s}^T &= -B_S {B_s}^T \\ {A_S}^T O_G + O_G A_S &= -{C_s}^T C_S \end{aligned} \tag{4.3}$$

The Lyapunov equations have unique solutions if and only if $\lambda(A_S) + \lambda(\overline{A_S}) \neq 0$

Find the Cholesky factors L_C and $L_O$of $C_G$and $O_G$respectively, such that:

$$C_G = L_C L_C^T, O_G = L_O L_O^T \tag{4.4}$$

Find the singular value decomposition (SVD) of the matrix$L_O^T L_C$, such that

$$L_O^T L_C = U \sum V^T \tag{4.5}$$

Compute,

$$\sum^{-1/2} = diag\left(\frac{1}{\sqrt{\sigma_1}}, \frac{1}{\sqrt{\sigma_2}}, \ldots\ldots, \frac{1}{\sqrt{\sigma_n}}\right) \tag{4.6}$$

where $\sum = diag(\sigma_1, \sigma_2, \ldots\ldots \sigma_n)$. The decreasing positive numbers $\sigma_1 \geq \sigma_2 \geq \ldots\ldots \geq \sigma_n$ in $\sum = diag(\sigma_1, \sigma_2, \ldots\ldots \sigma_n)$ are the Hankel singular values (HSV)

Then, form the transformation matrix

$$T = L_C V \sum^{-1/2} \tag{4.7}$$

Compute the matrices of the balanced realization:

$$\begin{aligned}\tilde{A} &= T^{-1}A_S T \\ \tilde{B} &= T^{-1}B_S \\ \tilde{C} &= C_S T\end{aligned} \tag{4.8}$$

Here transformation matrix T is such that the transformed controllability Grammians are diagonalized and equal to each other, i.e. $C_G = O_G = \sum = diag(\sigma_1, \sigma_2, \ldots \ldots \sigma_n)$ [165]. The reduced order model is obtained by truncating the states corresponding to the smaller HSVs. Partition the balanced realization in the form

$$\tilde{A} = \begin{pmatrix} A_R & A_{12} \\ A_{21} & A_{22} \end{pmatrix}, \tilde{B} = \begin{pmatrix} B_R \\ B_2 \end{pmatrix}, \tilde{C} = \begin{pmatrix} C_R & C_2 \end{pmatrix} \tag{4.9}$$

Where A_R is of order q (reduced order) and B_R and C_R are similarly defined. Now, find the reduced order model $G_{RS}(s)$ of the stable part as

$$G_{RS}(s) = C_R(sI - A_R)^{-1}B_R \tag{4.10}$$

Step 3: The reduced–order model $G_R(s)$ of $G(s)$ is then given by

$$G_R(s) = G_{RS}(s) + G_U(s) \tag{4.11}$$

4.3 Reduced Order Modelling for PHWR System

The PHWRs are an extremely vital part of the present-day power generation industry. The reactor power in Indian PHWR is controlled by the three components in reactor regulating system (RRS) viz. control rods (CR), adjust rods (AR), and zone control compartments (ZCC). The fast startup of reactor is dealt by ARs. Coarse control is provided by CRs and fine control of power load is provided by ZCCs. The parameters of this highly nonlinear system fluctuate with time as a function of initial power of reactor and control drop level [166]. This is usually required that there is a rapid drop of the bulk power in a nuclear reactor under load following operations or some unusual operating situations. For the diminution of global power in the Indian PHWRs, the control rods are pushed in to a pre-specified level inside the reactor and simultaneously the set point of the stipulated power is gradually decreased. This operation is known as step-back [167] which is governed by RRS. In RRS with passive step-back, proportional controllers are very commonly used for controlling the reactor power. However, this technique results in a power undershoot and also slow performance which is not desirable. Also, a low power undershoot may poison out the

PHWR due to thermal neutron flux reduction [168]. Therefore, it is very significant to have an effective and robust control algorithm to regulate the step back mechanism in a PHWR.

In [169], a 72-order model of 540 MWe PHWR has been reduced to 26^{th} reduced order model by aggregation method and a spatial controller has been designed using periodic output feedback. Kakhki *et al.* [18] designed a fractional order IMC (FOIMC) controller by applying a reduction technique to approximate the complex FO models. To obtain the reduced model of the original FO model, the effects of the dominant dynamics and also the low order coefficients of numerator and denominator of a FO transfer function have been taken.

The FOPTD and SOPTD systems can be used to approximate higher order systems in most of the process control areas. But, approximating very high order processes like PHWR with these techniques may introduce error while modelling which leads to inadequate controller design [170]. Das *et al.* [171] carried out the reduction of the identified models of PHWR into FOPTD and SOPTD models and designed an LQR based tuner augmented with a FO phase shaper. A Nyquist-based MOR technique using a genetic algorithm for modelling in FOPTD and SOPTD templates has been proposed by Das *et al.* [172] which performs better than the existing H2-norm-based model reduction technique. Further, an objective function composed of the error index and controller effort has been minimized and GA has been used to tune PID and FOPID controllers. In [173], Characteristic Ratio Assignment (CRA) method has been utilized for design of PID controller design using reduced FOPTD model of the corresponding system. In [174], new FO templates called Non-Integer Order Plus Time Delay (NIOPTD-I and NIOPTD-II) for reduced parameter modelling of higher order processes have been introduced which guarantee low modelling errors than the integer FOPTD and SOPTD reduced order models. Two controller design methodologies have been employed. Frequency domain based specifications are used for tuning the FOPID controller. Also, the time domain based method minimizes a suitable time domain integral performance index and searches for an optimal set of controller parameters. The MOR in NIOPTD templates have proved to be efficient [168], allowing robust tuning of controllers and assured accuracy. However, the dominant dynamics of the original system of higher order can be retained by using NIOPTD templates as they allow the reduced model to attain any random fractional values. Bongulwar *et al.* [175] utilized NIOPTD-I plant of PHWR to fulfill the design descriptions such as phase margin and gain crossover frequency with the help of an FOPID

controller. In this case, no undershoot is observed and the performance is robust over a large span of frequencies.

The identified models of PHWR systems have been taken from [167] and are shown in Table 4.1. Here, the input is the position of the control rod and the output of the PHWR is the percentage of the actual power that is produced. Table 4.1 shows the PHWR models for 30% rod drop case, having 100%, 90%, 80% and 70% initial levels of power, respectively [167].

Table 4.1 Transfer function models of the PHWR plant at different power levels

Identified model		Transfer Function
G_1	P_{100}^{30}	$\frac{(44.79s^5 + 8408s^4 + 7.687 \times 10^4 s^3 + 8.42 \times 10^6 s^2 - 2.561 \times 10^7 s + 1.336 \times 10^7)}{(s^6 + 12.31s^5 + 1088s^4 + 6624s^3 + 5.75 \times 10^4 s^2 + 7.683 \times 10^5 s + 6.946 \times 10^4)}$
G_2	P_{90}^{30}	$\frac{(-81.59s^5 + 8625s^4 - 2.028 \times 10^4 s^3 + 9.119 \times 10^6 s^2 - 2.544 \times 10^7 s + 1.682 \times 10^7)}{(s^6 + 17.41s^5 + 1129s^4 + 9406s^3 + 5.397 \times 10^4 s^2 + 9.21 \times 10^5 s + 9.474 \times 10^4)}$
G_3	P_{80}^{30}	$\frac{(22.75s^5 + 9232s^4 + 6.87 \times 10^4 s^3 + 7.943 \times 10^6 s^2 - 2.047 \times 10^7 s + 1.4 \times 10^7)}{(s^6 + 14.49s^5 + 1101s^4 + 7680s^3 + 5.278 \times 10^4 s^2 + 8.547 \times 10^5 s + 8.839 \times 10^4)}$
G_4	P_{70}^{30}	$\frac{(-61.92s^5 + 9106s^4 - 1.907 \times 10^4 s^3 + 7.272 \times 10^6 s^2 - 2.017 \times 10^7 s + 1.215 \times 10^7)}{(s^6 + 15.31s^5 + 1105s^4 + 8861s^3 + 5.144 \times 10^4 s^2 + 9.169 \times 10^5 s + 8.911 \times 10^4)}$

Using the MOR technique described in the above section, each higher order transfer function is reduced to second and third order transfer functions. Consider the first transfer function G_1 corresponding to operating condition P_{100}^{30}.

$$G_1(s) = \frac{(44.79s^5 + 8408s^4 + 7.687 \times 10^4 s^3 + 8.42 \times 10^6 s^2 - 2.561 \times 10^7 s + 1.336 \times 10^7)}{(s^6 + 12.31s^5 + 1088s^4 + 6624s^3 + 5.75 \times 10^4 s^2 + 7.683 \times 10^5 s + 6.946 \times 10^4)} \quad (4.12)$$

The transfer function matrix $G_1(s)$ has been decomposed into stable and unstable parts and written as

$$G_1(s) = G_{1S}(s) + G_{1U}(s) \quad (4.13)$$

where $G_{1S}(s)$ is the stable part and $G_{1U}(s)$ is the unstable part of $G_1(s)$. Here,

$$G_{1S}(s) = \frac{-493.5s^3 - 3741s^2 - 4.946e^5 s + 1.407e^5}{s^4 + 15.93s^3 + 1061s^2 + 9122s + 821.5} \quad (4.14)$$

$$G_{1U}(s) = \frac{538.3s + 1785}{s^2 - 3.623s + 84.56} \quad (4.15)$$

Convert the transfer function $G_{1S}(s)$ into state space form. The corresponding matrices are given as:

$$A_{1S} = \begin{bmatrix} -15.93 & -1061 & -9122 & -821.5 \\ 1 & 0 & 0 & 0 \\ 0 & 1 & 0 & 0 \\ 0 & 0 & 1 & 0 \end{bmatrix}$$
$$B_{1S} = [1 \quad 0 \quad 0 \quad 0]^T$$
$$C_{1S} = [-493.5 \quad -3741 \quad -4.946e+05 \quad 1.407e+05] \tag{4.16}$$
$$D_{1S} = [0]$$

Finding the controllability and observability Gramians C_G and O_G

$$C_{1G} = \begin{bmatrix} 0.068298 & 3.2526e\text{-}19 & -6.4459e\text{-}05 & -1.5882e\text{-}21 \\ 3.2526e\text{-}19 & 6.4459e\text{-}05 & -2.647e\text{-}23 & -1.1257e\text{-}07 \\ -6.4459e\text{-}05 & -2.647e\text{-}23 & 1.1257e\text{-}07 & 3.1019e\text{-}24 \\ -1.5882e\text{-}21 & -1.1257e\text{-}07 & 3.1019e\text{-}24 & 6.6919e\text{-}08 \end{bmatrix}$$
$$O_{1G} = \begin{bmatrix} 15049 & 1.1796e+05 & 1.4879e+07 & 1.2049e+07 \\ 1.1796e+05 & 1.1214e+06 & 1.1816e+08 & 2.7374e+08 \\ 1.4879e+07 & 1.1816e+08 & 1.4738e+10 & 1.3407e+10 \\ 1.2049e+07 & 2.7374e+08 & 1.3407e+10 & 1.9172e+11 \end{bmatrix} \tag{4.17}$$

The Cholesky factors L_C and L_O of C_G and O_G are given by equation (4.18)

$$L_{1c} = \begin{bmatrix} 0.26134 & 0 & 0 & 0 \\ 1.2446e-18 & 0.0080286 & 0 & 0 \\ -0.00024665 & 3.4938e-20 & 0.00022744 & 0 \\ -6.0771e-21 & -1.4021e-05 & 9.2017e-21 & 0.00025831 \end{bmatrix}$$
$$L_{1o} = \begin{bmatrix} 122.67 & 0 & 0 & 0 \\ 961.57 & 443.63 & 0 & 0 \\ 1.2128e+05 & 3459.1 & 4024.5 & 0 \\ 98219 & 4.0415e+05 & 24045 & 1.3475e+05 \end{bmatrix} \tag{4.18}$$

Find the singular value decomposition (SVD) of the matrix $L_O^T L_C$

$$U_1 = \begin{bmatrix} 0.23861 & -0.97063 & 0.0067606 & 0.029984 \\ 0.91978 & 0.22162 & 0.25277 & -0.20247 \\ 0.055261 & -0.012458 & -0.73308 & -0.67778 \\ 0.30661 & 0.092793 & -0.63139 & 0.7062 \end{bmatrix}$$

$$\Sigma_1 = \begin{bmatrix} 113.33 & 0 & 0 & 0 \\ 0 & 27.609 & 0 & 0 \\ 0 & 0 & 1.1242 & 0 \\ 0 & 0 & 0 & 1.0342 \end{bmatrix}$$

$$V_1 = \begin{bmatrix} -0.0028917 & -0.081816 & 0.46835 & 0.87974 \\ -0.0090026 & -0.24609 & 0.84583 & -0.47321 \\ 0.06491 & -0.96391 & -0.2541 & 0.045846 \\ 0.99785 & 0.060245 & 0.025518 & -0.0047021 \end{bmatrix} \quad (4.19)$$

Next,

$$\sum_1{}^{-1/2} = \begin{pmatrix} 0.0939 & 0 & 0 & 0 \\ 0 & 0.1903 & 0 & 0 \\ 0 & 0 & 0.9456 & 0 \\ 0 & 0 & 0 & 0.9862 \end{pmatrix} \quad (4.20)$$

The transformation matrix is given by Eq. (4.21)

$$T_1 = \begin{bmatrix} -7.0987e\text{-}05 & -0.0040693 & 0.11544 & 0.22608 \\ -6.7893e\text{-}06 & -0.00037602 & 0.0064047 & -0.0037358 \\ 1.4538e\text{-}06 & -3.7884e\text{-}05 & -0.00016345 & -0.00020311 \\ 2.4223e\text{-}05 & 3.6183e\text{-}06 & -4.9681e\text{-}06 & 5.3296e\text{-}06 \end{bmatrix} \quad (4.21)$$

Compute the matrices of the balanced realization

$$\tilde{A}_1 = \begin{bmatrix} -0.033354 & -0.72684 & 0.019166 & -0.086955 \\ 0.72684 & -9.3001 & 0.61689 & -3.0843 \\ -0.019166 & 0.61689 & -0.2721 & 31.428 \\ -0.086955 & 3.0843 & -31.428 & -6.3244 \end{bmatrix}$$

$$\tilde{B}_1 = \begin{bmatrix} 2.7496 \\ -22.661 \\ 0.78218 \\ 3.6169 \end{bmatrix} \quad (4.22)$$

$$\tilde{C}_1 = [2.7496 \quad 22.661 \quad -0.78218 \quad 3.6169]$$

The reduced order model has been obtained by truncating the states corresponding to the smaller Hankel Singular Values (HSVs). The dominant states are the states of the system having high energy content. This can be judged by calculating the HSVs corresponding to each state. The higher hankel singular value denotes higher energy state and hence higher dominance. Figure 4.1 shows the quantifiable measurement of the energies of different states.

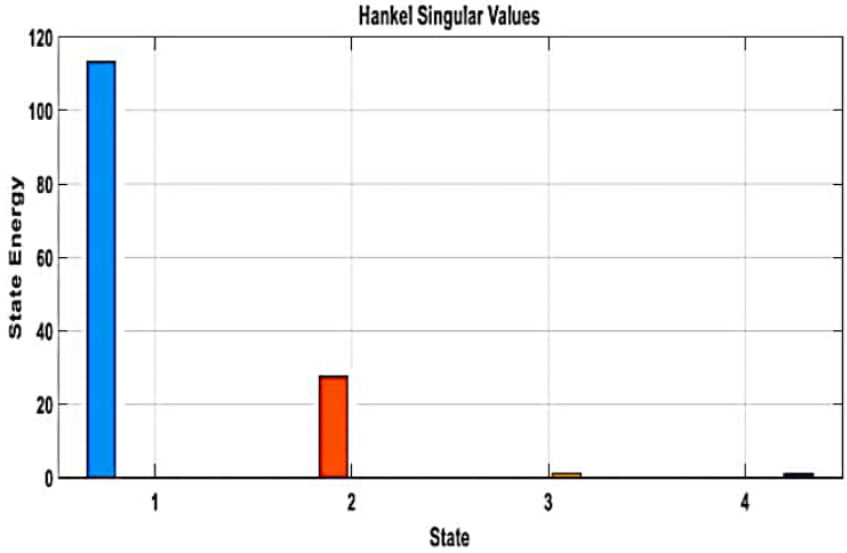

Figure 4.1 Hankel Singular Values

Only one state out of the four stable states (third order reduction; two unstable states being retained) has to be retained with most dominant state (highest HSV) of the system. Therefore, the reduced order matrices become

$$\begin{aligned} A_{1R} &= [\text{-}0.033354] \\ B_{1R} &= [2.7496] \\ C_{1R} &= [2.7496] \end{aligned} \tag{4.23}$$

The corresponding reduced order transfer function is given by Eq. (4.24)

$$G_{1RS}(s) = \frac{7.558}{s + 0.03335} \tag{4.24}$$

Substituting the values of $G_{1U}(s)$ from Eq. (4.15) and $G_{1RS}(s)$ from Eq. (4.24), the reduced–order model $G_{R1}(s)$ of $G_1(s)$ is obtained as in Eq. (4.25).

$$G_{R1}(s) = \frac{545.8s^2 + 1775s + 698.6}{s^3 - 3.59s^2 + 84.43s + 2.82} \tag{4.25}$$

Table 4.2 shows the second and third order reduced order models for P_{100}^{30}. Here, $G_{13}(s)$ represents the third order model corresponding to $G_1(s)$ and $G_{12}(s)$ represents the second order model corresponding to $G_1(s)$.The open loop poles of the original and corresponding reduced models are shown in Table 4.3. From Table 4.3, it has been observed that the original P_{100}^{30} model has two positive poles i.e. the system is unstable. When the system is reduced to 3rd and 2nd order models using the balanced truncation method, then the unstable poles have been retained as such.

Therefore, the instability of the system has been preserved in the reduced order models also. This can also be visualized from the step responses of original and corresponding reduced order models shown in Figures 4.2-4.5.

Table 4.2 Reduced order models of P_{100}^{30}

Third Order Reduced Model	Second Order Reduced Model
$G_{13}(s) = \frac{545.8s^2 + 1775s + 698.6}{s^3 - 3.59s^2 + 84.43s + 2.82}$	$G_{12}(s) = \frac{538.3s + 1785}{s^2 - 3.623s + 84.56}$

Table 4.3 Poles of different transfer function of P_{100}^{30}

Original Poles	Poles of reduced order Model: 3rd Order	Poles of reduced order Model: 2nd Order
-3.4006+31.411i -3.4006-31.411i -9.041+0i 1.8116+9.0152i 1.8116-9.0152i -0.091021+0i	1.8116+9.0152i 1.8116-9.0152i -0.033348+0i	1.8116+9.0152i 1.8116-9.0152i

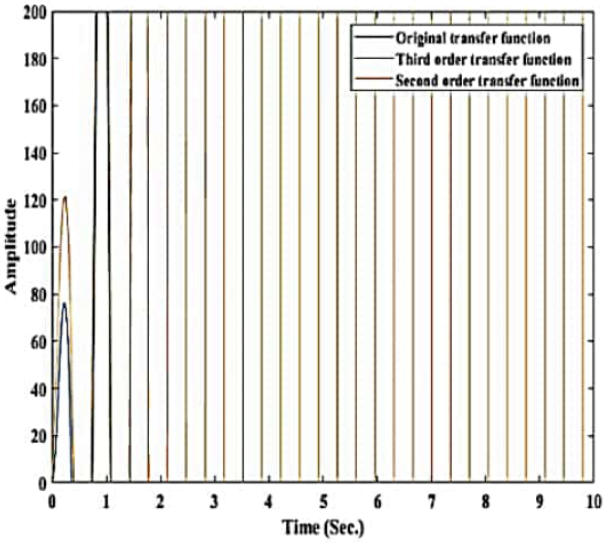

(a) Step responses of original and reduced P_{100}^{30} models

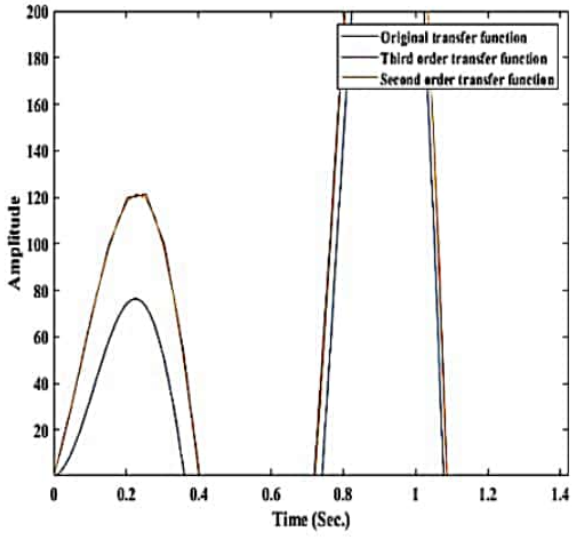

(b) Expanded view of step responses of original and reduced P_{100}^{30} models

Figure 4.2 Step response and expended view of original and reduced P_{100}^{30} models

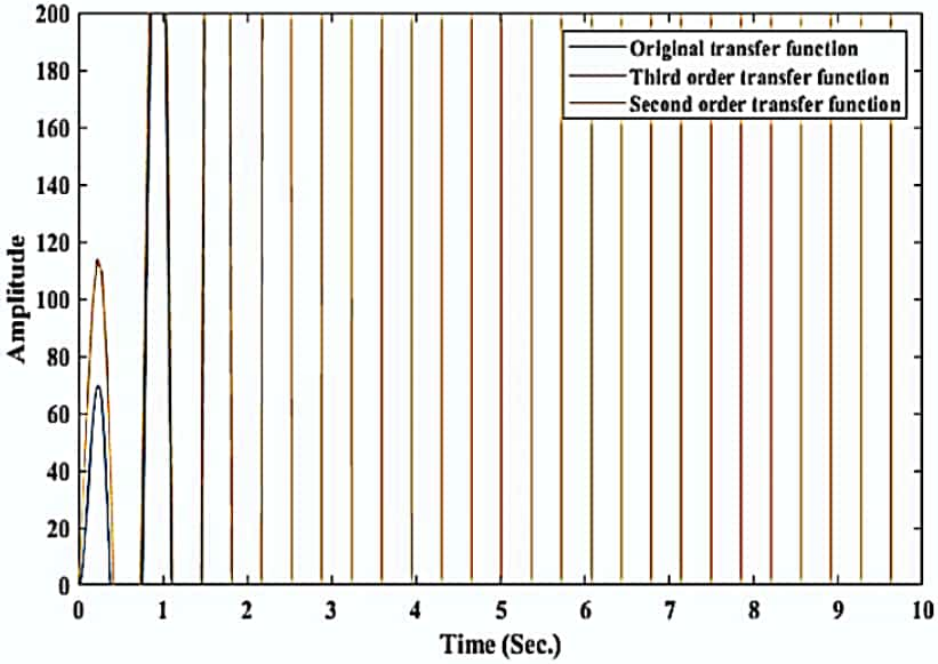

(a) Step responses of original and reduced P_{90}^{30} models

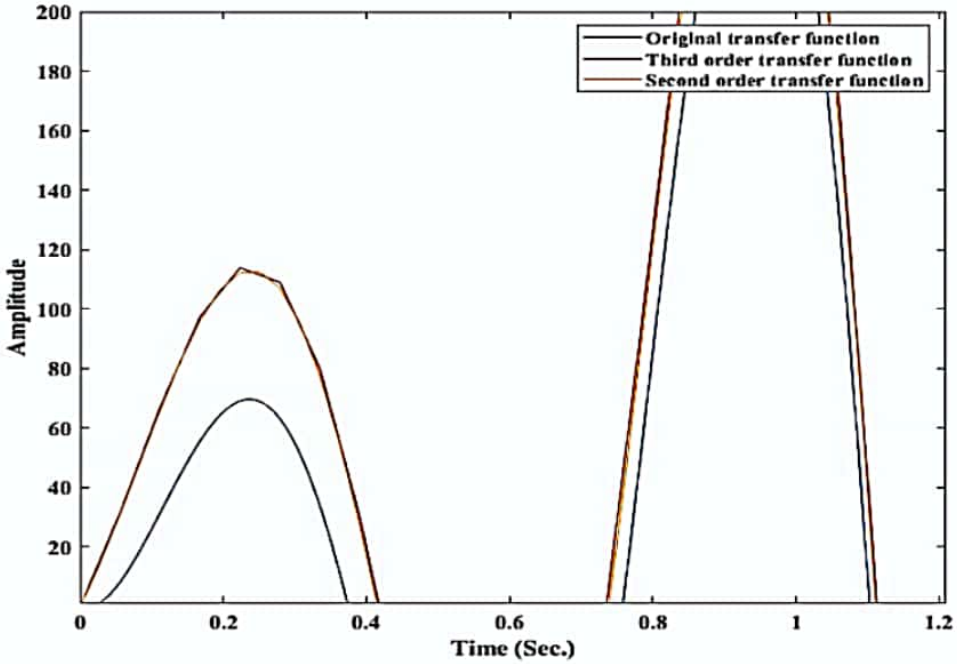

(b) Expanded view of step responses of original and reduced P_{90}^{30} models

Figure 4.3 Step response and expended view of original and reduced P_{90}^{30} models

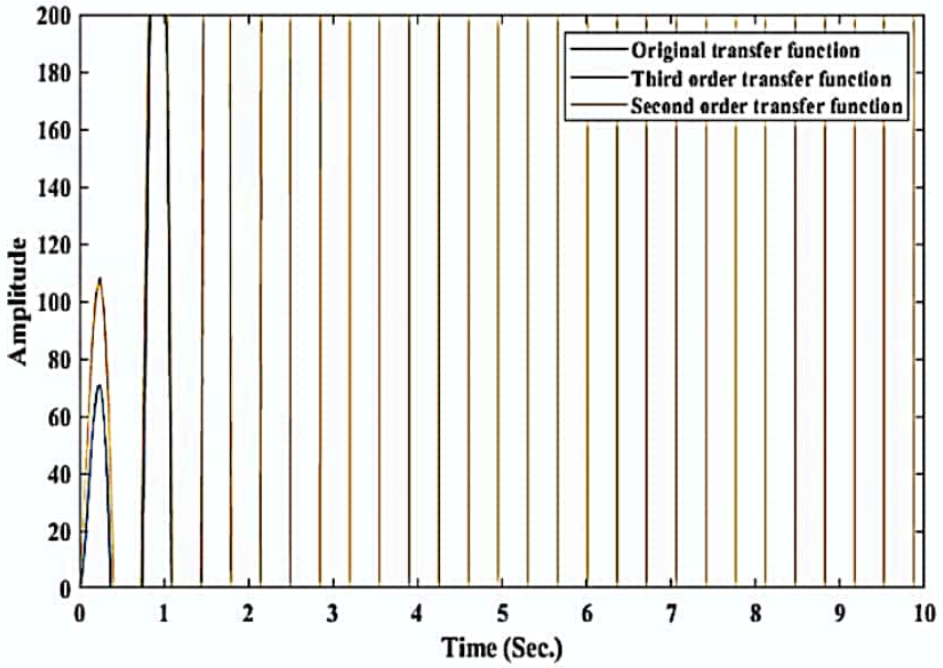

(a) Step responses of original and reduced P_{80}^{30} models

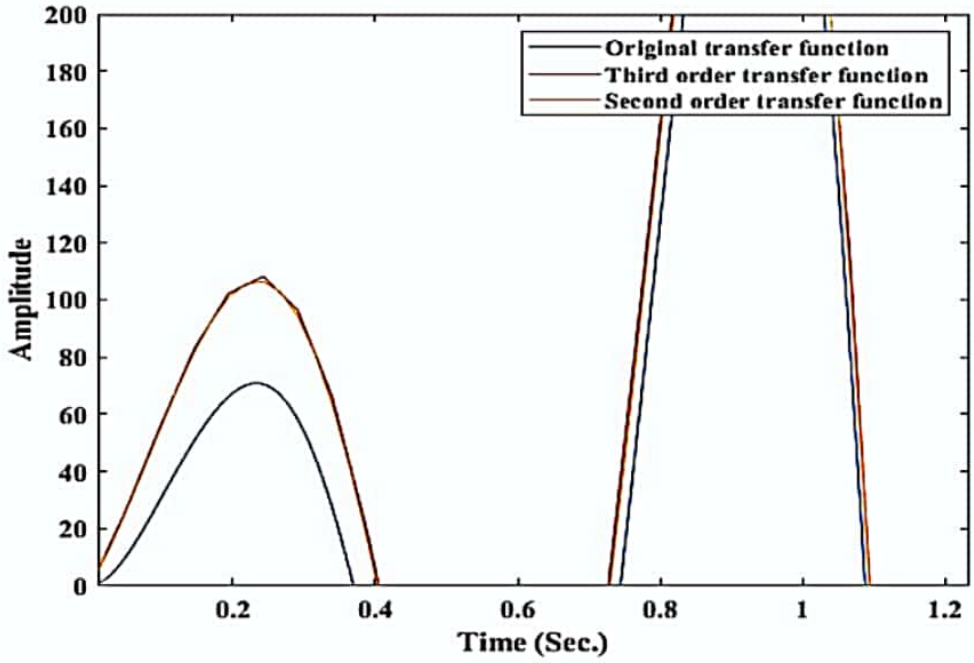

(b) Expanded view of step responses of original and reduced P_{80}^{30} models

Figure 4.4 Step response and expended view of original and reduced P_{80}^{30} models

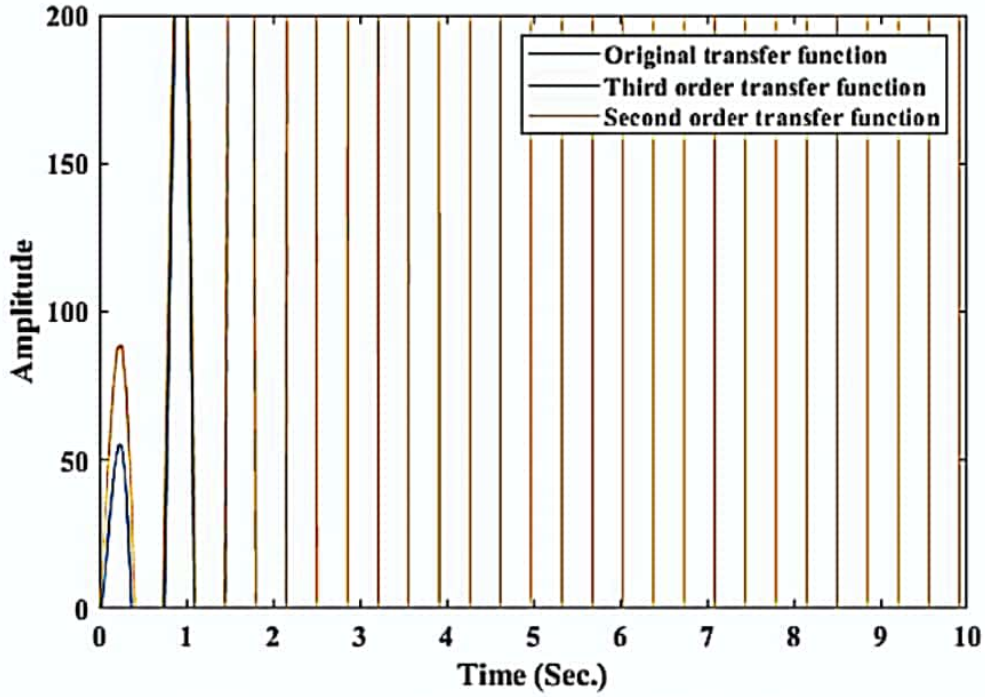

(a) Step responses of original and reduced P_{70}^{30} models

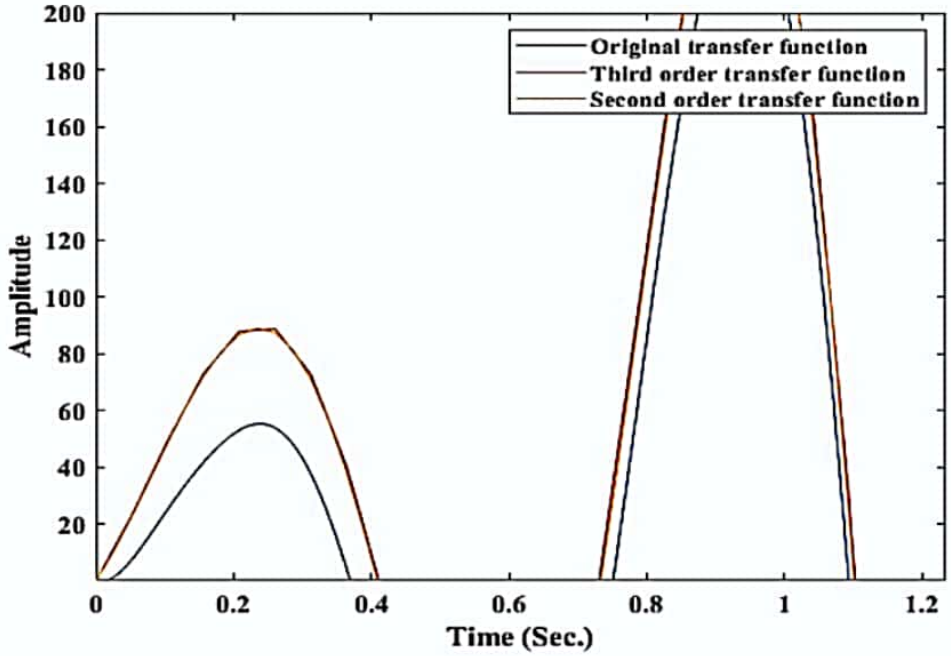

(b) Expanded view of step responses of original and reduced P_{70}^{30} models

Figure 4.5 Step response and expended view of original and reduced P_{70}^{30} models

Similarly, the reduced order models for all the transfer function models of PHWR have been found out and are tabulated in Tables 4.4, 4.6, 4.8 and their respective poles have been tabulated in Tables 4.5, 4.7, 4.9 respectively.

Table 4.4 Reduced order models of P_{90}^{30}

Third Order Reduced Model	Second Order Reduced Model
$G_{23}(s) = \frac{488.4s^2 + 1776s + 698.6}{s^3 - 3.263s^2 + 80.92s + 3.063}$	$G_{22}(s) = \frac{480.6s + 1784}{s^2 - 3.301s + 81.04}$

Table 4.5 Poles of different transfer functions of P_{90}^{30}

Original Poles	Poles of reduced order Model: 3rd Order	Poles of reduced order Model: 2nd Order
-4.7045 +31.412i -4.7045 -31.412i -11.198 +0i 1.6503 +8.8498i 1.6503 -8.8498i -0.10348 +0i	1.6503 +8.8498i 1.6503 -8.8498i -0.037799 +0i	1.6503 +8.8498i 1.6503 -8.8498i

Table 4.6 Reduced order models of P_{80}^{30}

Third Order Reduced Model	Second Order Reduced Model
$G_{33}(s) = \frac{466s^2 + 1499s + 669.9}{s^3 - 3.759s^2 + 83.37s + 3.329}$	$G_{32}(s) = \frac{458.7s + 1508}{s^2 - 3.799s + 83.52}$

Table 4.7 Poles of different transfer functions of P_{80}^{30}

Original Poles	Poles of reduced order Model: 3rd Order	Poles of reduced order Model: 2nd Order
-4.0256 +31.421i -4.0256 -31.421i -10.134 1.8995 +8.9393i 1.8995 -8.9393i -0.10408+0i	1.8995 +8.9393i 1.8995 -8.9393i -0.039862 +0i	1.8995 +8.9393i 1.8995 - 8.9393i

Table 4.8 Reduced order models of P_{70}^{30}

Third Order Reduced Model	Second Order Reduced Model
$G_{43}(s) = \frac{386.4s^2 + 1340s + 516.2}{s^3 - 3.503s^2 + 82.37s + 2.946}$	$G_{42}(s) = \frac{380.7s + 1347}{s^2 - 3.539s + 82.5}$

Table 4.9 Poles of different transfer functions of P_{70}^{30}

Original Poles	Poles of reduced order Model: 3rd Order	Poles of reduced order Model: 2nd Order
-3.8606 +31.421i -3.8606-31.421i -11.03 +0i 1.7695 +8.9088i 1.7695-8.9088i -0.097713 +0i	1.7695 +8.9088i 1.7695-8.9088i -0.035709 +0i	1.7695 +8.9088i 1.7695 -8.9088i

From the step responses obtained above for the original higher order PHWR system and its equivalent reduced third and second order system, it can be concluded that the Balanced truncation technique could successfully perform the model reduction of the higher order system. The reduced order models obtained have successfully retained the important dynamics of the original system. This property is extremely essential in order to have a successful controller design.

Summary

In this chapter, balanced truncation MOR technique has been applied to a PHWR model. The sixth order PHWR system has been reduced to equivalent third order system for all the step-back conditions. It was observed from the analysis of the obtained results that all the dominant dynamics of the original PHWR system were retained in the obtained reduced order models specially the unstable ones. This property makes it very useful for designing an efficient controller as the mathematical complexity of the design procedure reduces without compromising on the overall system performance.

CHAPTER 5

CONTROLLER DESIGN AND STABILITY ANALYSIS

5.1 Introduction

In current era of industrialization, automation and control have become very important and integral aspects of the industry. Therefore, the demand for robust control strategies that can provide accurate performance is ever increasing. The controller design problems for dynamical systems have been investigated by various researchers. The existing controller design techniques include Ziegler-Nichols, adaptive control, internal model control etc. but most of these techniques suffer from performance limitations during the real time applications. There are two main issues of concern that affect the controller performance in real time i.e., parametric variations and the external disturbances. Most of the existing controller design methods are not able to provide accurate performance under such conditions. Hence, the formulation of the efficient control methodologies should be carried out in such a way that it tackles both the aforementioned issues i.e. the parametric variations and the external influences. The FO controllers are known to prove successful in the real time, uncertain and the disturbed operating environment.

A revolutionary change occurred in the control system area after the development of fractional integral and differentiation operators in calculus. The use of fractional calculus started gaining popularity in the field of control system, when the FOPID controller was proposed in 1999. Mathematically, FOPID controller is represented as [24]:

$$C(s) = K_p + \frac{K_i}{s^{\lambda}} + K_d s^{\mu} \tag{5.1}$$

where, μ and λ can take any values within the range$(0,2)$. Since then, a lot of contribution have been made by various researchers to design efficient FO control algorithms which has proved more accurate and efficient. FO controllers have proven its efficacy in dealing with real time systems experiencing external disturbances and parametric variations [167], [169], [170], [176]–[182]. Some of the successfully used techniques for designing FO controllers are internal model control (IMC) [13], [42], [43], [183]–[186], adaptive control, intelligent control, optimization techniques etc.[28], [35], [115], [116], [187]–[196]. Many techniques like QFT, LMI, pole placement, H∞,

etc. exist in the literature for carrying out the controller design for interval systems [197]–[209]. However, most of the techniques are either mathematically complicated or do not behave efficiently under the varying operating circumstances for large and complex systems. The stability boundary locus technique has also been used successfully for design of FO controllers [19], [207], [210], [211]. The use of conventional tools like Kharitonov theorem and Edge theorem for interval systems have been illustrated in [41], [206], [210], [212], [213].

There are number of techniques proposed by the various researchers in past for designing FO controllers, but still the satisfactory performance of controllers while working in an uncertain or dynamic environment becomes an issue of concern. The controllers reveal a certain level of robustness when the control algorithms are formulated using fixed values of the system parameters, however, if these parameters are deviated due to some abnormal system behavior or external disturbance, there is always very high probability that the controller designed using fixed values of parameters may fail to deliver satisfactory performance. Hence, still there is need of such controller designing methodology which should be able to provide satisfactory reference tracking and disturbance rejection capabilities even for wider parametric variation of the system. Therefore, in this chapter FO control algorithms have been designed for perturbed PHWR as well as two area interconnected power system. Also, reduced order modelling described in Chapter 4 has been employed for controller design of PHWR system.

This chapter comprises of four sections. Section 5.2 discusses the proposed technique for designing the FOPID controller for power control in perturbed PHWR system. Section 5.3 illustrates reduced order modelling based controller design for the PHWR system. Section 5.4 discusses the proposed FOPID controller design technique for LFC in perturbed two area interconnected power system.

5.2 Fractional Order Controller Design for PHWR System

The FO controller design for PHWR system has been discussed in the following section.

5.2.1 Mathematical Modelling of PHWR System

While designing a controller, modelling a highly non-linear system like PHWR is not an easy task. The transfer function of PHWR is highly dependent on its operating conditions like its initial power and control rod position [214]. Various PID controllers have been designed for different linearized models of this non-linear plant as cited in [214]–[216] under different operating conditions. Liu *et*

al. [215] shows that the nonlinear behavior of the reactor can be tackled by switching to different controllers with the change in operating conditions. However, for each linearized model, it is not practical to design an independent controller. Talange *et al.* [169] and Shimjith *et al.* [217] proposed a controller designing technique for PHWR by developing its linearized mathematical model around specified operating points. In [218], optimal linear state feedback regulator is shown to give efficient results with the change in conditions of the system. The frequency domain tuning methods have been employed by Das *et al.* [168] to design FOPID controller for fractional reduced order models of PHWR. Although, this controller provides an isodamped response; however, an undershoot is seen at all operating points. A robust FOPI controller employing 'Stability Boundary Locus' technique has been proposed by Bhase *et al.* [170] for the nonlinear FO model of PHWR. The proposed method provides the satisfactory performance at the cost of increased settling time of the system.

Saha *et al.* [167] presented an active step back mechanism with robust controller which utilizes an LQR tuned PID along with FO phase shaper. It depicts enhancements in robustness and high frequency noise rejection but as a downside, at low frequencies an increase in sensitivity function has been observed. A robust FOPID controller has been proposed by Das *et al.* [168] which uses frequency domain tuning technique based on solving of simultaneous non-linear equations. The reduced order models have been obtained in fractional form giving minimum modelling error. However, an undershoot is obtained at all operating points. Das *et al.* [219] also proposed a continuous order PID like controller using optimized pole assignment like approach. Bhase *et al.* [170] proposed a robust FOPI controller for stabilizing the nonlinear FO PHWR plant using 'stability domain boundaries' in parameter plane. Although, the proposed controller ensures the iso-damped response in time domain with no undershoot for all (NIOPTD-II) reactor models, but with an increase in settling time of the system.

The mathematical models for the various step back conditions of the PHWR have been identified by Das in [219]. In this work, system and noise model identification based scheme has been employed to estimate the mathematical model of the reactor using real-time test data and regression based modelling techniques. Further, FO templates have been utilized to obtain the ROMs from the actual models. In [21], [220]–[222] it has been shown that the FO differential equations are more efficient to describe the kinematics of the nuclear reactor.

Table 5.1 shows the various identified FO models of a PHWR system for different operating conditions [219]. The subscript and superscript of transfer function model denotes initial reactor power and rod drop level, respectively.

Table 5.1 FO models of the PHWR for various operating conditions

Identified model	Reduced FO Models
P_{100}^{30}	$\frac{1522.8947}{s^{2.0971}+8.1944s^{1.0036}+7.7684}e^{-2.0043X10^{-12}s}$
P_{90}^{30}	$\frac{1359.2345}{s^{2.0972}+8.1906s^{1.0036}+7.7075}e^{-1.5968X10^{-9}s}$
P_{80}^{30}	$\frac{1027.3027}{s^{2.0163}+6.7859s^{0.99388}+6.5268}e^{-2.5346X10^{-5}s}$
P_{70}^{30}	$\frac{1074.396}{s^{2.0961}+8.2663s^{1.0037}+7.8641}e^{-3.1431X10^{-10}s}$
P_{100}^{50}	$\frac{529.1365}{s^{2.1002}+7.1111s^{1.0002}+9.0873}e^{-1.6049X10^{-5}s}$
P_{90}^{50}	$\frac{604.2541}{s^{2.2986}+8.871s^{1.0321}+11.2993}e^{-6.5X10^{-6}s}$
P_{80}^{50}	$\frac{337.846}{s^{2.2038}+6.7453s^{1.0132}+7.4275}e^{-1.8479X10^{-7}s}$
P_{70}^{50}	$\frac{325.2142}{s^{2.1969}+7.1459s^{1.0113}+8.3167}e^{-2.343X10^{-7}s}$

In [168], it has been illustrated that the P_{100}^{30} model has minimum phase margin and highest DC gain. This shows that the controller designed to meet the performance specifications for this condition would also produce suitable results for all the other conditions. Therefore, for designing the FO control algorithm, P_{100}^{30} has been considered as the worst case model. This model is converted into interval form by considering $\pm 50\%$ upper and lower bound uncertainties. Considering P_{100}^{30} model from Table 5.1 in interval form as in Eq. (5.2).

$$G(s)=\frac{N(s)}{D(s)}=\frac{a}{s^{2.0971}+b_1 s^{1.0036}+b_0} \tag{5.2}$$

where $a \in [761.44735,2284.3420], b_1 \in [4.0972,12.2916], b_0 \in [3.8842,11.6526]$.

In the next section, the FOPID controller designing procedure has been presented for an interval FO model employing edge theorem. It adopts a range of values of the parameters rather than using their fix values for controller design. Hence, the designed controller poses the capability to

stabilize the system output for any variation within the predefined range with moderate accuracy. Thus, the proposed method of controller designing incorporates higher robustness in the system for a large range of variations in system parameters.

5.2.2 Proposed INFOPID Controller Design for Power Control in Perturbed PHWR System

This section proposes the Interval Fractional Order PID (INFOPID) controller design methodology for power control in PHWR using the concepts of Stability Boundary Locus [19] and Edge theorem[11]. Figure 5.1 shows the block diagram representation of overall control system.

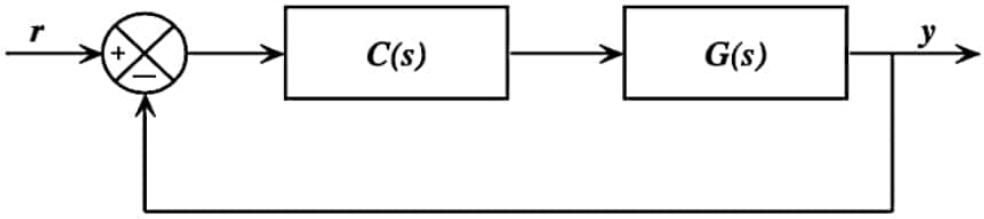

Figure 5.1 Closed loop control system

where, the controller is represented by $C(s)$ and the system model is represented by $G(s)$. The obtained closed loop transfer function of the complete system is $\frac{G(s)C(s)}{1+G(s)C(s)}$. Thus, the characteristic equation of the complete system comes to be

$$p(s; k_p, k_i, k_d, \lambda, \mu) = 1 + C(s)G(s) = 0 \tag{5.3}$$

Consider P_{100}^{30} model as in Eq. (5.2) for designing an INFOPID controller. According to Edge theorem, the numerator $N(s)$ in Eq.(5.2) has two values i.e.

$$N_1(s) = 761.44735 \;\&\; N_2(s) = 2284.3420 \tag{5.4}$$

Consider the denominator polynomial from (5.2)

$$D(s) = s^{2.0971} + b_1 s^{1.0036} + b_0 \tag{5.5}$$

According to edge theorem [11], the 4 edge polynomials for Eq. 5.5 has been formed as:

$$D_1(s) = s^{2.0971} + 4.0972s^{1.0036} + 3.8842 \tag{5.6}$$
$$D_2(s) = s^{2.0971} + 4.0972s^{1.0036} + 11.6526 \tag{5.7}$$
$$D_3(s) = s^{2.0971} + 12.2916s^{1.0036} + 3.8842 \tag{5.8}$$
$$D_4(s) = s^{2.0971} + 12.2916s^{1.0036} + 11.6526 \tag{5.9}$$

Using Eqns. (5.4) & (5.6)-(5.9), a group of eight edge transfer functions for the interval model of P_{100}^{30} PHWR presented in Eq. (5.2) has been formed as given by Eq. (5.10) and shown in Table 5.2.

$$G_i(s) = \frac{N_j(s)}{D_l(s)}, i = 1,2.....8, j = 1,2, l = 1,2,3,4 \tag{5.10}$$

Table 5.2 Transfer function for the interval model of P_{100}^{30} PHWR

Label name	Transfer function for the interval model of P_{100}^{30} PHWR
$G_1(s)$	$\frac{761.44735}{s^{2.0971} + 4.0972s^{1.0036} + 3.8842}$
$G_2(s)$	$\frac{761.44735}{s^{2.0971} + 4.0972s^{1.0036} + 11.6526}$
$G_3(s)$	$\frac{761.44735}{s^{2.0971} + 12.2916s^{1.0036} + 3.8842}$
$G_4(s)$	$\frac{761.44735}{s^{2.0971} + 12.2916s^{1.0036} + 11.6526}$
$G_5(s)$	$\frac{2284.3420}{s^{2.0971} + 4.0972s^{1.0036} + 3.8842}$
$G_6(s)$	$\frac{2284.3420}{s^{2.0971} + 4.0972s^{1.0036} + 11.6526}$
$G_7(s)$	$\frac{2284.3420}{s^{2.0971} + 12.2916s^{1.0036} + 3.8842}$
$G_8(s)$	$\frac{2284.3420}{s^{2.0971} + 12.2916s^{1.0036} + 11.6526}$

Taking the FOPID controller given in Eq. (5.1) and using Eq. (5.3), characteristic equation is found as

$$p(s; k_p, k_i, k_d, \lambda, \mu) = 1 + \left\{k_p + \frac{k_i}{s^\lambda} + k_d s^\mu\right\}\left\{\frac{a}{s^{2.0971} + b_1 s^{1.0036} + b_0}\right\} = 0 \tag{5.11}$$

$$p(s; k_p, k_i, k_d, \lambda, \mu) = (s)^{2.0971+\lambda} + b_1(s)^{1.0036+\lambda} + [b_0 + ak_p](s)^\lambda + ak_d(s)^{\lambda+\mu} + ak_i = 0 \tag{5.12}$$

The closed loop system as shown in Figure 5.1 will be stable if all the roots of Eq. (5.12) lie in left side of the s -plane. If the above condition is followed, the region for which, when $p(s; k_p, k_i, k_d, \lambda, \mu) \in S'$, is termed as the stability domain S' The boundary of the stability domain for a FOPID controller has been marked by the real root boundary (RRB) and the complex root boundary (CRB). These boundaries are described as

$$\begin{aligned} RRB: P(0; k_p, k_i, k_d, \lambda, \mu) = 0, for \omega \in (0, \infty), \\ CRB: P(j\omega; k_p, k_i, k_d, \lambda, \mu) = 0, for \omega \in (0, \infty). \end{aligned} \tag{5.13}$$

To attain RRB, replace $s = 0$ in Eq. (5.12). The RRB comes out to be k_i=0. To obtain the CRB, $s = j\omega$ has been substituted in Eq. (5.12),

$$\begin{aligned} & p(j\omega; k_p, k_i, k_d, \lambda, \mu) \\ & = (j\omega)^{2.0971+\lambda} + b_1(j\omega)^{1.0036+\lambda} + [b_0 + ak_p](j\omega)^{\lambda} + ak_d(j\omega)^{\lambda+\mu} + ak_i = 0 \end{aligned} \tag{5.14}$$

Solving Eq. (5.14) using the mathematical identity,

$$j^{\lambda} = cos(\frac{\lambda\pi}{2}) + j\, sin(\frac{\lambda\pi}{2}) \tag{5.15}$$

following equation has been obtained,

$$\begin{aligned} & \omega^{2.0971+\lambda}\left\{cos(\lambda + 2.0971)\frac{\pi}{2} + j\, sin(\lambda + 2.0971)\frac{\pi}{2}\right\} \\ & \quad + b_1\omega^{1.0036+\lambda}\left\{cos(\lambda + 1.0036)\frac{\pi}{2} + j\, sin(\lambda + 1.0036)\frac{\pi}{2}\right\} \\ & + \omega^{\lambda}[b_0 + ak_p]\left\{cos\,\lambda\frac{\pi}{2} + j\, sin\,\lambda\frac{\pi}{2}\right\} + ak_d\omega^{\lambda+\mu}\left\{cos(\lambda + \mu)\frac{\pi}{2} + j\, sin(\lambda + \mu)\frac{\pi}{2}\right\} + ak_i = 0 \end{aligned} \tag{5.16}$$

Express Eq. (5.16) in the form given in Eq. (5.17) and equalizing the real and imaginary segment to zero:

$$P(\omega, k_p, k_i, k_d, \lambda, \mu) = Re\{P(\omega, k_p, k_i, k_d, \lambda, \mu)\} + j\, Im\{P(\omega, k_p, k_i, k_d, \lambda, \mu)\} \tag{5.17}$$

Segregating the real and imaginary parts and equalizing to zero:

Real part:

$$\begin{aligned} & \omega^{2.0971+\lambda}\, cos(\lambda + 2.0971)\frac{\pi}{2} + b_1\omega^{1.0036+\lambda}\, cos(\lambda + 1.0036)\frac{\pi}{2} \\ & + \omega^{\lambda}\, cos\,\lambda\frac{\pi}{2}(b_0 + ak_p) + ak_d\omega^{\lambda+\mu}\, cos(\lambda + \mu)\frac{\pi}{2} + ak_i = 0 \end{aligned} \tag{5.18}$$

Imaginary part:

$$\begin{aligned} & \omega^{2.0971+\lambda}\, sin(\lambda + 2.0971)\frac{\pi}{2} + b_1\omega^{1.0036+\lambda}\, sin(\lambda + 1.0036)\frac{\pi}{2} \\ & + \omega^{\lambda}\, sin\,\lambda\frac{\pi}{2}(b_0 + ak_p) + ak_d\omega^{\lambda+\mu}\, sin(\lambda + \mu)\frac{\pi}{2} = 0 \end{aligned} \tag{5.19}$$

Eq. (5.18) and Eq. (5.19) have been obtained in terms of three variables k_p, k_i and k_d. It is required to solve these equations and obtain the expressions of k_p and k_i so that the stability region can be plotted in the $(k_p - k_i)$ plane. This can be achieved in two ways:

- The value of k_d is set arbitrarily and CRB and RRB are plotted in the $(k_p - k_i)$ plane for various values of $\lambda \in (0,2)$ and $\mu \in (0,2)$.
- The value of k_i is set arbitrarily and CRB and RRB are plotted in the $(k_p - k_d)$ plane for various values of $\lambda \in (0,2)$ and $\mu \in (0,2)$.

Now, $k_d = 0.05$ has been chosen and Eq. (5.18) & Eq. (5.19) have been concurrently solved to get k_p and k_i. The expressions obtained are given in Eq. (5.20) and Eq. (5.21). Using these values, the CRB and RRB have been traced in the $(k_p - k_i)$ plane for a preset value of $\mu \in (0,2)$ and $\lambda \in (0,2)$ as ω varies from $(0, \infty)$.

$$k_p = \frac{-1}{a\omega^{\lambda} \cos\lambda\left(\frac{\pi}{2}\right)} \begin{Bmatrix} ak_d\omega^{\lambda+\mu}\cos(\lambda+\mu)\frac{\pi}{2} + ak_i + b_1\omega^{1.0036+\lambda}\cos(\lambda+1.0036)\frac{\pi}{2} + \\ \omega^{2.0971+\lambda}\cos(\lambda+2.0971)\frac{\pi}{2} + b_0\omega^{\lambda}\cos\lambda\frac{\pi}{2} \end{Bmatrix} \quad (5.20)$$

$$k_i = \frac{\omega^{2.0971+\lambda}\sin 2.0971\frac{\pi}{2} + b_1\omega^{1.0036+\lambda}\sin 1.0036\frac{\pi}{2} + ak_d\omega^{\mu+\lambda}\sin\mu\frac{\pi}{2}}{a\sin\lambda\frac{\pi}{2}} \quad (5.21)$$

The area that has been obtained by sketching the CRB and the RRB in the $k_p - k_i$ plane is termed as stability region for that value of λ and μ i.e., all the values of k_p and k_i that lie inside this region will stabilize the system. Hence, by varying $\lambda \in (0,2)$and $\mu \in (0,2)$, the stability regions have been produced for all combinations of λ and μ.

Subsequently, the values of k_p, k_i, λ and μ have been calculated to obtain suitable performance for all the edge transfer functions obtained in Eq. (5.10). This has been accomplished with the subsequent steps:

Step 1: Firstly, taking into account the first edge transfer function

$G_1(s) = \frac{761.44735}{s^{2.0971}+4.0972s^{1.0036}+3.8842}$ as obtained from Table 5.2.

Step 2: Using the mathematical equations of k_p and k_i as obtained in Eq. (5.20) and Eq. (5.21), sketch the graphs of stability region as elaborated above, in the $k_p - k_i$ plane for entire values of $\lambda \in (0,2)$ and $\mu \in (0,2)$. The global stability region for the first edge transfer function $G_1(s)$ hence obtained is shown in Figure 5.2(a).

Step 3: Follow step 2 for all $G_i(s), i = 2, \ldots\ldots\ldots, 8$ to get the global stability region for the all other transfer functions. Figures 5.2(b)-(h) show the individual global stability regions for all other transfer functions.

Step 4: Now, only one controller that would be able to stabilize all the eight edge transfer functions has to be obtained. Hence, the intersection of eight individual graphs shown in Figures 5.2(a)-(h) has been achieved. This is termed as the common global stability region. This region is valid to all the eight edge transfer functions presented in Eq. (5.10).

Step 5: Values of λ and μ providing biggest intersection of the stability regions has been chosen. The values of $\lambda = 0.9$ and $\mu = 0.95$ have been selected, (Figure 5.3) so that it would be able to stabilize all the transfer functions presented in Eq. (5.10). Further, the same region has been utilized to estimate k_p and k_i.

Step 6: An appropriate combination of k_p and k_i providing paramount controller performance has been selected from the region attained in Step 5. In this case, the selected value is $k_p = 0.011$ and $k_i = 0.03$ which has been shown in the zoomed view within the intersection stability region in Figure 5.4.

Hence, the controller parameters attained are $k_p = 0.011, k_i = 0.03, k_d = 0.05, \lambda = 0.9, \mu = 0.95$ i.e., the designed INFOPID controller is represented as,

$$C(s) = 0.011 + \frac{0.03}{s^{0.9}} + 0.05s^{0.95} \tag{5.22}$$

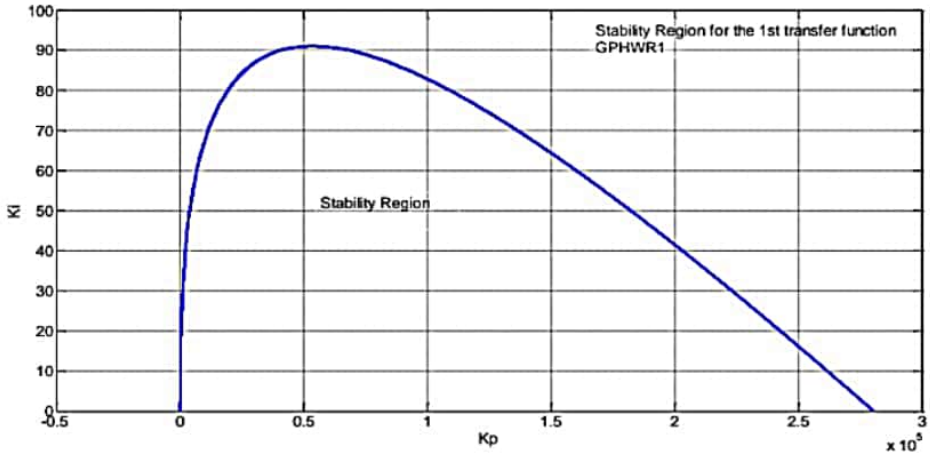

(a) Stability region for $G_1(s)$

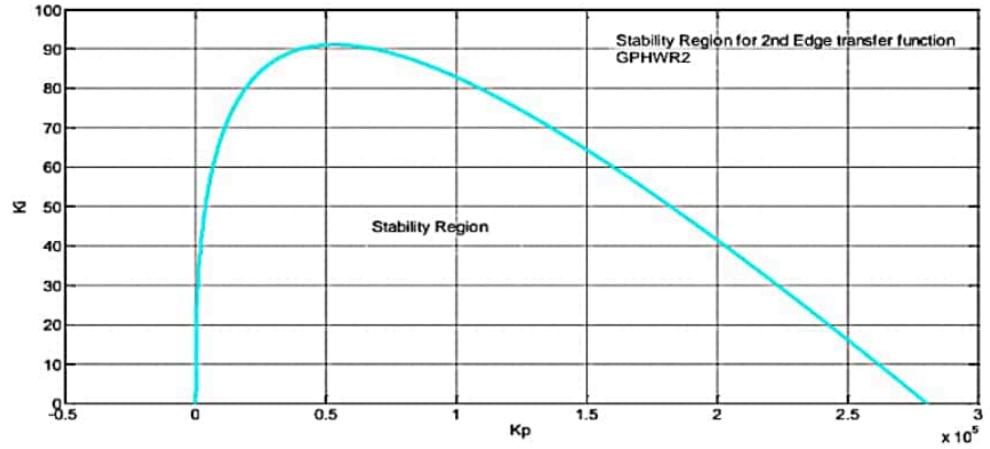

(b) Stability region for $G_2(s)$

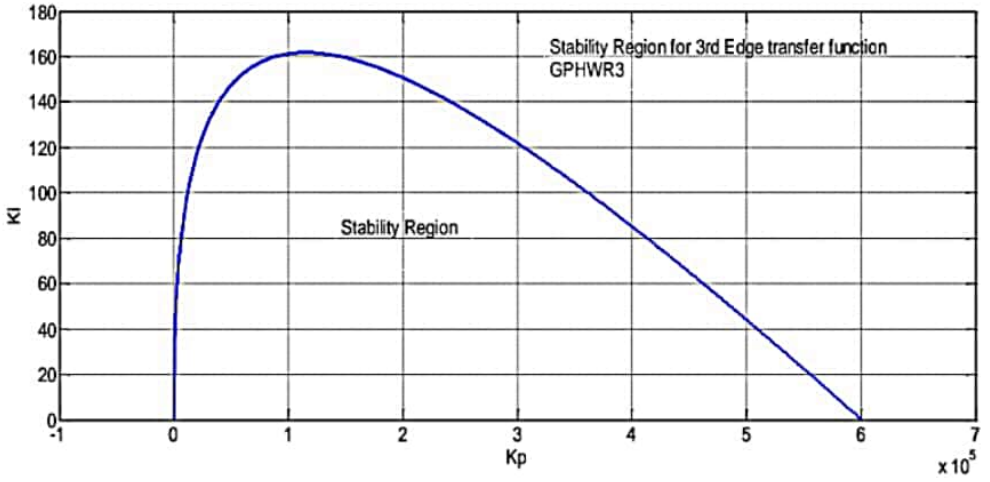

(c) Stability region for $G_3(s)$

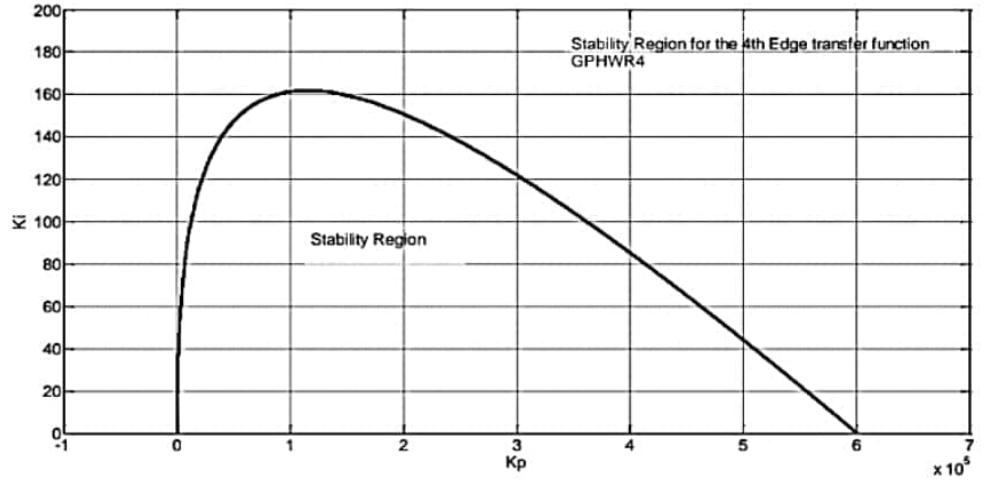

(d) Stability region for $G_4(s)$

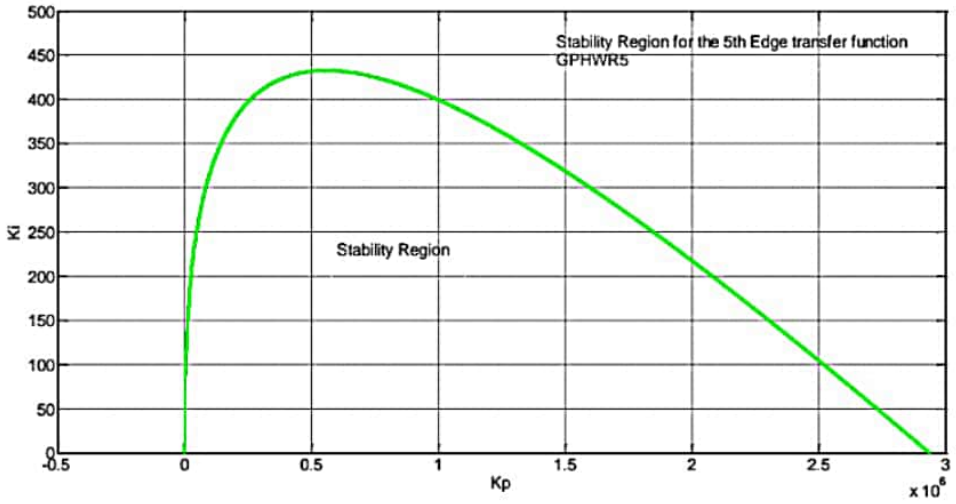

(e) Stability region for $G_5(s)$

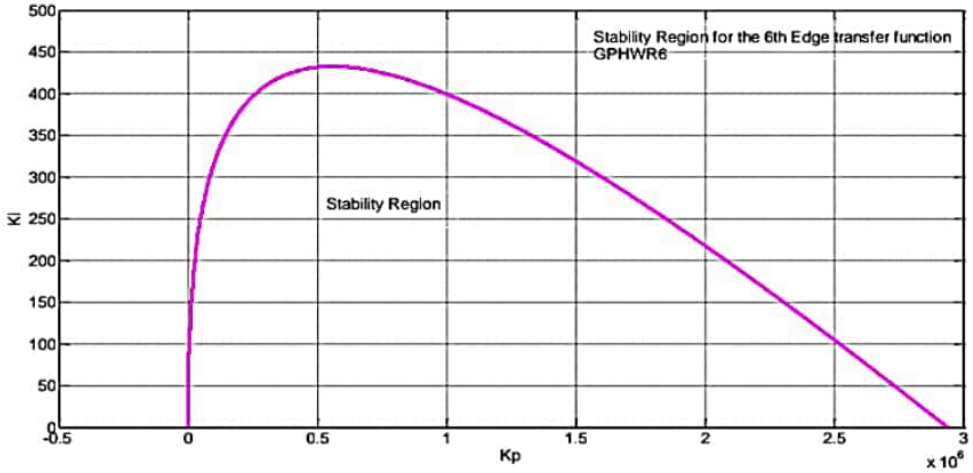

(f) Stability region for $G_6(s)$

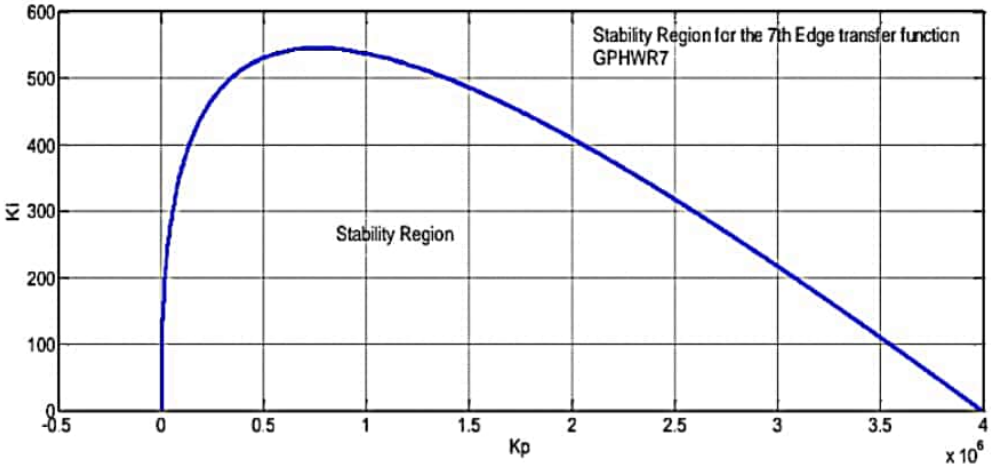

(g) Stability region for $G_7(s)$

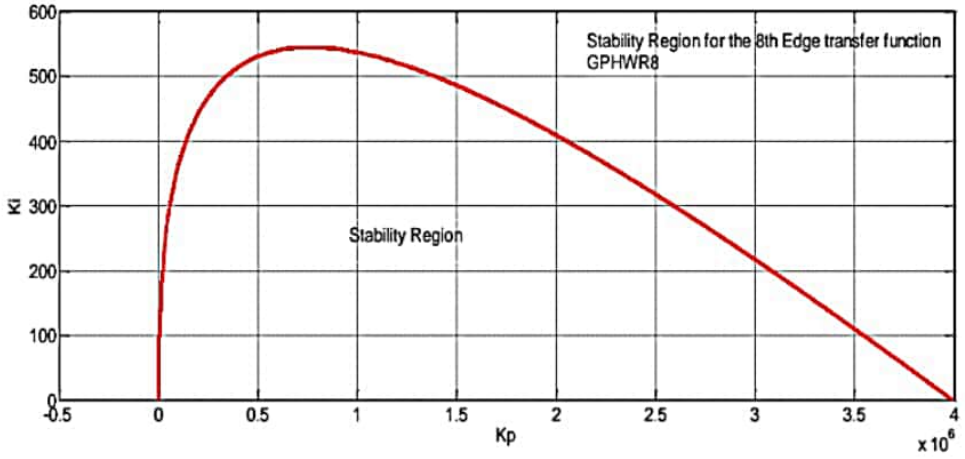

(h) Stability region for $G_8(s)$

Figure 5.2 Stability regions for edge transfer functions

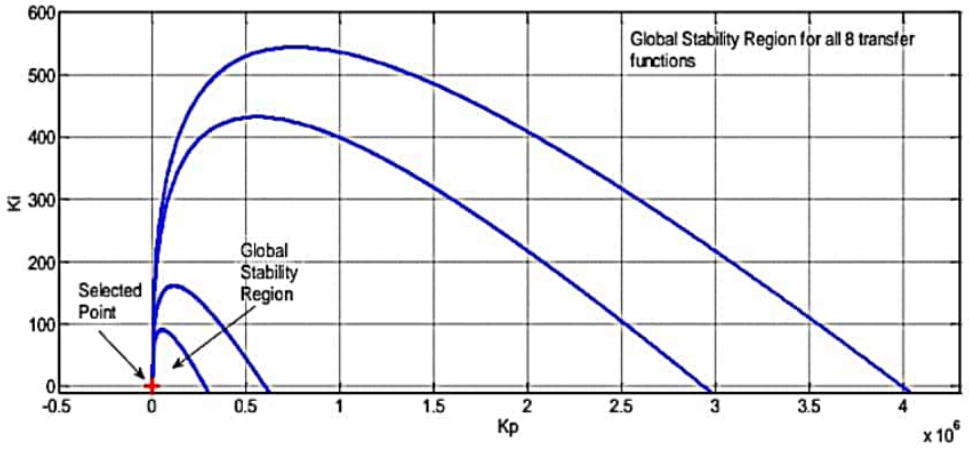

Figure 5.3 Global stability region for all the 8 transfer functions

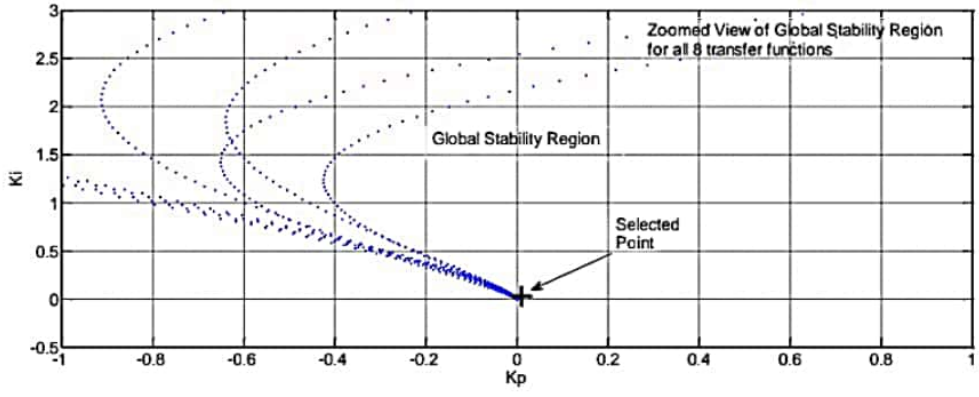

Figure 5.4 Zoomed view of global stability region of all the 8 transfer functions

5.2.2.1 Stability Analysis

In this section, stability testing of the closed loop PHWR system has been illustrated for one of the interval transfer functions of P_{100}^{30} given by $G_1(s)$. The analysis of stability for this system has been carried out by evaluating characteristic equation. The characteristic equation of the system is,

$$P(s) = 1 + \left(\frac{761.44735}{s^{2.0971} + 4.0972s^{1.0036} + 3.8842}\right)\left(0.011 + \frac{0.03}{s^{0.9}} + 0.05s^{0.95}\right) = 0 \quad (5.23)$$

The characteristic equation can be written as:

$$P(s) = s^{2.99} + 4.0972s^{1.90} + 12.2601s^{0.90} + 38.0723s^{1.85} + 22.8434 = 0 \quad (5.24)$$

As per the stability analysis technique given in [45], firstly FO polynomial has been transformed into the integer order polynomial as:

$$P(s) = s^{\frac{299}{100}} + 4.0972s^{\frac{190}{100}} + 12.2601s^{\frac{90}{100}} + 38.0723s^{\frac{185}{100}} + 22.8434 = 0 \quad (5.25)$$

In Eq. (5.25), substituting $s^{\frac{1}{100}} = w$, the following equation has been obtained,

$$P(s) = w^{299} + 4.0972w^{190} + 38.0723w^{185} + 12.2601w^{90} + 22.8434 = 0 \quad (5.26)$$

The roots obtained for Eq. (5.26) have been given in the Table 5.3.

Table 5.3: Roots of characteristic polynomial $P(s)$

-0.9999+ *i* 0.0000	-0.8336-*i* 0.5458	1.0235+*i* 0.1425
0.9210+ *i* 0.3773	-0.9170+*i* 0.3943	0.6434-*i* 0.7594
0.5671+ *i* 0.8221	0.1289+*i* 0.9873	0.7674+*i* 0.6415
0.8930- *i* 0.5164	-0.8878+*i* 0.4553	-0.4901-*i* 0.9080
-0.0013-*i* 1.0325	-0.6336-*i* 0.7677	0.7202+*i* 0.7389
0.8931-*i* 0.4393	-0.8684-*i* 0.4878	-0.4394+*i* 0.9331
0.8807+*i* 0.4730	0.2248-*i* 0.9716	-0.8952+*i* 0.5162
-0.1704+*i* 1.0174	-0.3349-*i* 0.9754	-0.6776+*i* 0.7795
-1.0279+*i* 0.0848	-0.9463+*i* 0.4142	-0.7323-*i* 0.6752
-1.0128+*i* 0.1967	0.4762-*i* 0.8746	0.3893-*i* 0.9180
0.9951-*i* 0.0485	0.4157-*i* 0.9051	0.3893+*i* 0.9180
-0.2088-*i* 0.9732	0.7963-*i* 0.6551	0.2810+*i* 0.9945
0.3892-*i* 0.9575	0.5099+*i* 0.8581	-0.4643+*i* 0.8805
0.8611+*i* 0.4994	-0.7949+*i* 0.6012	0.2248+*i* 0.9716
-0.2261-*i* 1.0064	-0.7598-*i* 0.7004	-0.9978+*i* 0.0676
-0.5517+*i* 0.8329	0.9850-*i* 0.3094	-0.6586-*i* 0.7502

-0.2088+*i* 0.9732	-0.3089-*i* 0.9512	-0.7198+*i* 0.7411
0.6348-*i* 0.8140	0.5344+*i* 0.8399	0.2899-*i* 0.9536
-0.7073+*i* 0.7035	0.6218+*i* 0.7821	-0.5234-*i* 0.8467
0.9857+*i* 0.1536	-0.9676+*i* 0.3612	0.3535-*i* 0.9314
-0.6065+*i* 0.7935	-0.8654+*i* 0.5650	0.5902+*i* 0.8015
0.9789+*i* 0.1825	-0.1778+*i* 0.9839	0.4417+*i* 0.9343
-0.8329-*i* 0.6121	-0.6065-*i* 0.7935	0.8248+*i* 0.5572
0.2255+*i* 1.0084	0.5892+*i* 0.8479	0.9361+*i* 0.3495
0.9446+*i* 0.4153	0.6218-*i* 0.7821	0.8307+*i* 0.6107
-0.8654-*i* 0.5650	-0.2439+*i* 0.9697	-0.9221-*i* 0.4658
0.8930+*i* 0.5164	-0.4030-*i* 0.9100	-0.3089+*i* 0.9512
0.2614-*i* 0.9615	0.5418+*i* 0.8793	-0.3727+*i* 0.9282
0.4926-*i* 0.9082	0.7674-*i* 0.6415	0.1695+*i* 1.0193
0.6939+*i* 0.7137	0.9850+*i* 0.3094	-0.9900+*i* 0.1021
-0.9807+*i* 0.1695	1.0010+*i* 0.2547	0.8470+*i* 0.5315
-0.9900-*i* 0.1021	0.1955-*i* 0.9765	0.6434+*i* 0.7594
0.9966-*i* 0.0190	0.5892-*i* 0.8479	-0.8174-*i* 0.5703
-1.0279-*i* 0.0848	0.9571-*i* 0.2852	-0.1106-*i* 0.9936
-0.2439-*i* 0.9697	-0.7598+*i* 0.7004	0.8470-*i* 0.5315
-1.0128-*i* 0.1967	-0.6586+*i* 0.7502	0.9735-*i* 0.2198
0.0917+*i* 0.9939	0.3356-*i* 0.9775	-0.9807-*i* 0.1695
-0.5395-*i* 0.8799	0.6733+*i* 0.7385	-0.8544+*i* 0.5140
0.9892+*i* 0.1157	-0.3727-*i* 0.9282	-0.2809-*i* 0.9924
-1.0217+*i* 0.1409	0.7963+*i* 0.6551	-0.7073-*i* 0.7035
-0.2750+*i* 0.9567	0.5902-*i* 0.8015	-0.9948+*i* 0.0341
-0.5875-*i* 0.8491	-0.9221+*i* 0.4658	0.7411+*i* 0.6645
0.1128-*i* 1.0270	0.6786+*i* 0.7777	-0.9625-*i* 0.2674
0.9789-*i* 0.1825	0.1586-*i* 0.9850	0.7219-*i* 0.6916
-0.4944+*i* 0.8685	0.9571+*i* 0.2852	0.2614+*i* 0.9615
0.1695-*i* 1.0193	0.6786-*i* 0.7777	-1.0009-*i* 0.2522
-0.7949-*i* 0.6012	0.9640+*i* 0.2487	0.5418-*i* 0.8793
-0.8329+*i* 0.6121	-0.1778-*i* 0.9839	-0.9858-*i* 0.3071
0.7595+*i* 0.6980	-0.7976-*i* 0.6574	0.4926+*i* 0.9082
-0.0430+*i* 0.9982	-0.4394-*i* 0.9331	-0.6335+*i* 0.8155
-0.9670-*i* 0.2361	0.8807-*i* 0.4730	0.2899+*i* 0.9536
-0.7198-*i* 0.7411	-0.9170-*i* 0.3943	0.3356+*i* 0.9775
1.0330-*i* 0.0286	0.4417-*i* 0.9343	0.0615+*i* 0.9937
0.8093+*i* 0.5879	-0.9260+*i* 0.3655	0.2810-*i* 0.9945

-1.0310+*i* 0.0283	-0.0064-*i* 0.9954	-0.4944-*i* 0.8685
-0.4348+*i* 0.9004	-0.8336+*i* 0.5458	0.4505+*i* 0.8900
0.9203+*i* 0.4666	-0.6845-*i* 0.7231	0.5099-*i* 0.8581
-0.1418+*i* 0.9851	0.3261-*i* 0.9419	0.2255-*i* 1.0084
-0.5517-*i* 0.8329	0.4157+*i* 0.9051	0.0558+*i* 1.0314
0.9966+*i* 0.0190	0.9892-*i* 0.1157	0.9857-*i* 0.1536
0.5344-*i* 0.8399	1.0139+*i* 0.1990	-0.9419+*i* 0.3316
-0.7976+*i* 0.6574	0.3535+*i* 0.9314	0.8611-*i* 0.4994
0.9203-*i* 0.4666	-0.5875+*i* 0.8491	-0.8684+*i* 0.4878
1.0299-*i* 0.0856	0.0615-*i* 0.9937	0.8631+*i* 0.5645
0.7847-*i* 0.6122	-0.9858+*i* 0.3071	0.7847+*i* 0.6122
-0.8992-*i* 0.4276	1.0299+*i* 0.0856	-0.1106+*i* 0.9936
-1.0009+*i* 0.2522	0.1289-*i* 0.9873	0.6939-*i* 0.7137
-0.7528+*i* 0.6538	-0.1145+*i* 1.0253	-0.9676-*i* 0.3612
0.9447+*i* 0.3137	-0.8174+*i* 0.5703	-0.0581-*i* 1.0305
-0.9260-*i* 0.3655	0.1586+*i* 0.9850	-0.2261+*i* 1.0064
-0.3349+*i* 0.9754	0.8931+*i* 0.4393	-0.8878-*i* 0.4553
0.9662-*i* 0.3629	0.9106+*i* 0.4123	0.9935+*i* 0.0865
0.3261+*i* 0.9419	-0.8544-*i* 0.5140	-0.9790-*i* 0.2020
0.8093-*i* 0.5879	-0.9978-*i* 0.0676	0.9446-*i* 0.4153
-0.0743-*i* 0.9925	0.4762+*i* 0.8746	-0.8952-*i* 0.5162
-1.0310-*i* 0.0283	-0.0430-*i* 0.9982	-0.1704-*i* 1.0174
-0.9487+*i* 0.3016	-0.2750-*i* 0.9567	1.0330+*i* 0.0286
0.6733-*i* 0.7385	0.3892+*i* 0.9575	-0.7767+*i* 0.6241
-0.1418-*i* 0.9851	0.9951+*i* 0.0485	0.7219+*i* 0.6916
-0.6336+*i* 0.7677	0.9735+*i* 0.2198	-0.9909+*i* 0.1351
-0.6776-*i* 0.7795	0.0558-*i* 1.0314	-0.5395+*i* 0.8799
-0.8992+*i* 0.4276	0.7202-*i* 0.7389	-0.7528-*i* 0.6538
0.6348+*i* 0.8140	1.0010-*i* 0.2547	-0.4643-*i* 0.8805
-0.0013+*i* 1.0325	-0.9909-*i* 0.1351	-0.6335-*i* 0.8155
-0.9790+*i* 0.2020	-0.9419-*i* 0.3316	0.9447-*i* 0.3137
0.9640-*i* 0.2487	0.4505-*i* 0.8900	-0.9487-*i* 0.3016
0.9935-*i* 0.0865	0.0244+*i* 0.9982	-0.6845+*i* 0.7231
-0.7323+*i* 0.6752	-0.4901+*i* 0.9080	-0.9948-*i* 0.0341
-0.9625+*i* 0.2674	0.9210-*i* 0.3773	-0.3399+*i* 0.9355
0.9361-*i* 0.3495	-0.4348-*i* 0.9004	-0.3877-*i* 0.9555
-0.9463-*i* 0.4142	-0.0743+*i* 0.9925	-0.2809+*i* 0.9924
0.1955+*i* 0.9765	-0.3877+*i* 0.9555	-1.0217-*i* 0.1409

-0.5234+*i* 0.8467	0.8248-*i* 0.5572	-0.5799-*i* 0.8090
-0.4030+*i* 0.9100	0.9106-*i* 0.4123	-0.9670+*i* 0.2361
0.1128+*i* 1.0270	0.8631-*i* 0.5645	1.0139-*i* 0.1990
0.8307-*i* 0.6107	-0.5799+*i* 0.8090	-0.7767-*i* 0.6241
-0.1145-*i* 1.0253	0.7595-*i* 0.6980	0.0917-*i* 0.9939
0.5671-*i* 0.8221	1.0235-*i* 0.1425	-0.0064+*i* 0.9954
0.7411-*i* 0.6645	-0.3399-*i* 0.9355	0.9662+*i* 0.3629
-0.0581+*i* 1.0305	0.0244-*i* 0.9982	

Now, from the roots of the polynomial (5.26) obtained above, the set of physically realizable roots ϕ_i, have been determined using the condition $|arg(\phi_i)| < \frac{\pi}{100}$. The obtained physically realizable roots are presented below in Eq. (5.27) - (5.30). Further, the stability condition $|arg(\phi_i)| > \frac{\pi}{200}$ has been checked for all physically realizable roots. If all the realizable roots of the system satisfy the given condition, only then the system is said to be stable. From Eq. (5.27) - (5.30) the system is found to be stable.

$$|arg(\phi_1)| = 0.0190 \quad (5.27)$$

$$|arg(\phi_2)| = 0.0276 \quad (5.28)$$

$$|arg(\phi_3)| = 0.0190 \quad (5.29)$$

$$|arg(\phi_4)| = 0.0276 \quad (5.30)$$

5.2.2.2 Simulation Results

The simulation outcomes achieved by carrying out the design of an INFOPID controller using the proposed technique for power control in PHWR under step back condition has been presented in this section. The response of the proposed controller for the 8 edge transfer functions (signifying varying operating conditions due to incidental parameter changes) as well as the various step back conditions (signifying varying operating conditions due to different control rod position) has been shown here.

Figures 5.5(a)-(h) reveal the performance of the proposed INFOPID controller for various interval transfer functions of the PHWR. These interval transfer functions signify possible changes in the system parameters due to any unintentional cause. The proposed INFOPID controller has been designed by considering a range of possible variations of each parameter value. In this system, a negative unit step input has been given to the system at time 1sec. From Figure 5.5, it has been

observed that the proposed controller exhibits good set point tracking in all the different interval conditions. Also, the response of the proposed INFOPID has been compared to the IOPID controller tuned using conventional Ziegler Nichol's tuning, FOPID controller proposed in [168] by Das *et al.*, FOPI controller proposed in [170] by Bhase *et al.*, COPID controller proposed in [219] by Das *et al.* and FOIMCPID controller proposed in [182] by Sumeet *et al.* It has been perceived from the results that the existing controllers (devised using the nominal parameter values), exhibit a sluggish response and have a slow set point tracking ability as compared to the proposed INFOPID controller when subjected to interval conditions. It has also been perceived that the proposed controller has faster set point tracking capability than the existing controllers even under interval conditions. Hence the proposed controller has a higher robustness.

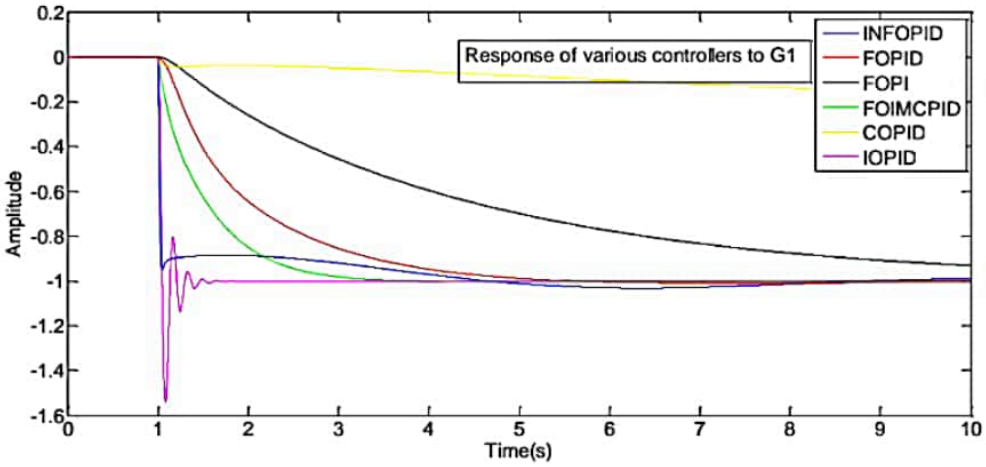

(a) Response of various controllers to G_1

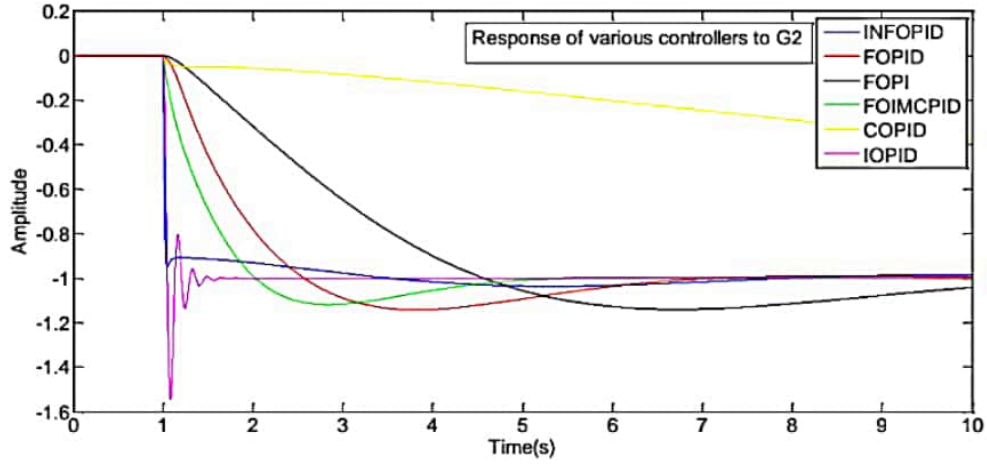

(b) Response of various controllers to G_2

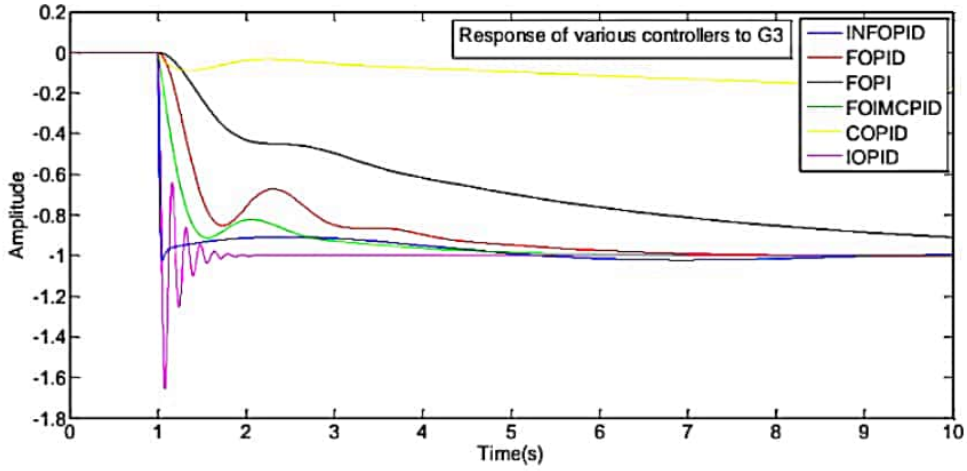

(c) Response of various controllers to G_3

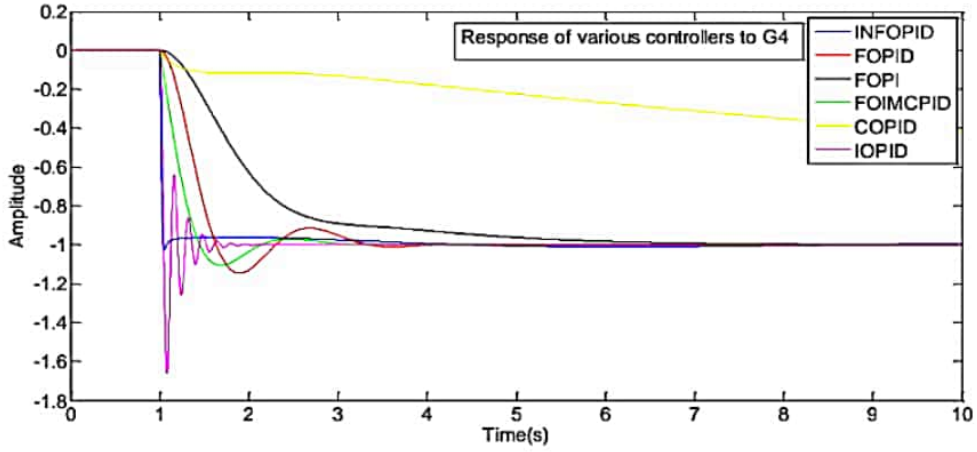

(d) Response of various controllers to G_4

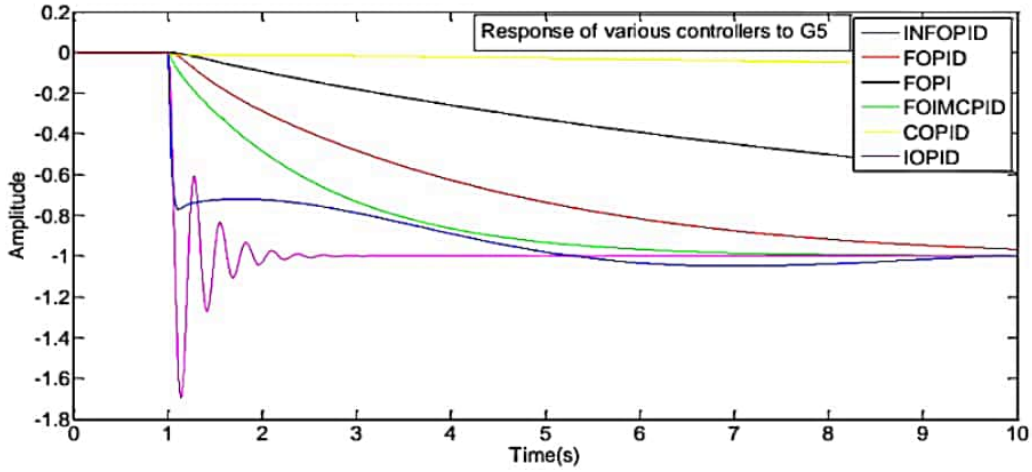

(e) Response of various controllers to G_5

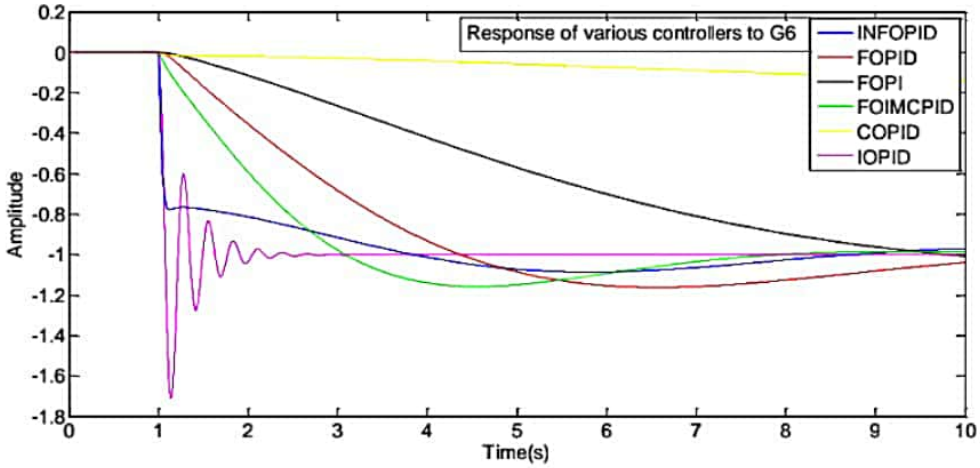

(f) Response of various controllers to G_6

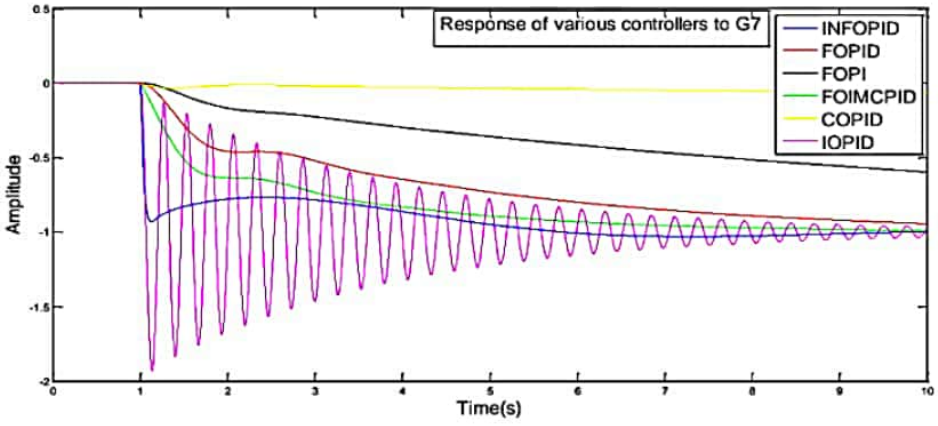

(g) Response of various controllers to G_7

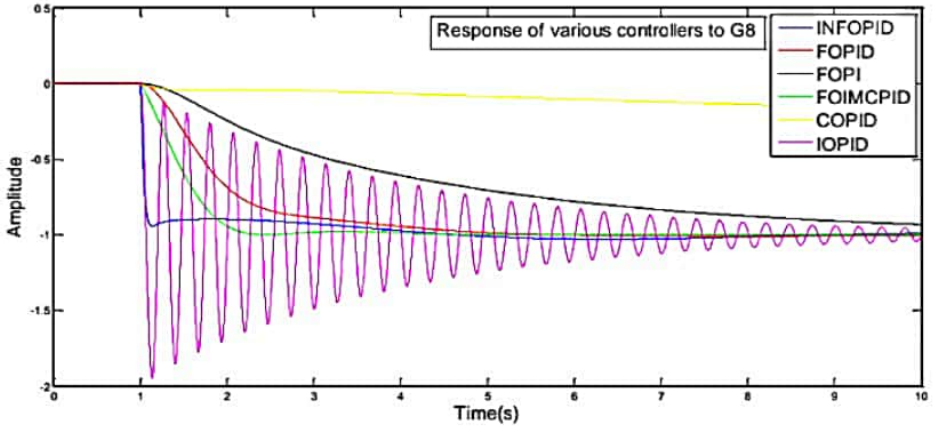

(h) Response of various controllers to G_8

Figure 5.5 Response of various controllers to different interval conditions of P_{100}^{30}

Figures 5.6(a)-(h) present the performance of the proposed INFOPID controller for the different reactor models. These models signify the different operating conditions with respect to different positions of the control rod. The responses have been compared to the conventional IOPID controller, FOPID controller proposed by Das *et al.*[168], FOPI controller suggested by Bhase *et al.* [170], COPID controller proposed in [219] by Das *et al.* and FOIMCPID controller proposed by Sumeet *et al.* [182]. Although the proposed INFOPID controller produces a small undershoot but the system settles quickly as compared to other existing controllers. It illustrates that the proposed controller has a faster set point tracking ability as compared to existing controllers under different step back conditions.

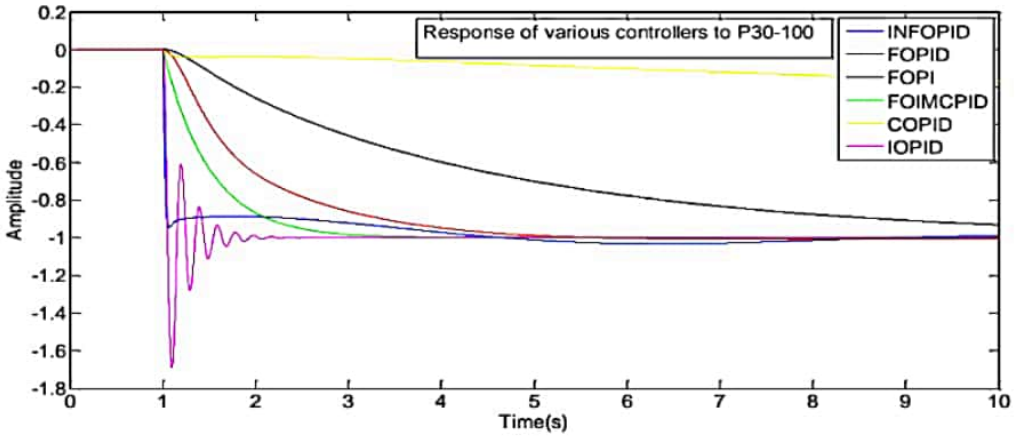

(a) Response of various controllers for transfer function model P_{100}^{30}

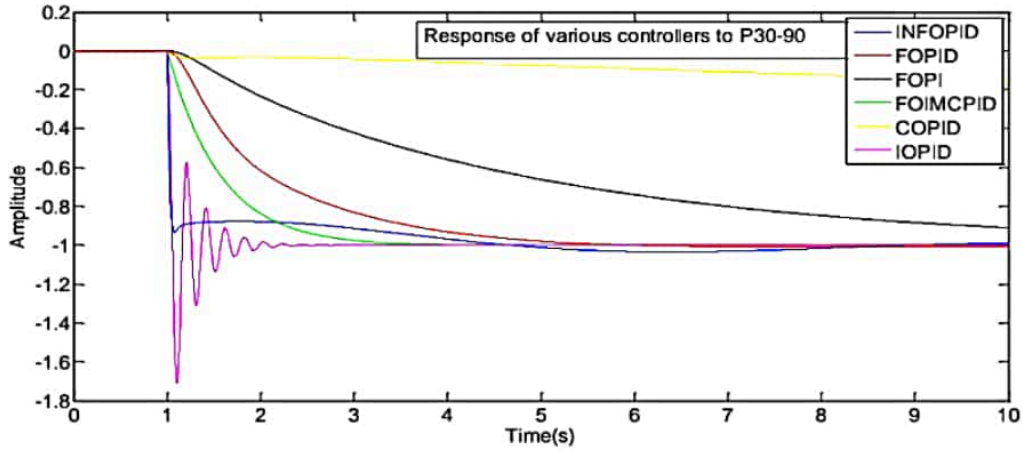

(b) Response of various controllers for transfer function model P_{90}^{30}

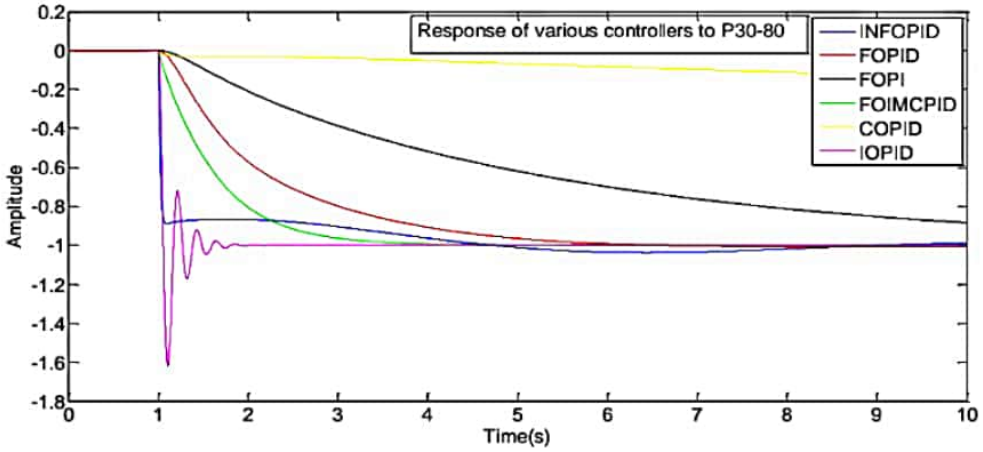

(c) Response of various controllers for transfer function model P_{80}^{30}

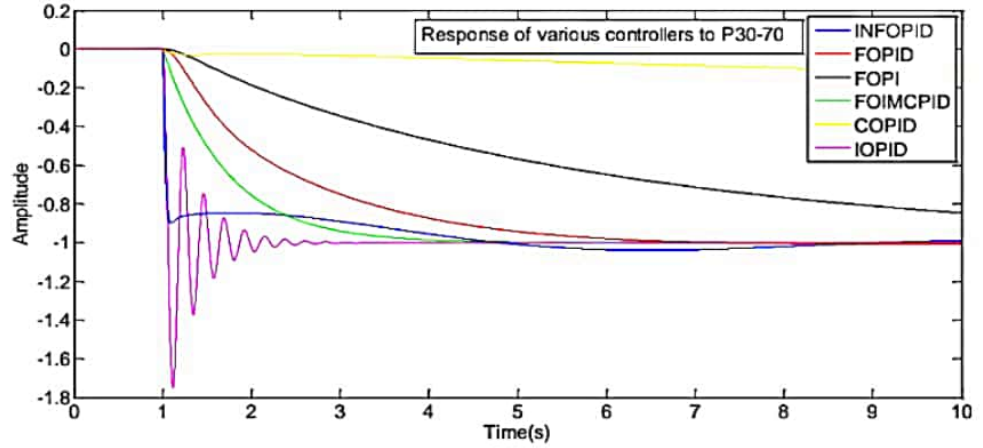

(d) Response of various controllers for transfer function model P_{70}^{30}

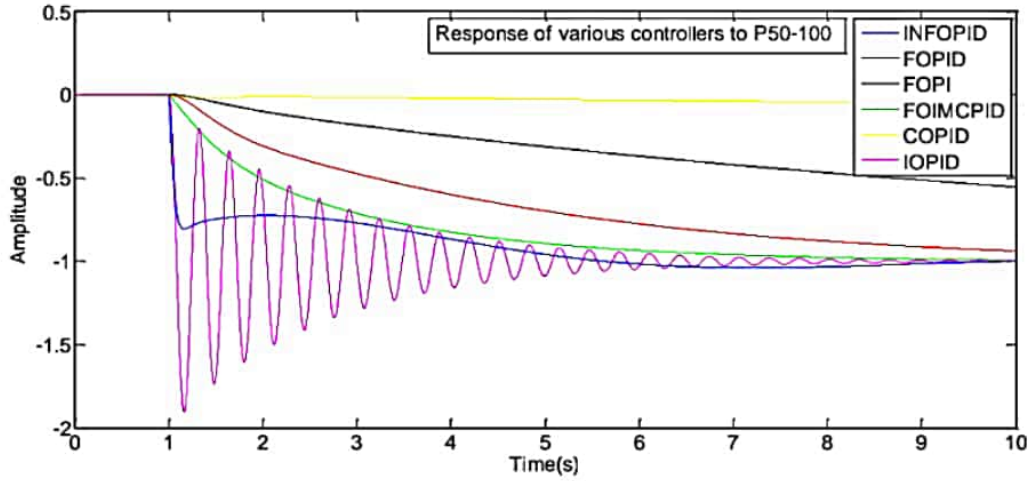

(e) Response of various controllers for transfer function model P_{100}^{50}

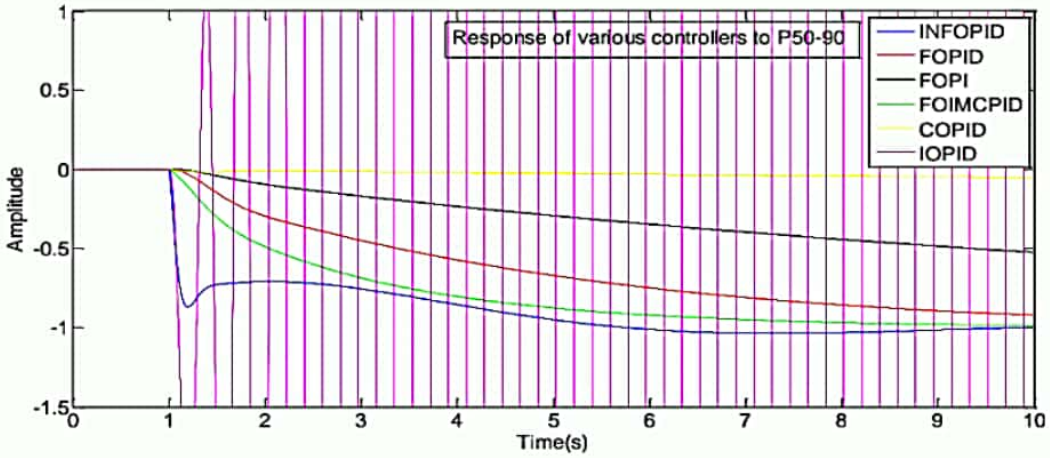

(f) Response of various controllers for transfer function model P_{90}^{50}

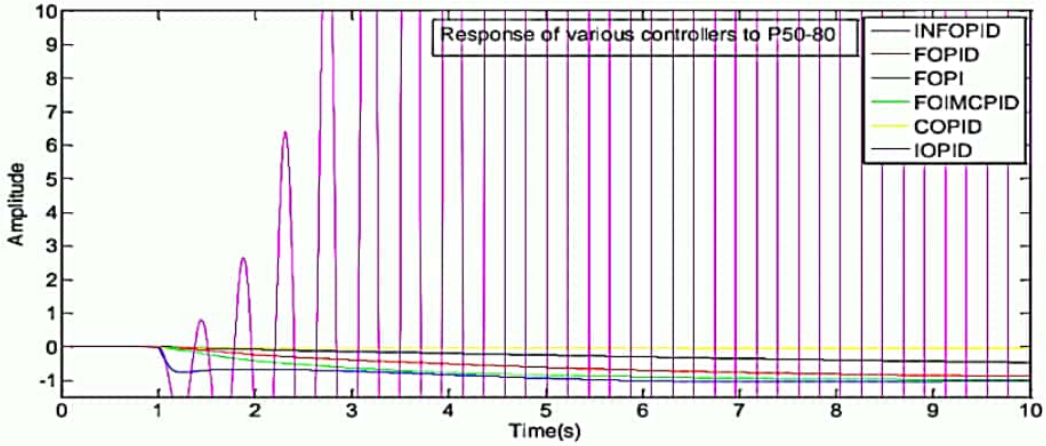

(g) Response of various controllers for transfer function model P_{80}^{50}

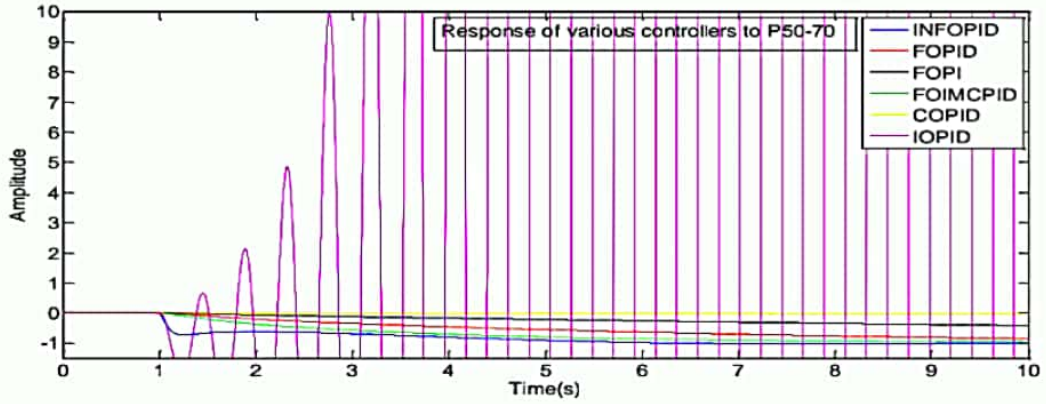

(h) Response of various controllers for transfer function model P_{70}^{50}

Figure 5.6 Response of various controllers to different step back conditions

5.2.2.3 Performance Analysis

In this section, the quantitative analysis of the designed INFOPID controller with the already existent controllers has been carried out by using different integral error criteria namely, Integral Time-Weighted Absolute Error (ITAE), Integral Squared Error (ISE), and Integral Absolute Error (IAE) The different error criterion for the designed controller and the controllers suggested in [168], [170], [219] and [182] has been given in Table 5.4 and Table 5.5. The collation of different error criterion for the different interval conditions for P_{100}^{30} described in section 5.2.2 has been presented in Table 5.4. Further, Table 5.5 presents the comparison of different error criterions for different step back conditions of the PHWR model. As seen from comparison, the designed INFOPID controller provides the best performance under the given perturbed situations as well as varying step back operating conditions and is hence, much more robust than the nominal controllers.

Table 5.4 Comparison of performance of various controllers under interval conditions

Interval Model	Controller	ITAE	ISE	IAE
G_8	FOPID	2.177	0.5123	1.026
	IMCFOPID	0.7757	0.2391	0.5036
	FOPI	11.51	1.677	3.122
	COPID	43.82	7.396	8.149
	Proposed INFOPID	**1.279**	**0.03741**	**0.3757**
G_7	FOPID	2.64	0.4482	1.017
	IMCFOPID	1.181	0.2229	0.5778
	FOPI	7.218	1.136	2.153
	COPID	37.87	6.044	7.318
	Proposed INFOPID	**1.032**	**0.02282**	**0.2715**
G_6	FOPID	2.375	0.3788	0.965
	IMCFOPID	1.07	0.1564	0.4951
	FOPI	11.7	1.409	2.982
	COPID	43.3	7.212	8.047
	Proposed INFOPID	**1.144**	**0.02896**	**0.3231**
G_5	FOPID	0.801	0.2691	0.4813
	IMCFOPID	0.3491	0.1255	0.2551
	FOPI	2.358	0.627	1.117

	COPID	34.88	5.221	6.788
	Proposed INFOPID	**0.4534**	**0.01297**	**0.1337**
G_4	FOPID	9.654	1.502	2.81
	IMCFOPID	3.64	0.7413	1.485
	FOPI	28.76	4.193	5.948
	COPID	47.5	8.415	8.702
	Proposed INFOPID	**2.892**	**0.194**	**0.9048**
G_3	FOPID	7.434	1.062	2.127
	IMCFOPID	3.829	0.5969	1.336
	FOPI	13.35	2.478	3.762
	COPID	45.22	7.828	8.386
	Proposed INFOPID	**2.593**	**0.1107**	**0.6988**
G_2	FOPID	10.01	1.242	2.692
	IMCFOPID	4.387	0.5487	1.461
	FOPI	27.75	3.838	5.704
	COPID	47.292	8.339	8.662
	Proposed INFOPID	**2.543**	**0.1479**	**0.7842**
G_1	FOPID	2.047	0.5685	1.008
	IMCFOPID	0.7398	0.2935	0.4967
	FOPI	11.43	1.696	3.117
	COPID	43.82	7.4	8.151
	Proposed INFOPID	**1.201**	**0.04616**	**0.3632**

Table 5.5 Performance comparison under different step back conditions

Step Back Condition	**Controller**	**ITAE**	**ISE**	**IAE**
P_{100}^{30}	FOPID	2.142	0.5231	1.021
	IMCFOPID	0.7501	0.2513	0.4985
	FOPI	11.49	1.681	3.121
	COPID	43.82	7.397	8.15
	Proposed INFOPID	**1.26**	**0.03969**	**0.3726**
P_{90}^{30}	FOPID	2.439	0.5802	1.127
	IMCFOPID	0.8617	0.2806	0.5543
	FOPI	12.99	1.863	3.393

	COPID	44.35	7.541	8.231
	Proposed INFOPID	**1.376**	**0.04649**	**0.4091**
P_{80}^{30}	FOPID	2.805	0.6963	1.25
	IMCFOPID	1.011	0.3142	0.6216
	FOPI	14.74	2.075	3.696
	COPID	44.87	7.682	8.309
	Proposed INFOPID	**1.501**	**0.05319**	**0.4495**
P_{70}^{30}	FOPID	3.346	0.7383	1.419
	IMCFOPID	1.221	0.3585	0.7133
	FOPI	16.93	2.356	4.067
	COPID	45.44	7.836	8.393
	Proposed INFOPID	**1.678**	**0.06703**	**0.5056**
P_{100}^{50}	FOPID	11.25	1.576	3.04
	IMCFOPID	4.65	0.7561	1.652
	FOPI	30	4.369	6.112
	COPID	47.64	8.452	8.721
	Proposed INFOPID	**2.892**	**0.2054**	**0.9217**
P_{90}^{50}	FOPID	12.35	1.7	3.235
	IMCFOPID	5.24	0.8192	1.783
	FOPI	31.08	4.573	6.276
	COPID	47.78	8.49	8.741
	Proposed INFOPID	**3.012**	**0.2362**	**0.9702**
P_{80}^{50}	FOPID	14.78	2.057	3.694
	IMCFOPID	6.438	1.023	2.09
	FOPI	33.45	5.072	6.648
	COPID	48.06	8.575	8.785
	Proposed INFOPID	**3.45**	**0.31**	**1.123**
P_{70}^{50}	FOPID	17.15	2.345	4.084
	IMCFOPID	7.966	1.1766	2.394
	FOPI	35.21	5.432	6.909
	COPID	48.25	8.63	8.813
	Proposed INFOPID	**3.753**	**0.3709**	**1.237**

5.2.3 Proposed FOPID Controller for Power Control in PHWR using ROM

This section discusses the design of the FOPID controller for control of power in PHWR that has been carried out using the concepts of MOR [12] and Stability Boundary Locus using specific gain-phase margin technique [164]. FOPID controllers provide improved control than conventional PID controller due to the two extra DOFs to better adjust the dynamic behavior of the system.

Figure 5.7 shows the feedback control system. Here, $C_t(A,\phi)$ represents a virtual compensator which is physically not present in the system. This gain phase tester has been used only for design or getting analytical information about FOPID controller.$C(s)$ denotes the controller and $G(s)$ denotes system model.

$$C_t(A,\phi) = Ae^{-j\phi} \tag{5.31}$$

The controller parameters for given value of gain margin A can be obtained by putting $\phi = 0$ and A can be set to 1 to find controller parameters for a given phase marginϕ.

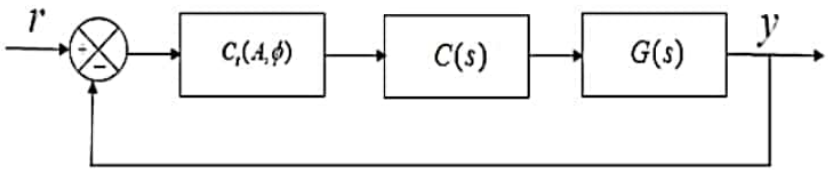

Figure 5.7 Feedback control system

The transfer function of the closed loop system shown in Figure 5.7 is obtained as

$$\frac{G(s)C(s)C_t(A,\phi)}{1+G(s)C(s)C_t(A,\phi)} \tag{5.32}$$

Hence, overall system's characteristic equation is of the form

$$p(s;k_p,k_i,k_d,\lambda,\mu) = 1 + C(s)G(s)C_t(A,\phi) = 0 \tag{5.33}$$

In order to design a robust control algorithm, the worst-case model has been taken into consideration i.e. P_{100}^{30}. G(s) has been taken as the ROM obtained from original higher order model of PHWR. While considering a second order reduced model, the following characteristic equation of system has been obtained by using Eq. (5.1) and (5.32) in Eq. (5.34)

$$p(s;k_p,k_i,k_d,\lambda,\mu) = 1 + Ae^{-j\phi}\left\{k_p + \frac{k_i}{s^\lambda} + k_d s^\mu\right\}\left\{\frac{ds+e}{as^2+bs+c}\right\} = 0 \tag{5.34}$$

$$\begin{gathered} p(s;k_p,k_i,k_d,\lambda,\mu) = 0 \\ a(s)^{2+\lambda} + b(s)^{1+\lambda} + c(s)^\lambda\left[dk_p(s)^{1+\lambda} + dk_i s + dk_d(s)^{1+\lambda+\mu} + ek_p(s)^\lambda + ek_i + ek_d(s)^{\lambda+\mu}\right] = 0 \end{gathered} \tag{5.35}$$

The stability of the system can be analyzed by seeing the location of the roots of the characteristic polynomial. The closed loop system is said to be stable if entire roots of Eq. (5.35) come in left side of the s - plane. If the equation in (5.35) has no roots in right half s -plane, then the region for which $p(s;k_p,k_i,k_d,\lambda,\mu) \in S'$ is called the stability region. The real root boundary (RRB) and the complex root boundary (CRB) define the boundary of stability domain for a FOPID controller. The boundaries are defined as

$$\begin{gathered} RRB: P(0;k_p,k_i,k_d,\lambda,\mu) = 0, for\omega \in (0,\infty), \\ CRB: P(j\omega;k_p,k_i,k_d,\lambda,\mu) = 0, for\omega \in (0,\infty) \end{gathered} \tag{5.36}$$

By putting $s = 0$ in (5.35), the RRB has been obtained as $k_i = 0$

Put $s = j\omega$ in (5.35) to find the CRB,

$$\begin{gathered} p(j\omega;k_p,k_i,k_d,\lambda,\mu) = a(j\omega)^{2+\lambda} + b(j\omega)^{1+\lambda} + c(j\omega)^\lambda + Ae^{-j\phi}[dk_p(j\omega)^{1+\lambda} + dk_i(j\omega) + \\ dk_d(j\omega)^{1+\lambda+\mu} + ek_p(j\omega)^\lambda + ek_i + ek_d(j\omega)^{\lambda+\mu}] = 0 \end{gathered} \tag{5.37}$$

The following mathematical identity has been used to solve Eq. (5.37),

$$j^\lambda = cos(\frac{\lambda\pi}{2}) + j\,sin(\frac{\lambda\pi}{2}) \tag{5.38}$$

The equation obtained is,

$$\begin{gathered} a\omega^{2+\lambda}\left\{cos(\lambda+2)\frac{\pi}{2} + j\,sin(\lambda+2)\frac{\pi}{2}\right\} + b\omega^{1+\lambda}\left\{cos(\lambda+1)\frac{\pi}{2} + j\,sin(\lambda+1)\frac{\pi}{2}\right\} + c\omega^\lambda\left\{cos\,\lambda\frac{\pi}{2} + j\,sin\,\lambda\frac{\pi}{2}\right\} \\ + A(cos\,\phi - j\,sin\,\phi)\begin{Bmatrix} dk_p w^{1+\lambda}[cos(\lambda+1)\frac{\pi}{2} + j\,sin(\lambda+1)\frac{\pi}{2}] + dk_i jw + \\ dk_d w^{\lambda+\mu+1}[cos(\lambda+\mu+1)\frac{\pi}{2} + j\,sin(\lambda+\mu+1)\frac{\pi}{2}] \\ +ek_p w^\lambda[cos\,\lambda\frac{\pi}{2} + j\,sin\,\lambda\frac{\pi}{2}] + ek_i + ek_d w^{\lambda+\mu}[cos(\lambda+\mu)\frac{\pi}{2} + j\,sin(\lambda+\mu)\frac{\pi}{2}] \end{Bmatrix} = 0 \end{gathered} \tag{5.39}$$

Eq. (5.39) has been expressed in form of Eq. (5.40)

$$P(\omega,k_p,k_i,k_d,\lambda,\mu) = Re\{P(\omega,k_p,k_i,k_d,\lambda,\mu)\} + j\,Im\{P(\omega,k_p,k_i,k_d,\lambda,\mu)\} \tag{5.40}$$

Next, equate imaginary and real parts equal to zero:

Real part:

$$a\omega^{2+\lambda}\cos(\lambda+2)\frac{\pi}{2}+b\omega^{1+\lambda}\cos(\lambda+1)\frac{\pi}{2}+c\omega^{\lambda}\cos\lambda\frac{\pi}{2}+dAk_pw^{1+\lambda}[\cos(1+\lambda)\frac{\pi}{2}-\phi] + dAk_iw\sin\phi+dAk_dw^{\lambda+\mu+1}[\cos(1+\lambda+\mu)\frac{\pi}{2}-\phi]+eAk_pw^{\lambda}[\cos(\lambda\frac{\pi}{2} - \phi)]+eAk_i\cos\phi+eAk_dw^{\lambda+\mu}[\cos(\mu+\lambda)\frac{\pi}{2}-\phi]=0 \quad (5.41)$$

Imaginary part:

$$a\omega^{2+\lambda}\sin(\lambda+2)\frac{\pi}{2}+b\omega^{1+\lambda}\sin(\lambda+1)\frac{\pi}{2}+c\omega^{\lambda}\sin\lambda\frac{\pi}{2}+dAk_pw^{1+\lambda}[\sin(1+\lambda)\frac{\pi}{2}-\phi] + dAk_iw\cos\phi+dAk_dw^{\lambda+\mu+1}[\sin(1+\lambda+\mu)\frac{\pi}{2}-\phi]+eAk_pw^{\lambda}[\sin(\lambda\frac{\pi}{2} - \phi)]-eAk_i\sin\phi+eAk_dw^{\lambda+\mu}[\sin(\mu+\lambda)\frac{\pi}{2}-\phi]=0 \quad (5.42)$$

Eq. (5.41) and Eq. (5.42) have been attained in terms of k_d, k_p and k_i. There are two ways in which these equations can be solved [164]:

- The RRB & CRB are plotted in the $(k_p - k_i)$ plane for several values of $\lambda \in (0,2)$ and $\mu \in (0,2)$ fixing the value of k_d arbitrarily.
- The value of k_i can be fixed capriciously and RRB & CRB are plotted in the $(k_p - k_d)$ plane for numerous values of $\lambda \in (0,2)$ and $\mu \in (0,2)$.

The value of k_d has been kept fixed and Eq. (5.41) and Eq. (5.42) have been solved concurrently to obtain k_p and k_i. The CRB and RRB has been traced using these equations in the $(k_p - k_i)$ plane for fix value of $\mu \in (0,2)$ and $\lambda \in (0,2)$ as ω varies from$(0,\infty)$ [164].

$$k_p = \frac{-\begin{Bmatrix} Adk_dw^{\lambda+\mu+1}\cos((1+\lambda+\mu)\frac{\pi}{2}-\phi)+eAk_dw^{\lambda+\mu}\cos((\lambda+\mu)\frac{\pi}{2}-\phi) \\ +aw^{2+\lambda}\cos(2+\lambda)\frac{\pi}{2}+bw^{1+\lambda}\cos(1+\lambda)\frac{\pi}{2}+cw^{\lambda}\cos\lambda\frac{\pi}{2} \\ +eA\cos\phi\,k_i+dAk_iw\sin\phi \end{Bmatrix}}{dAw^{1+\lambda}\cos((1+\lambda)\frac{\pi}{2}-\phi)+eAw^{\lambda}\cos(\lambda\frac{\pi}{2}-\phi)} \quad (5.43)$$

$$k_i = \frac{-\begin{Bmatrix} adAw^{2\lambda+3}\sin(\frac{\pi}{2}+\phi)+bdAw^{2\lambda+2}\sin\phi+cdAw^{1+2\lambda}\sin(\frac{-\pi}{2}+\phi)+ \\ d^2A^2k_dw^{2+2\lambda+\mu}\sin\mu\frac{\pi}{2}+edA^2k_dw^{1+2\lambda+\mu}\sin(\mu\frac{\pi}{2}-\frac{\pi}{2})+aeAw^{2+2\lambda}\sin(\pi+\phi)+ \\ beAw^{1+2\lambda}\sin(\frac{\pi}{2}+\phi)+ceAw^{2\lambda}\sin\phi+deA^2k_dw^{1+2\lambda+\mu}\sin(\mu+1)\frac{\pi}{2}+e^2A^2k_dw^{2\lambda+\mu}\sin\mu\frac{\pi}{2} \end{Bmatrix}}{d^2A^2w^{2+\lambda}\cos(1+\lambda)\frac{\pi}{2}+edA^2w^{1+\lambda}(\cos\lambda\frac{\pi}{2}-\sin(1+\lambda)\frac{\pi}{2})-A^2e^2w^{\lambda}\sin\lambda\frac{\pi}{2}} \quad (5.44)$$

A plot has been obtained between $k_p$and k_i for fixed value of λ and μ; the region that has been obtained is termed the stability region i.e., all the values of $k_p$and k_i that lie within this area possess a capability to stabilize the system. Hence, the stability regions for all combinations of λ and μ have been acquired by varying $\lambda \in (0,2)$and $\mu \in (0,2)$.

In order to design a robust control algorithm, the worst-case model has been taken into consideration i.e. P_{100}^{30}. Its second order reduced model is given by Eq. (5.45)

$$G_{12}(s) = \frac{538.3s + 1785}{s^2 - 3.623s + 84.56} \tag{5.45}$$

Using the method discussed above, the following expressions of $k_p$and $k_i$have been obtained for second order reduced model of P_{100}^{30} . Here, $k_d = 0.005, \phi = 45^{\circ}, A = 3dB$ is chosen.

$$k_p = \frac{-\begin{Bmatrix} 8.0745w^{\lambda+\mu+1}\cos((1+\lambda+\mu)\frac{\pi}{2} - \frac{\pi}{4}) + 26.775w^{\lambda+\mu}\cos((\lambda+\mu)\frac{\pi}{2} - \frac{\pi}{4}) \\ +w^{2+\lambda}\cos(2+\lambda)\frac{\pi}{2} - 3.623w^{1+\lambda}\cos(1+\lambda)\frac{\pi}{2} + 84.56w^{\lambda}\cos\lambda\frac{\pi}{2} \\ +3786.55k_i + 1141.9k_iw \end{Bmatrix}}{1614.9w^{1+\lambda}\cos((1+\lambda)\frac{\pi}{2} - \frac{\pi}{4}) + 5355w^{\lambda}\cos(\lambda\frac{\pi}{2} - \frac{\pi}{4})} \tag{5.46}$$

$$k_i = \frac{-\begin{Bmatrix} 1141.9w^{2\lambda+3} - 7924.254w^{2\lambda+2} - 110280.21w^{1+2\lambda}) \\ +13039.51w^{2+2\lambda+\mu}\sin\mu\frac{\pi}{2} + \\ +320191.24w^{2\lambda} + 143380w^{2\lambda+\mu}\sin\mu\frac{\pi}{2} \end{Bmatrix}}{2.6079 \times 10^6 w^{2+\lambda}\cos(1+\lambda)\frac{\pi}{2} + -28676025w^{\lambda}\sin\lambda\frac{\pi}{2}} \tag{5.47}$$

Next, the appropriate values of k_p, k_i, λ and μ have to be calculated that can give suitable performance for the third order reduced order system as well.

The third order reduced model is given by Eq. (5.48)

$$G_{13}(s) = \frac{545.8s^2 + 1775s + 698.6}{s^3 - 3.59s^2 + 84.43s + 2.82} \tag{5.48}$$

The values of k_p and k_i can be obtained utilizing the similar method for the third order reduced model as well. The equations for k_p, k_i for obtaining the stability region of third order model as given as:

$$k_p = \frac{\begin{bmatrix} -w^{3+\lambda}\cos(3+\lambda)\frac{\pi}{2} + 3.59w^{2+\lambda}\cos(2+\lambda)\frac{\pi}{2} - 84.43w^{1+\lambda}\cos(1+\lambda)\frac{\pi}{2} \\ -2.82w^{\lambda}\cos\lambda\frac{\pi}{2} + 1157.8k_i w^2 - 3765.3k_i w - 1482k_i \\ -8.187w^{\lambda+\mu+2}\cos((\lambda+\mu+2)\frac{\pi}{2} - \frac{\pi}{4}) \\ -26.625w^{\lambda+\mu+1}\cos((\lambda+\mu+1)\frac{\pi}{2} - \frac{\pi}{4}) - 10.479w^{\lambda+\mu}\cos((\lambda+\mu)\frac{\pi}{2} - \frac{\pi}{4}) \end{bmatrix}}{1637.4w^{2+\lambda}\cos((\lambda+2)\frac{\pi}{2} - \frac{\pi}{4}) + 5325w^{1+\lambda}\cos((\lambda+1)\frac{\pi}{2} - \frac{\pi}{4}) + 2095.8w^{\lambda}\cos(\lambda\frac{\pi}{2} - \frac{\pi}{4})} \quad (5.49)$$

$$k_i = \frac{\begin{matrix} -(11157.8w^{5+2\lambda} - 391.3w^{4+2\lambda} - 112754w^{3+2\lambda} + 3.1996\times10^5 w^{2+2\lambda} - 1.3574\times10^5 w^{1+2\lambda} + 13405w^{4+2\lambda+\mu}\sin\mu\frac{\pi}{2} \\ +43596w^{3+2\lambda+\mu}(\sin(\mu\frac{\pi}{2} - \frac{\pi}{2}) + \sin(\mu\frac{\pi}{2} + \frac{\pi}{2})) + w^{2+2\lambda+\mu}(17158\sin(\mu\frac{\pi}{2} - \pi) + 1.4178\times10^5\sin\mu\frac{\pi}{2} \\ +17158\sin(\mu+2)\frac{\pi}{2}) + 55801w^{1+2\lambda+\mu}(\sin(\mu+1)\frac{\pi}{2} + \sin(\mu\frac{\pi}{2} - \frac{\pi}{2})) + 4179.1w^{2\lambda} + 21962w^{2\lambda+\mu}\sin\mu\frac{\pi}{2}) \end{matrix}}{\begin{matrix} 2.6811\times10^6 w^{4+\lambda}\sin(\lambda+2)\frac{\pi}{2} + 8.7192\times10^6 w^{3+\lambda}(\cos(\lambda+2)\frac{\pi}{2} + \sin(\lambda+1)\frac{\pi}{2}) + w^{2+\lambda}(-3.4317\times10^6\sin(\lambda+2)\frac{\pi}{2} + \\ 28355625\cos(\lambda+1)\frac{\pi}{2} + 3.4317\times10^6\sin\lambda\frac{\pi}{2}) + 11160135w^{1+\lambda}(\cos\lambda\frac{\pi}{2} - \sin(\lambda+1)\frac{\pi}{2}) - 4.3924\times10^6 w^{\lambda}\sin\lambda\frac{\pi}{2} \end{matrix}} \quad (5.50)$$

In this case, the controller parameters have been selected as, $k_p = 0.015, k_i = 0.004, k_d = 0.005,$ $\lambda = 0.9, \mu = 0.9$ the FOPID controller attained is given by Eq. (5.51).

$$C(s) = 0.015 + \frac{0.004}{s^{0.9}} + 0.005s^{0.9} \quad (5.51)$$

5.2.3.1 Stability Analysis

In this section, stability testing of the closed loop PHWR system has been illustrated for one of the operating conditions P_{100}^{30} (transfer function$G_1(s)$) of PHWR given in Table 4.1. The stability analysis of the original higher order system has been done by estimating the location of the roots of its characteristic equation. The characteristic equation can be written as,

$$P_1(s) = 1 + \left(\frac{(44.79s^5 + 8408s^4 + 7.687X\times10^4 s^3 + 8.42\times10^6 s^2 - 2.561\times10^7 s + 1.336\times10^7)}{(s^6 + 12.31s^5 + 1088s^4 + 6624s^3 + 5.75\times10^4 s^2 + 7.683\times10^5 s + 6.946\times10^4)}\right) * \left(0.015 + \frac{0.004}{s^{0.9}} + 0.005s^{0.9}\right) = 0 \quad (5.52)$$

The characteristic equation can be written as,

$$\begin{aligned} P_1(s) = {} & s^{6.9} + 0.22395s^{6.8} + 12.981s^{5.9} + 42.04s^{5.8} + 0.17916s^5 + 1214.12s^{4.9} \\ & + 384.35s^{4.8} + 33.632s^4 + 7777.05s^{3.9} + 42100s^{3.8} + 307.48s^3 \\ & + 183800s^{2.9} - 128000s^{2.8} + 33680s^2 + 384000s^{1.9} + 66800s^{1.8} \\ & - 102400s + 269860s^{0.9} + 53440 = 0 \end{aligned} \quad (5.53)$$

To perform the stability analysis, the FO polynomial has been first transformed into the integer order polynomial:

$$P_1(s) = s^{\frac{69}{10}} + 0.22395s^{\frac{68}{10}} + 12.981s^{\frac{59}{10}} + 42.04s^{\frac{58}{10}} + 0.17916s^{\frac{50}{10}} + 1214.12s^{\frac{49}{10}} + 384.35s^{\frac{48}{10}} + 33.632s^{\frac{40}{10}} + 7777.05s^{\frac{39}{10}} + 42100s^{\frac{38}{10}} + 307.48s^{\frac{30}{10}} + 183800s^{\frac{29}{10}} - 128000s^{\frac{28}{10}} + 33680s^{\frac{20}{10}} + 384000s^{\frac{19}{10}} + 66800s^{\frac{18}{10}} - 102400s + 269860s^{\frac{9}{10}} + 53440 = 0 \quad (5.54)$$

In Eq. (5.54), substituting $s^{\frac{1}{10}} = w$, the following equation is obtained,

$$P_1(s) = w^{69} + 0.22395w^{68} + 12.981w^{59} + 42.04w^{58} + 0.17916w^{50} + 1214.12w^{49} + 384.35w^{48} + 33.632w^{40} + 7777.05w^{39} + 42100w^{38} + 307.48w^{30} + 183800w^{29} - 128000w^{28} + 33680w^{20} + 384000w^{19} + 66800w^{18} - 102400w^{10} + 269860w^{9} + 53440 = 0 \quad (5.55)$$

The roots obtained for Eq. (5.55) have been given in Table 5.6.

Table 5.6: Roots of characteristic polynomial $P_1(s)$

-0.8026+*i* 0.0000	-0.6284+*i* 0.5042	0.7829-*i* 0.3641
-0.7858+*i* 0.7171	-0.9219-*i* 0.5136	0.3695-*i* 0.7470
-0.8298+*i* 1.6037	-1.7847-*i* 0.2779	0.7684+*i* 0.7041
-0.9245+*i* 0.4047	0.2037+*i* 1.0213	1.2566-*i* 1.2772
1.0405-*i* 0.1154	-0.2170-*i* 1.0400	-0.9719-*i* 0.2273
-1.6133+*i* 0.8180	0.7829+*i* 0.3641	-0.1764+*i* 0.7960
0.4332-*i* 0.9657	0.6102-*i* 0.7498	0.4332+*i* 0.9657
-1.0546-*i* 0.1226	0.8834+*i* 0.2078	-0.2884-*i* 1.7676
-0.2884+*i* 1.7676	-0.9245-*i* 0.4047	0.6102+*i* 0.7498
-0.6294-*i* 0.7628	-0.4409+*i* 0.9491	-0.6284-*i* 0.5042
0.8077-*i* 1.5922	1.7625+*i* 0.2896	-0.7858-*i* 0.7171
-1.7847+*i* 0.2779	1.7625-*i* 0.2896	-1.2786+*i* 1.2655
-1.2786-*i* 1.2655	0.6090+*i* 0.8073	0.9905-*i* 0.3152
-0.5131+*i* 0.8792	0.6090-*i* 0.8073	-1.0546+*i* 0.1226
0.9137-*i* 0.5231	-0.5131-*i* 0.8792	-0.1764-*i* 0.7960
0.2664+*i* 1.7791	0.3695+*i* 0.7470	-0.0290+*i* 0.9835
-0.6294+*i* 0.7628	-0.8298-*i* 1.6037	1.5911-*i* 0.8065
0.9905+*i* 0.3152	0.9137+*i* 0.5231	-0.2170+*i* 1.0400
0.8834-*i* 0.2078	0.2664-*i* 1.7791	0.2037-*i* 1.0213
-0.4409-*i* 0.9491	0.0876-*i* 1.0107	-0.0290-*i* 0.9835
-1.6133-*i* 0.8180	-0.9719+*i* 0.2273	0.7684-*i* 0.7041
-0.9219+*i* 0.5136	1.5911+*i* 0.8065	1.0405+*i* 0.1154
0.0876+*i* 1.0107	0.8077+*i* 1.5922	1.2566+*i* 1.2772

Now, from the roots of the polynomial (5.55) obtained above, the set of physically realizable rootsϕ_i, have been determined using the condition $|arg(\phi_i)| < \frac{\pi}{10}$. In this case, the physically realizable roots have been obtained as:

$$|arg(\phi_1)| = 0.308 \quad (5.56)$$

$$|arg(\phi_2)| = 0.231 \quad (5.57)$$

$$|arg(\phi_3)| = 0.162 \quad (5.58)$$

$$|arg(\phi_4)| = 0.308 \quad (5.59)$$

$$|arg(\phi_5)| = 0.231 \quad (5.60)$$

$$|arg(\phi_6)| = 0.162 \quad (5.61)$$

For all the physically realizable roots obtained above, the stability condition $|arg(\phi_i)| > \frac{\pi}{20}$ has been checked. If all the realizable roots of the polynomial follow this condition, then the system is considered as a stable system. Since, all the values given by Eq. (5.56) - (5.61) lies within the range of 0.157 to 0.314 (stability boundary values); thus, with the proposed controller the system becomes stable which was earlier unstable.

5.2.3.2 Simulation Results and Performance Analysis

Three integral error criteria (IAE, ITAE, ISE) have been used for the performance analysis of the designed FOPID controller for the original higher order model of PHWR (under step back condition). The collation of the suggested controller with the existent controllers [175][167] as presented by Saha *et al.* and Patre *et al.* has been shown in the Figure 5.8 and Table 5.7 for P_{100}^{30} operating condition of PHWR.

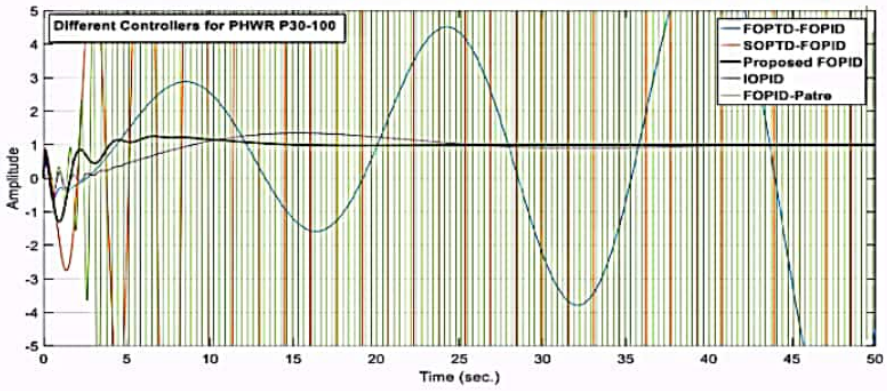

Figure 5.8 Performance of different controllers for P_{100}^{30}

Table 5.7 Integral error measures for P_{100}^{30} operating condition of PHWR

Model	Controller	ISE	IAE	ITAE	Settling time
P_{100}^{30}	**Proposed FOPID**	**4.95**	**4.98**	**24.9**	**13 sec.**
	FOPTD-FOPID	641.7	140.3	4672	Oscillatory
	SOPTD-FOPID	3.2×10^{14}	4.02×10^{7}	1.8×10^{9}	Unstable
	IOPID	5.86	10.33	115.6	24 sec.
	FOPID-Patre	1.33×10^{54}	1.276×10^{27}	6.283×10^{28}	Unstable

As evident from Figure 5.8, the controllers designed by Saha *et al.* [167] using FOPTD and SOPTD ROMs give unstable results when applied to original higher order system whereas the proposed FOPID gives a stable response. It has also been observed that the integer order PID controller has a higher settling time in comparison to the proposed FOPID controller. The same has been observed from the quantitative analysis shown in Table 5.7. The error is exponentially increasing for the controllers designed by Saha *et al.* [167] and Patre *et al.* [175] .

The performance of the various controllers on operating condition P_{90}^{30}, P_{80}^{30}, P_{70}^{30} has been shown in Figures 5.9, 5.10, 5.11 and Tables 5.8, 5.9, 5.10 respectively. The settling time of the proposed system has been observed to be lesser in comparison to other controllers when the proposed controller has been applied to different operating conditions of the original PHWR model.

The percentage improvement of the proposed controller over conventional integer order PID controller in terms of settling time has been calculated as:

$$\%\ improvement = \frac{Settling\ time\ of\ proposed\ FOPID - Settling\ time\ of\ IOPID}{Settling\ time\ of\ IOPID} \times 100$$

From Table 5.7, it has been observed that the proposed controller gives a reduction by 45.833% in settling time of the worst case operating condition. Similarly, for other operating conditions, a reduction by 40%, 41.37% and 42.42% in settling time has been observed as shown in Tables 5.8, 5.9 and 5.10 respectively.

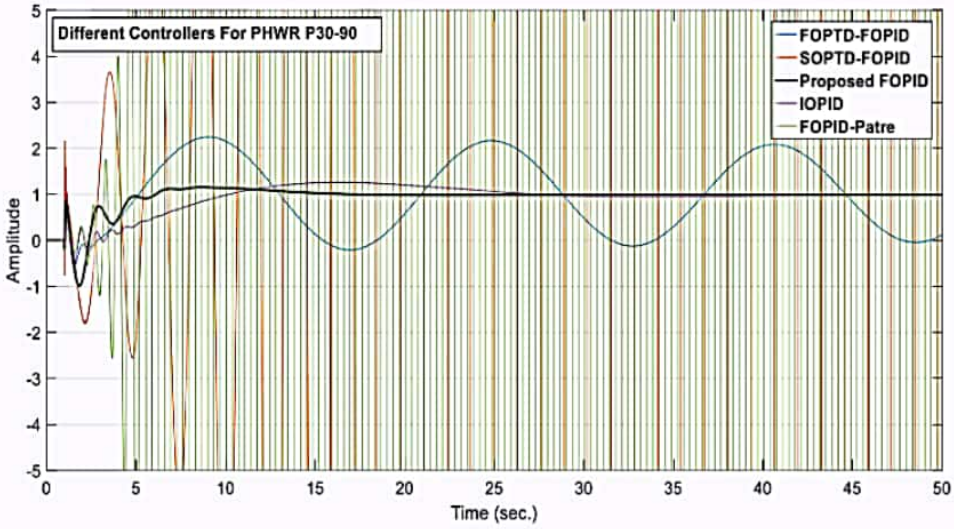

Figure 5.9 Performance of different controllers for P_{90}^{30}

Table 5.8 Integral error measures of various controllers for P_{90}^{30} operating condition

Model	Controller	ISE	IAE	ITAE	Settling time
P_{90}^{30}	**Proposed FOPID**	**3.516**	**4.125**	**25.31**	**6 sec.**
	FOPTD-FOPID	33.82	36.69	916.4	Oscillatory
	SOPTD-FOPID	1.104×10^{11}	8.563×10^{5}	3.93×10^{7}	Unstable
	IOPID	4.816	8.572	90.49	10 sec.
	FOPID-Patre	2.166×10^{48}	1.692×10^{24}	8.324×10^{25}	Unstable

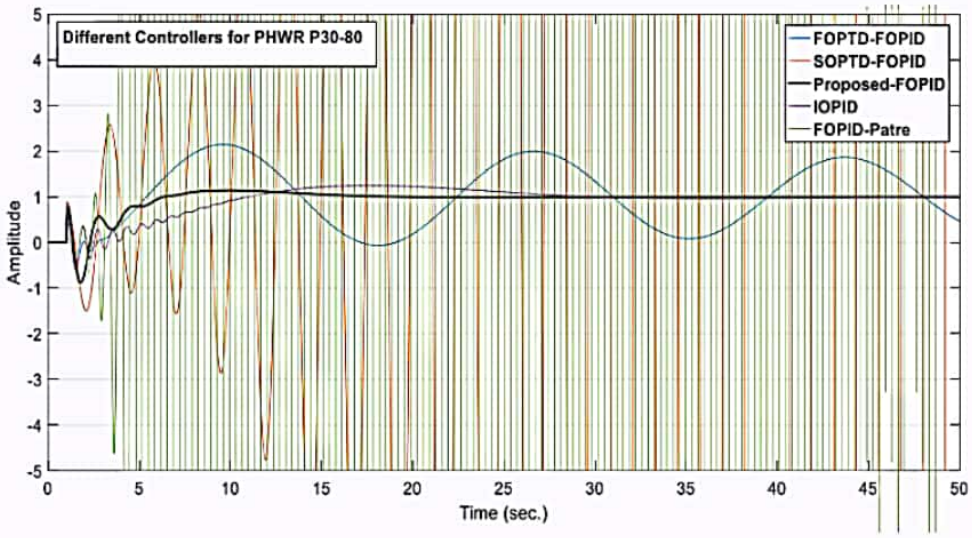

Figure 5.10 Performance of different controllers for P_{80}^{30}

Table 5.9 Integral error measures of various controllers for P_{80}^{30} operating condition

Model	Controller	ISE	IAE	ITAE	Settling time
P_{80}^{30}	**Proposed FOPID**	**3.34**	**4.338**	**28.21**	**17 sec.**
	FOPTD-FOPID	24.83	30.97	725.6	Oscillatory
	SOPTD-FOPID	1.604×10^{6}	4393	1.87×10^{5}	Unstable
	IOPID	5.023	8.852	95.75	29 sec.
	FOPID-Patre	4.26×10^{59}	6.812×10^{29}	3.36×10^{31}	Unstable

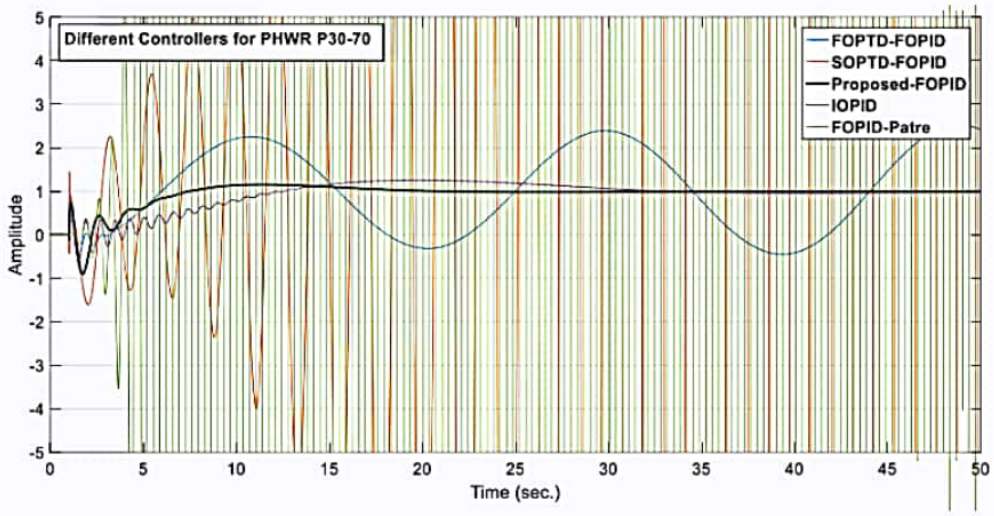

Figure 5.11 Performance of different controllers for P_{70}^{30}

Table 5.10 Integral error measures of various controllers for P_{70}^{30} operating condition

Model	Controller	ISE	IAE	ITAE	Settling time
P_{70}^{30}	**Proposed FOPID**	**3.79**	**5.172**	**36.64**	**19 sec.**
	FOPTD-FOPID	46.76	43	1154	Oscillatory
	SOPTD-FOPID	2.2×10^{6}	5150	2.19×10^{5}	Unstable
	IOPID	5.89	10.28	124.9	33 sec.
	FOPID-Patre	1.11×10^{57}	3.54×10^{28}	1.74×10^{30}	Unstable

It has been perceived from this comparison that the proposed FOPID controller performs very well under the different step back operating situations and is hence much more robust than the other controllers. The controller provides the faster set point tracking capability even under various operating situations of PHWR. The proposed controller responds satisfactorily well when applied to the original higher order model of PHWR using the ROM for its design.

5.3 Fractional Order Controller Design for Load Frequency Control in Perturbed Two Area Interconnected Power System

In multiarea power systems, the frequency deviations and the scheduled tie line power are mainly due to the variance in the generation and demand. The problem of acknowledging the real power variations in the system is referred to as LFC. So, the minimization of the frequency and tie-line scheduled power variations are the main objectives of LFC in an interconnected power system. It is also important to improve the stability of inter-area oscillations for the better system performance [223].With the advent of rise in complexity in modern power systems, the researchers are motivated to develop controller design techniques to solve these problems effectively. Different researchers have proposed various control schemes of LFC for single [41], [206], [224]–[226] as well as multi area systems [210], [224], [227]–[237]. Nowadays, many LFC control strategies have been presented to guarantee improved disturbance rejection in the wider range whilst maintaining robustness against systems parametric variations. Successful applications of optimal control [235], [238], [239], robust control using an iterative LMI [240][241], QFT scheme [242] , model based control using MPC [224], [236]and IMC [243]–[245], fractional-order control [41], [206], [246], PID control using artificial intelligence techniques [247]–[251], as well as human behavior adapted optimization algorithms [107], [190], [252], [253] have also been reported in literature for LFC.

When LFC is designed, the uncertainties arising in the power system because of alteration in the system parameters, variations in load or modelling errors become one of the critical problems. Hence, these uncertainties cannot be neglected while designing a controller. Otherwise, the designed controller may not meet the actual plant specifications as the system parameters are partially known. Earlier, the control laws were developed based on the linearized models with selected parameters and then experimented on the perturbed model. Today, the solutions for the best controller parameters are obtained considering the parametric uncertainties in advance. The controller evaluation is done either while carrying out the stability analysis of the control system or after designing the controller. Additionally, the fixed parameter PID which is commonly used in the LFC application may cause instability in the system because of its derivative action which augments the disturbances immensely.

Toulabi *et al.* [223] presented a new robust PI design for robust stability analysis and employed intelligent techniques to tune PI parameters. Majhi *et al.* [224] proposed a new control configuration in which plant dynamics is estimated using identification technique and then the controller is designed using the Laurent series. Then, the robust stability examination of the LFC under varying parametric perturbation of the plant has been carried out. Both the methods utilized Kharitonov's theorem to monitor the robustness while controller designing. Sondhi *et al.* [206] proposed a FOPID controller for the perturbed model of the single area LFC using the same theorem. Sahaj *et al.* [210] proposed the robust PID controller design for LFC problem using the above theorem for a multi-area power system. Saxena *et al.* [245] employed two methods, named Padé and Routh approximation model reduction techniques to create a controller for single-area power system. This controller satisfies robust and optimal response. Further, Saxena *et al.* proposed a FOPID controller for LFC of single and multi-area power system to improve power system performance via reduced-order modelling scheme [43]. Both the methods are capable of rejecting the disturbance and at the same time handling the parametric uncertainty very efficiently. A sliding mode controller has been designed in [225] using an equivalent ROM for single area power system consisting of two reheated thermal units.

5.3.1 Mathematical Modelling of LFC

The power system is an extensive system divided into areas. Each area is integrated to its neighboring areas with the help of tie lines through which power sharing occurs. LFC modulates the power flow between the areas keeping the frequency constant against any load change. Each area must also maintain the tie line power flow to the pre-specified value. The model of LFC is composed of a machine, a turbine, a governor, load and droop characteristics. The model of two area interconnected system with nonreheated turbine has been shown in Figure 5.12 [246]. The terminology of the parameters utilized in the two area interconnected system has been shown in Table 5.11 [246].

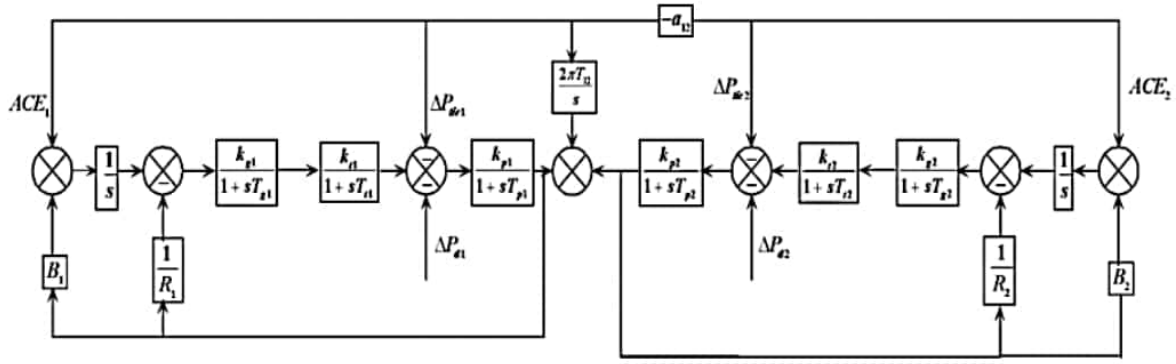

Figure 5.12 Block diagram of two area interconnected power system

Table 5.11 Nomenclature of power systems components

I	Subscript referred to area 1, 2, ...
H	Generator inertia constant
$\Delta P_d(t)$	Load disturbance (p.u. MW)
$\Delta X_G(t)$	Change in governor valve position (p.u. MW)
$\Delta P_G(t)$	Change in generator output (p.u. MW)
R	Speed regulation because of governor action (Hz/p.u. MW)
K_p	Electric system gain
$\Delta P_{T,i}(t)$	Overall tie-line flow in control area i (p.u. MW)
T_t	Time constant of turbine (s)
D	Frequency-sensitive load damping coefficient
T_g	Time constant of governor (s)
$\Delta f(t)$	Change in frequency (Hz)
B_i	Frequency Bias of control area i (p.u. MW/Hz)
T_{ij}	Tie-line synchronizing coefficient between area i and j
N	Number of control areas
T_r	Steam turbine reheat time constant(s)
K_r	Steam turbine reheat coefficient(s)

Mathematically, the system can be constituted as

$$G(s) = \frac{G_p(s)G_t(s)G_g(s)}{1 + G_p(s)G_t(s)G_g(s)/R} \tag{5.62}$$

Where $\frac{1}{R}$ depicts droop characteristics, $G_g(s)$ illustrates the governor dynamics

$$G_g(s) = \frac{1}{T_g s + 1} \tag{5.63}$$

$G_t(s)$ illustrates the turbine dynamics

$$G_t(s) = \frac{1}{T_t s + 1} \tag{5.64}$$

$G_p(s)$ illustrates the power system (load and machine) dynamics

$$G_p(s) = \frac{1}{2H(s) + D} \tag{5.65}$$

The model can be constituted as in Eq. (5.66) and Eq. (5.67) using Eqs. (5.62) -(5.65):

$$G_{TA}(s) = \frac{G_p(s)G_t(s)G_g(s)}{1 + G_p(s)G_t(s)G_g(s)/R} \tag{5.66}$$

$$G_{TA}(s) = \frac{R}{2T_g RT_T Hs^3 + (2T_T RH + 2HRT_g + RT_g T_T D)s^2 + (2RH + RT_T D + RT_g D)s + (RD + 1)} \tag{5.67}$$

Considering the variations in parameters for area 1:

$$R \in [0.025,0.075], H \in [2.5,7.5], T_g \in [0.10,0.30], D \in [0.30,0.90], T_t \in [0.25,0.75] \tag{5.68}$$

The intervals have been descripted by considering 50% of lower and upper limit uncertainties. Solving the model in Eq. (5.66) to the form given in Eq. (5.69) for area 1.

$$G_{TA1}(s) = \frac{N_{TA1}(s)}{D_{TA1}(s)} = \frac{c}{d_3 s^3 + d_2 s^2 + d_1 s + d_0} \tag{5.69}$$

The nominal parameter values are tabulated in Table 5.12 [246]

Table 5.12 Two-area interconnected system parameters

Component	Area 1	Area 2
Load change ΔP_L	0.01 p.u.	0
Base power (MVA) S_B	1,000	1,000
Turbine time constant T_t	0.50	0.60
Governor time constant T_g	0.20	0.30
Inertia constant H	5.00	4.00

Damping coefficient D	0.60	0.90
Speed regulation R	0.05	0.0625
Synchronizing power coefficientP_s	2	

For area 1

$$\begin{aligned} c &= R \in [0.025,0.075] \\ d_3 &= 2T_gRT_TH \in [0.003125,0.253125] \\ d_2 &= (2T_TRH + 2HRT_g + RT_gT_TD) \in [0.0439375,1.1964375] \\ d_1 &= (2RH + RT_TD + RT_gD) \in [0.127625,1.19585] \\ d_0 &= (RD + 1) \in [1.0075,1.0675] \end{aligned} \tag{5.70}$$

Considering the system parameter variations in area 2,

$$R \in [0.3125,0.9375], H \in [2,6], T_g \in [0.15,0.45], D \in [0.45,1.35], T_t \in [0.30,0.90] \tag{5.71}$$

For area 2, solving the model in Eq. (5.66) to the form given in Eq. (5.72) for area 2.

$$G_{TA2}(s) = \frac{N_{TA2}(s)}{D_{TA2}(s)} = \frac{e}{f_3s^3 + f_2s^2 + f_1s + f_0} \tag{5.72}$$

$$\begin{aligned} e &= R \in [0.3125,0.9375] \\ f_3 &= 2T_gRT_TH \in [0.05625,4.55625] \\ f_2 &= (2T_TRH + 2HRT_g + RT_gT_TD) \in [0.5688,15.7] \\ f_1 &= (2RH + RT_TD + RT_gD) \in [1.3131,12.9585] \\ f_0 &= (RD + 1) \in [1.1406,2.2656] \end{aligned} \tag{5.73}$$

5.3.2 Proposed INFOPID controller Design for LFC in Perturbed Two Area Interconnected Power System

In this segment, an INFOPID controller has been designed for the two area interconnected system under perturbed conditions. The complete feedback control system has been shown in Figure 5.1. Here, $G(s)$ is the system transfer function and$C(s)$ is the controller. The closed loop transfer function of the system is given as,

$$G'(s) = \frac{G(s)C(s)}{1 + G(s)C(s)} \tag{5.74}$$

The characteristic equation of the system is given as;

$$p(s; k_p, k_i, k_d, \lambda, \mu) = 1 + C(s)G(s) = 0 \tag{5.75}$$

For designing the INFOPID controller for the perturbed two area interconnected system, the interval model as obtained in Eq. (5.69) has been considered. According to Kharitonov theorem, the numerator $N_{TA1}(s)$ in Eq.(5.69) has two values i.e.$N_{TA11}(s) = 0.025$ and $N_{TA12}(s) = 0.075$. The denominator polynomial in (5.69) has been represented in terms of Kharitinov polynomials as given by Eq. (5.76) - (5.79)

$$D_{TA11}(s) = 1.0075 + 0.127625s + 1.1964375s^2 + 0.253125s^3 \quad (5.76)$$

$$D_{TA12}(s) = 1.0075 + 1.195875s + 1.1964375s^2 + 0.003125s^3 \quad (5.77)$$

$$D_{TA13}(s) = 1.0675 + 0.127625s + 0.0439375s^2 + 0.253125s^3 \quad (5.78)$$

$$D_{TA14}(s) = 1.0675 + 1.195875s + 0.0439375s^2 + 0.003125s^3 \quad (5.79)$$

Similarly, expressing the numerator and denominator polynomial in Eq. (5.72) in terms of Kharitinov polynomials, numerator has two values i.e. $N_{TA21}(s) = 0.3125$ and $N_{TA22}(s) = 0.9375$; and four Kharitonov polynomials have been obtained as in Eq. (5.80)-(5.83)

$$D_{TA21}(s) = 1.1406 + 1.3131s + 15.7s^2 + 4.55625s^3 \quad (5.80)$$

$$D_{TA22}(s) = 1.1406 + 12.9585s + 15.7s^2 + 0.05625s^3 \quad (5.81)$$

$$D_{TA23}(s) = 2.2656 + 1.3131s + 0.5688s^2 + 4.55625s^3 \quad (5.82)$$

$$D_{TA24}(s) = 2.2656 + 12.9585s + 0.5688s^2 + 0.05625s^3 \quad (5.83)$$

For the interval model of the two areas, the group of 8 Kharitonov transfer functions have been formed as

$$G_{TAki}(s) = \frac{N_{TAkj}(s)}{D_{TAkl}(s)}, i = 1,2.....8, j,k = 1,2, l = 1,2,3,4 \quad (5.84)$$

The characteristic equation of the system is found by contemplating the FOPID controller given in Eq. (5.1) and using Eq. (5.69) and Eq. (5.75);

$$p(s; k_p, k_i, k_d, \lambda, \mu) = 1 + \left\{k_p + \frac{k_i}{s^\lambda} + k_d s^\mu\right\}\left\{\frac{c}{d_3 s^3 + d_2 s^2 + d_1 s + d_0}\right\} = 0 \quad (5.85)$$

$$p(s; k_p, k_i, k_d, \lambda, \mu) = d_3 s^{3+\lambda} + d_1 s^{2+\lambda} + d_1 s^{1+\lambda} + d_0 s^\lambda + ck_p s^\lambda + ck_d s^{\lambda+\mu} + ck_i = 0 \quad (5.86)$$

The stability condition for the closed loop system shown in Figure 5.1 is that all the roots of Eq. (5.69) should lie in left half of the s-plane. The stability domain S' can be defined as the region for which, when $p(s; k_p, k_i, k_d, \lambda, \mu) \in S'$, the characteristic equation of the system has no roots

in the right half s -plane. The boundary of the stability region for FOPID controller is marked by the two curves named real root boundary (RRB) and the complex root boundary (CRB) as explained by Eq. (5.13).

In this case, substituting $s = 0$ in Eq. (5.86), the RRB is acquired as $k_i = 0$. To obtain CRB, substitute $s = j\omega$ in Eq. (5.86), the following equation has been obtained,

$$\begin{aligned} p(j\omega; k_p, k_i, k_d, \lambda, \mu) \\ &= d_3(j\omega)^{3+\lambda} + d_1(j\omega)^{2+\lambda} + d_1(j\omega)^{1+\lambda} + d_0(j\omega)^{\lambda} + ck_p(j\omega)^{\lambda} \\ &+ ck_d(j\omega)^{\lambda+\mu} + ck_i = 0 \end{aligned} \tag{5.87}$$

Solving Eq. (5.87) by applying the mathematical identity (5.15), the equation obtained is as given by Eq. (5.88),

$$\begin{aligned} &d_3\omega^{3+\lambda}\left\{cos(\lambda+3)\frac{\pi}{2} + j\,sin(\lambda+3)\frac{\pi}{2}\right\} + d_2\omega^{2+\lambda}\left\{cos(\lambda+2)\frac{\pi}{2} + j\,sin(\lambda+2)\frac{\pi}{2}\right\} \\ &+ d_1\omega^{1+\lambda}\left\{cos(\lambda+1)\frac{\pi}{2} + j\,sin(\lambda+1)\frac{\pi}{2}\right\} + \omega^{\lambda}d_0\left\{cos\,\lambda\frac{\pi}{2} + j\,sin\,\lambda\frac{\pi}{2}\right\} \\ &+ ck_p\omega^{\lambda}\left\{cos\,\lambda\frac{\pi}{2} + j\,sin\,\lambda\frac{\pi}{2}\right\} \\ &+ ck_d\omega^{\lambda+\mu}\left\{cos(\lambda+\mu)\frac{\pi}{2} + j\,sin(\lambda+\mu)\frac{\pi}{2}\right\} + ck_i = 0 \end{aligned} \tag{5.88}$$

Eq. (5.88) has been further expressed as in Eq. (5.17). After segregating the real and imaginary parts and equating them to zero:

Real part:

$$\begin{aligned} &d_3\omega^{3+\lambda}\,cos(\lambda+3)\frac{\pi}{2} + d_2\omega^{2+\lambda}\,cos(\lambda+2)\frac{\pi}{2} + d_1\omega^{1+\lambda}\,cos(\lambda+1)\frac{\pi}{2} \\ &+ \omega^{\lambda}d_0\,cos\,\lambda\frac{\pi}{2} + ck_p\omega^{\lambda}\,cos\,\lambda\frac{\pi}{2} + ck_d\omega^{\lambda+\mu}\,cos(\lambda+\mu)\frac{\pi}{2} + ck_i = 0 \end{aligned} \tag{5.89}$$

Imaginary part:

$$\begin{aligned} &d_3\omega^{3+\lambda}\,sin(\lambda+3)\frac{\pi}{2} + d_2\omega^{2+\lambda}\,sin(\lambda+2)\frac{\pi}{2} + d_1\omega^{1+\lambda}\,sin(\lambda+1)\frac{\pi}{2} \\ &+ \omega^{\lambda}d_0\,sin\,\lambda\frac{\pi}{2} + ck_p\omega^{\lambda}\,sin\,\lambda\frac{\pi}{2} + ck_d\omega^{\lambda+\mu}\,sin(\lambda+\mu)\frac{\pi}{2} = 0 \end{aligned} \tag{5.90}$$

Eq. (5.89) and Eq. (5.90) have been solved simultaneously and $k_p$and k_i have been obtained as given in Eq. (5.91) and Eq. (5.92). The value of k_d has been set arbitrarily and CRB and RRB have been plotted in the $(k_p - k_i)$ plane for various values of $\lambda \in (0,2)$ and $\mu \in (0,2)$. Now, $k_d = 7$ has been chosen and Eq. (5.74) and Eq. (5.75) trace a curve called CRB in $(k_p - k_i)$ plane for fixed λ and μ as ω varies from $(0, \infty)$.

$$k_p = \frac{-1}{c\omega^{\lambda}\cos\lambda\left(\frac{\pi}{2}\right)}\begin{Bmatrix} ck_d\omega^{\lambda+\mu}\cos(\lambda+\mu)\frac{\pi}{2} + ck_i + d_3\omega^{3+\lambda}\cos(\lambda+3)\frac{\pi}{2} + \\ d_2\omega^{2+\lambda}\cos(\lambda+2)\frac{\pi}{2} + d_1\omega^{1+\lambda}\cos(\lambda+1)\frac{\pi}{2} + d_0\omega^{\lambda}\cos\lambda\frac{\pi}{2} \end{Bmatrix} \quad (5.91)$$

$$k_i = \frac{d_3\omega^{3+\lambda}\sin 3\frac{\pi}{2} + d_2\omega^{2+\lambda}\sin 2\frac{\pi}{2} + d_1\omega^{1+\lambda}\sin\frac{\pi}{2} + ck_d\omega^{\mu+\lambda}\sin\mu\frac{\pi}{2}}{c\sin\lambda\frac{\pi}{2}} \quad (5.92)$$

The region that is acquired by plotting the CRB and the RRB in the $k_p - k_i$ plane is called the stability region for that fixed value of λ and μ i.e., all the values of $k_p$and k_i that lie within this region will stabilize the system. Hence, by altering $\lambda \in (0,2)$and $\mu \in (0,2)$, the stability regions have been obtained for all combinations of λ and μ. Subsequently, the values of k_p and k_i have been calculated that can give suitable performance for all the Kharitonov transfer functions for area 1 as obtained in Eq.(5.84).

Consider the first transfer function

$$G_{TAki}(s) = \frac{N_{TAkj}(s)}{D_{TAkl}(s)}, k = 1, i = 1, j = 1, l = 1 \quad (5.93)$$

obtained in Eq. (5.84) .Using the mathematical equations of k_p and k_i as obtained in Eq. (5.91) and Eq. (5.92), obtain the stability region in the $k_p - k_i$ plane for all values of $\lambda \in (0,2)$and $\mu \in (0,2)$. This is shown in Figure 5.13 (a) and (b) for area 1 and 2 respectively. Similarly, the stability region for all $G_{TA1}(s), i = 2, \ldots\ldots\ldots, 8$ is obtained. The intersection of all the regions thus obtained is called global stability region for the eight Kharitonov transfer functions. The values of (k_p, k_i) that lie in this region are capable of stabilizing all the 8 Kharitonov transfer functions of the system. The combination of λ and μ that gives the largest intersection stability region has been selected. In this case $\lambda = 0.9$ and $\mu = 0.9$ has been selected. Further, this region has been utilized to select the values of k_p and k_i. From this region, an appropriate value of k_p and k_i that gives the paramount controller performance has to be selected. Here, $k_p = 4$ and $k_i = 27$ has been selected by trial and error method based on various integral error criterion. Hence, the controller parameters selected are $k_p = 4, k_i = 27, k_d = 7, \lambda = 0.9, \mu = 0.9$ i.e., the INFOPID controller obtained for area 1 is,

$$C(s) = 4 + \frac{27}{s^{0.9}} + 7s^{0.9} \quad (5.94)$$

Following the same procedure the controller parameters for area 2 have been calculated as, $k_p = 15, k_i = 8, k_d = 10, \lambda = 1.3, \mu = 1.2$ i.e., the INFOPID controller obtained for area 2 is,

$$C(s) = 15 + \frac{8}{s^{1.3}} + 10s^{1.2} \tag{5.95}$$

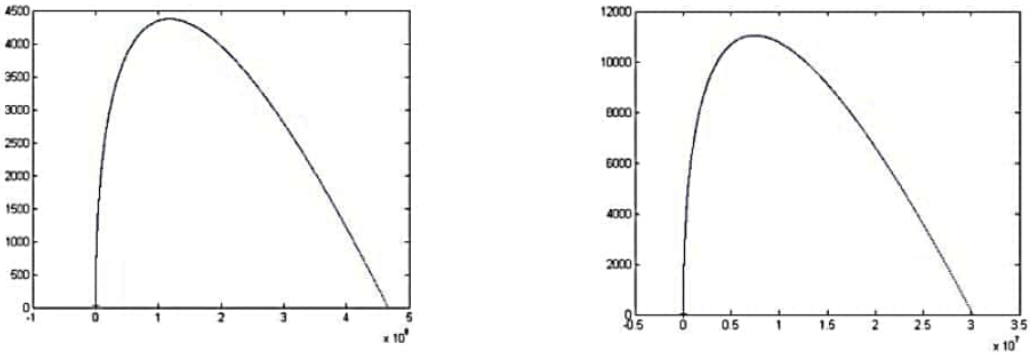

(a) Area 1 (b) Area 2

Figure 5.13 Stability region for area 1 and area 2

In practice, there are non-linearities in the LFC system. Typical non-linearities include Governor Dead Band (GDB) and Generation Rate Constraint (GRC). The total magnitude of continuous speed change within which the valve position does not change is termed as the governor dead band. The dead band is found mainly due to backlash in the linkage mechanism between the servo piston and the camshaft. The limiting value of dead band is specified as 0.0006 per unit or 0.06% which is the value allowed by the joint AIEE-ASME Standards for large steam-turbine speed governors [254].

In practical situations, the rate at which the generated output can be changed is limited by the mechanical inertia of the rotating parts in thermal power plants. This is termed as GRC [255]. The system is unable to respond instantaneously under transient conditions due to this constraint in the system. The performance of the system gets degraded and this may even cause instability in the system [255], [256]. The GRC is modelled by addition of saturation limiter to the turbine output for simulation studies.

Both the non-linearities (GRC and GDB) have been considered in the two area interconnected system and the better suited controller parameters have been selected from the stability region

obtained. In this case, the controller parameters selected for the system including non-linearities are:

Area 1:$k_p = 0.2, k_i = 0.5, k_d = 7, \lambda = 0.9, \mu = 0.9$ i.e., the INFOPID controller obtained for area 1 is,

$$C(s) = 0.2 + \frac{0.5}{s^{0.9}} + 7s^{0.9} \tag{5.96}$$

Area 2: $k_p = 15, k_i = 8, k_d = 10, \lambda = 1.3, \mu = 1.2$ i.e., the INFOPID controller obtained for area 2 is,

$$C(s) = 15 + \frac{8}{s^{1.3}} + 10s^{1.2} \tag{5.97}$$

5.3.3 Stability Analysis

In this section, stability testing of the closed loop PHWR system has been illustrated for one of the interval transfer functions of area 1 of the two area interconnected system given in Eq. 5.84. In this case, the stability analysis of the system can be done by evaluating the roots of the characteristic equation $1 + C(s)G(s) = 0$ of the system. The characteristic equation can be written as,

$$H(s) = 1 + \left(\frac{0.025}{1.0075 + 0.127625s + 1.1964375s^2 + 0.253125s^3}\right)\left(4 + \frac{27}{s^{0.9}} + 7s^{0.9}\right) = 0 \tag{5.98}$$

The characteristic equation becomes,

$$H(s) = 0.253s^{3.9} + 1.196s^{2.9} + 0.1275s^{1.9} + 0.175s^{1.8} + 1.1575s^{0.9} + 0.675 = 0 \tag{5.99}$$

According to the stability analysis technique given in [45], the FO polynomial has been first converted into the integer order polynomial as:

$$H(s) = 0.253s^{\frac{39}{10}} + 1.196s^{\frac{29}{10}} + 0.1275s^{\frac{19}{10}} + 0.175s^{\frac{18}{10}} + 1.1575s^{\frac{9}{10}} + 0.675 = 0 \tag{5.100}$$

In Eq. (5.100), substituting $s^{\frac{1}{10}} = w$, the equation becomes,

$$H(s) = 0.253w^{39} + 1.196w^{29} + 0.1275w^{19} + 0.175w^{18} + 1.1575w^{9} + 0.675 = 0 \tag{5.101}$$

The roots obtained for Eq. (5.101) have been given in the Table 5.13.

Table 5.13 Roots of characteristic polynomial $H(s)$

-0.7294+i 0.0000	0.4475+i 0.8813	0.1632-i 0.9935
-0.5592-i 0.4687	0.8851+i 0.4513	0.3649+i 0.6325
-0.5592+i 0.4687	-1.1158+i 0.3617	-0.8874+i 0.4625
-0.1272+i 0.7189	-0.4490+i 0.8993	0.8851-i 0.4513
-0.1272-i 0.7189	0.6850-i 0.9468	-0.9837+i.1472
0.7126+i 0.7085	-0.0027-i 1.1704	-0.7039+i 0.6951
-0.6906-i 0.9469	-0.6906+i 0.9469	0.4475-i 0.8813
0.6862-i 0.2498	0.7126-i 0.7085	0.6850+i 0.9468
-0.1579+i 0.9740	-0.9837-i 0.1472	-0.4490-i 0.8993
0.9877-i 0.1556	1.1101-i 0.3616	0.3649-i 0.6325
-0.7039-i 0.6951	-0.1579-i 0.9740	1.1101+i 0.3616
-0.0027+i 1.1704	0.1632+i.9935	0.9877+i 0.1556
0.6862+i 0.2498	-1.1158-i 0.3617	-0.8874-i 0.4625

Now, from the roots of the polynomial (5.101) obtained above, the set of physically realizable roots ϕ_i, have been determined using the condition $|arg(\phi_i)| < \frac{\pi}{10}$. The obtained physically realizable roots are presented below in Eq. (5.102) - (5.105). Further, the stability condition $|arg(\phi_i)| > \frac{\pi}{20}$ has been checked for all physically realizable roots. If all the realizable roots of the system satisfy the given condition, only then the system is said to be stable. From Eq. (5.102) - (5.105) the system is found to be stable.

$$|arg(\phi_1)| = 0.1753 \tag{5.102}$$

$$|arg(\phi_2)| = 0.3049 \tag{5.103}$$

$$|arg(\phi_3)| = 0.1753 \tag{5.104}$$

$$|arg(\phi_4)| = 0.3049 \tag{5.105}$$

5.3.4 Simulation Results

The simulation outcomes attained by implementing the INFOPID controller designed by the proposed technique for the two area interconnected system have been illustrated in this section. The designed INFOPID controller has been tested through simulation by disturbing the various parameters of the system from their nominal values. The responses obtained have been shown in Figures 5.14-5.19. The Step Load Perturbation (SLP) of 0.01 has been considered in all the cases.

Case i: Nominal parameters, without non-linearities

In the first case, the response of the INFOPID controller has been tested on the system with nominal parameters i.e. none of the parameters have been disturbed and no non- linearity has been added. SLP of 0.01 has been given to the system at time t = 0 and t = 8 sec. Figure 5.14 (a-b) shows that the designed INFOPID controller shows improved disturbance rejection as compared to the conventional FOPID and integer order PID controllers.

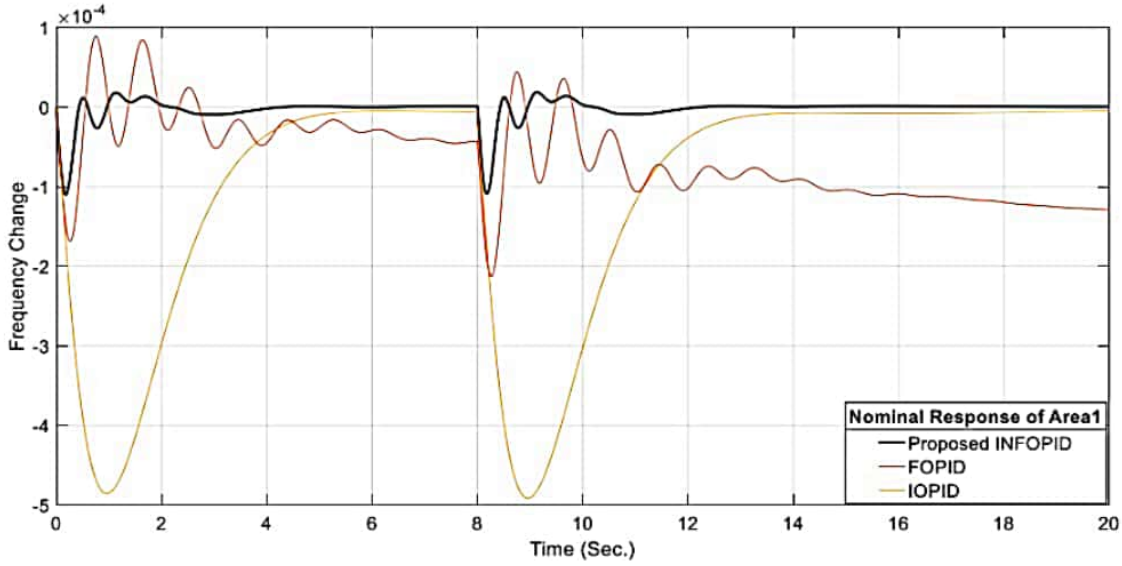

(a) Performance of controllers for area 1 under nominal conditions

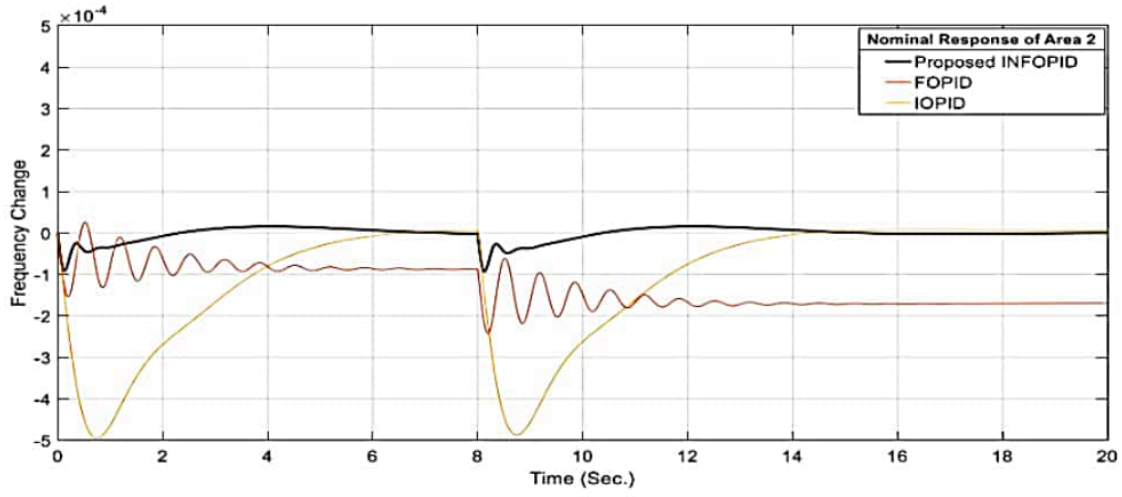

(b) Performance of controllers for area 2 under nominal conditions

Figure 5.14 Performance of various controllers under nominal conditions

Case ii: Parametric Uncertainty: Tg, T_t, R disturbed by ± 50%

The robustness of the controller has been evaluated by disturbing the parameters of the system one by one ± 50%. Figure 5.15 (a-b) presents the performance of various controllers when T_g has been disturbed by ± 50% and at the same time, SLP of 0.01 has been given to the system at time t = 0 and t = 8 sec. It has been noticed that the designed controller shows improved performance. Similarly, the performance of various controllers obtained by disturbing T_g, T_t and R for both the areas has been illustrated in Figure 5.15 (c-f).

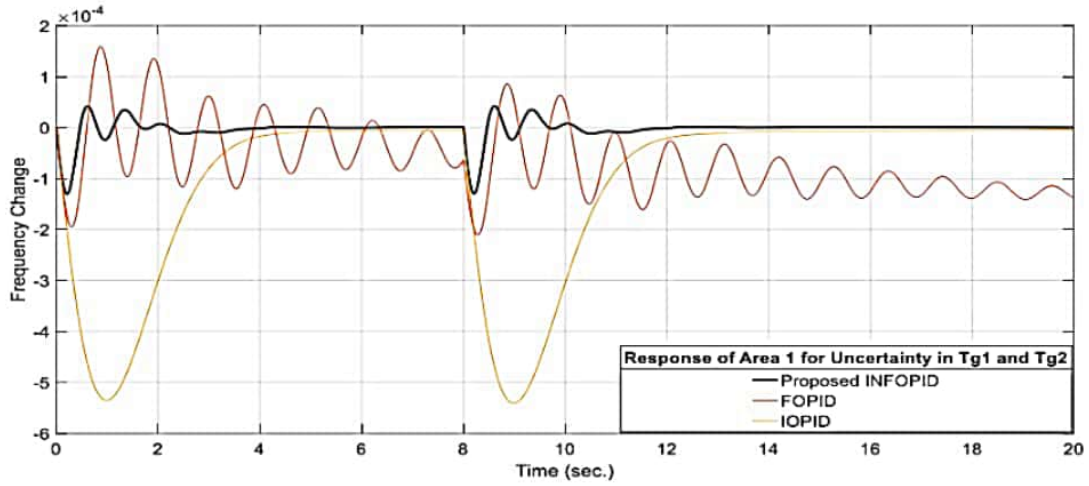

(a) Response of area 1 for uncertainty in T_{g1} and T_{g2}

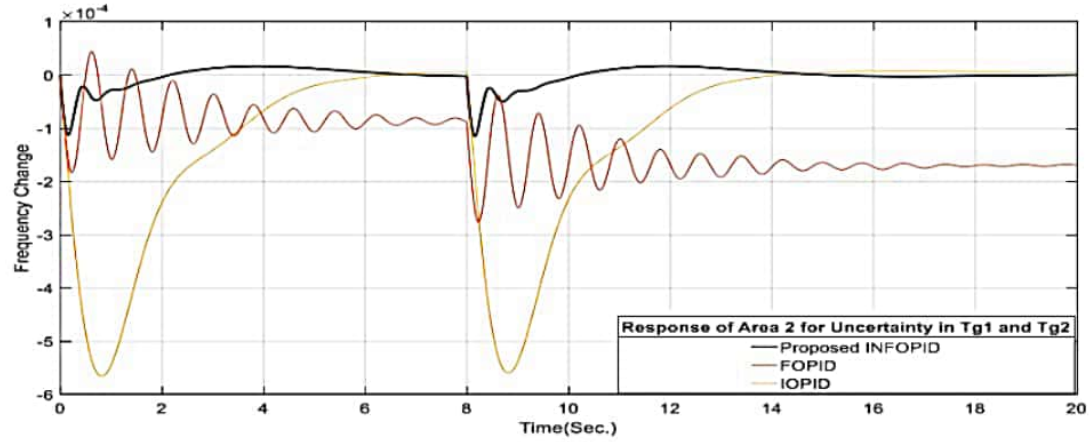

(b) Response of area 2 for uncertainty in T_{g1} and T_{g2}

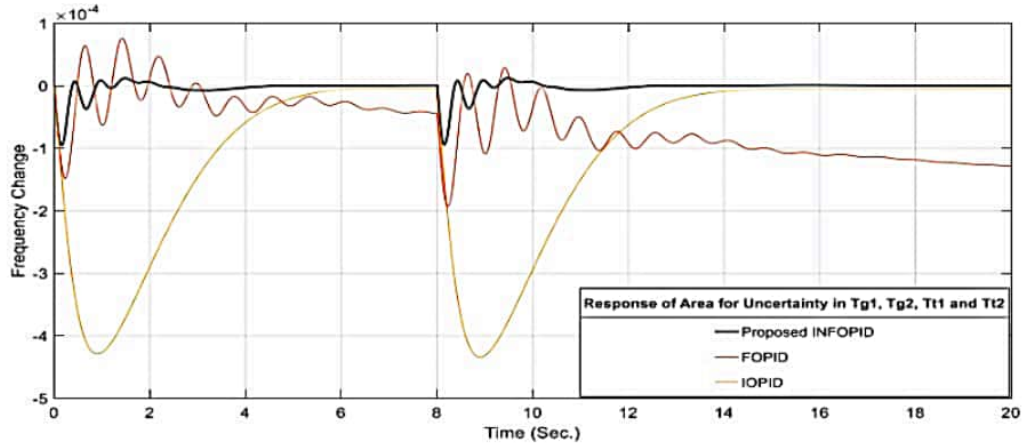

(c) Response of area 1 for uncertainty in T_{g1},T_{g2},T_{t1} and T_{t2}

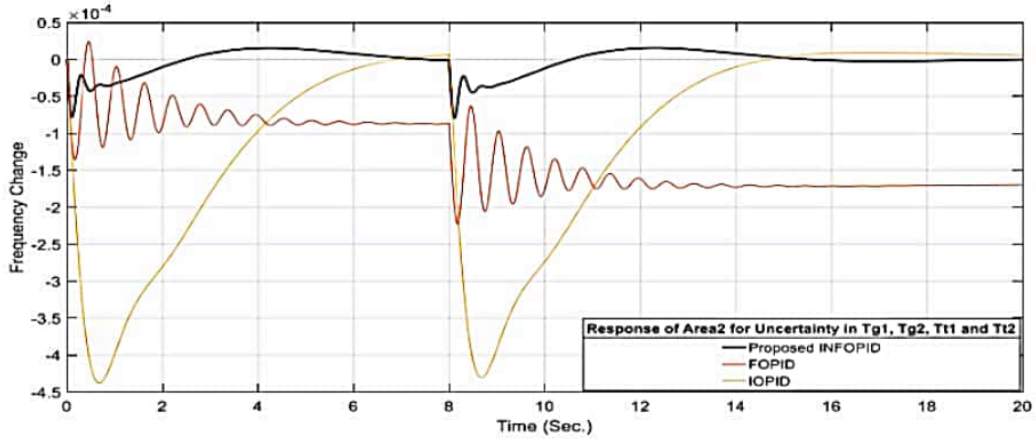

(d) Response of area 2 for uncertainty in T_{g1},T_{g2},T_{t1} and T_{t2}

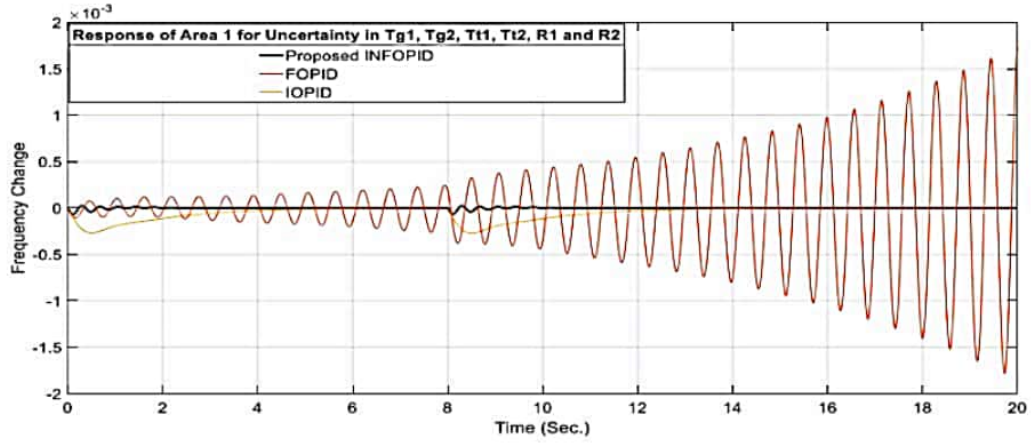

(d) Response of area 1 for uncertainty in T_{g1},T_{g2},T_{t1},T_{t2},R_1 and R_2

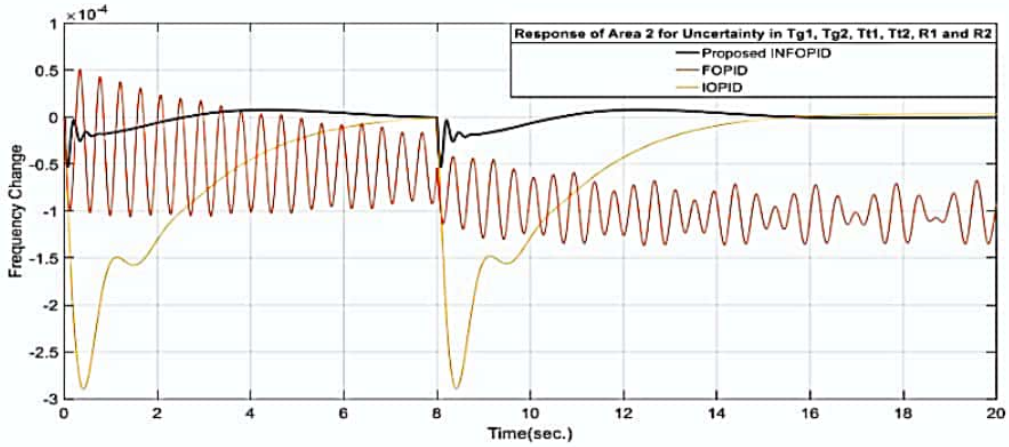

(e) Response of area 2 for uncertainty in T_{g1},T_{g2},T_{t1},T_{t2},R_1 and R_2

Figure 5.15 Performance of various controllers for area 1 and area 2 with parametric uncertainty

Figure 5.15 shows that even when the various parameters of the system have been disturbed from their nominal values, the proposed controller shows improved disturbance rejection as collated to the conventional FOPID controller. This increases the safety factor of the system when working in changing operating conditions.

Case iii: nominal parameters;with non-linearities

Figures 5.16 (a-b) and 5.17 (a-b) show performance of the various controllers on the system in presence of GRC and GDB non linearities. It has been found that the designed INFOPID controller shows enhanced disturbance rejection in this case as well.

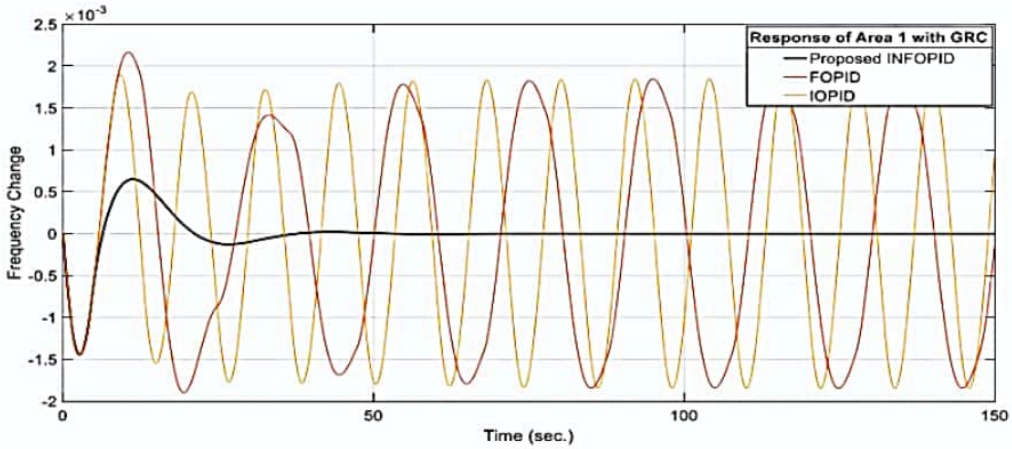

(a) Response of controllers for area 1with GRC under nominal conditions

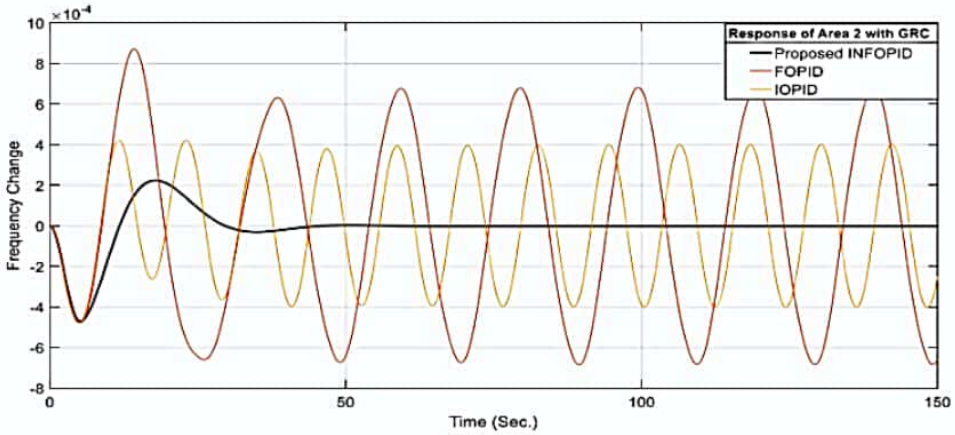

(b) Response of controllers for area 2 with GRC under nominal conditions

Figure 5.16 Performance of various controllers for area 1 and area 2 with GRC under nominal conditions

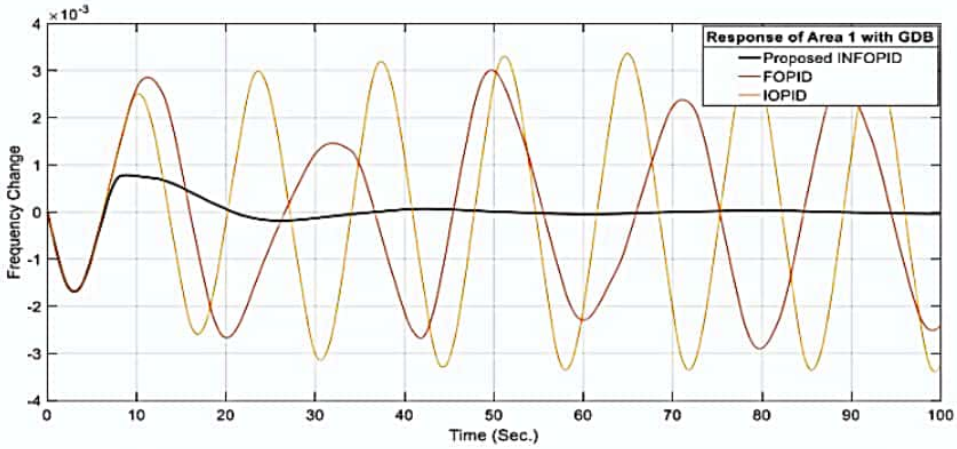

(a) Response of controllers for area 1with GDB under nominal conditions

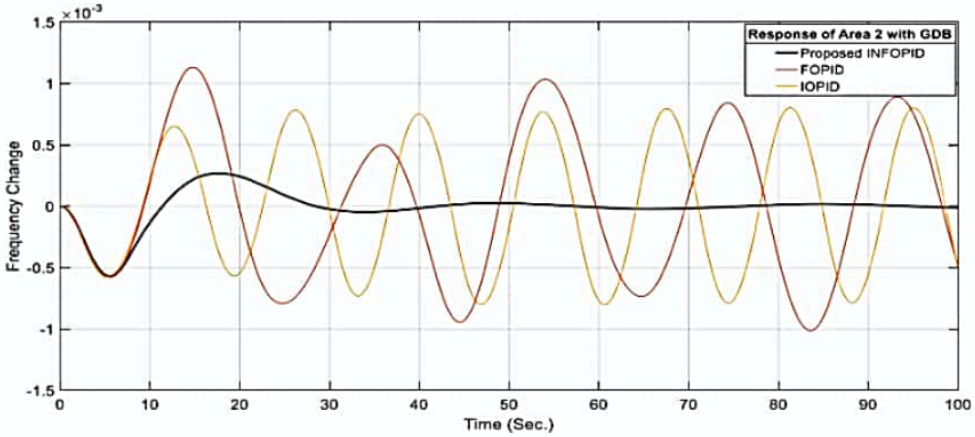

(b) Response of controllers for area 2 with GDB under nominal conditions

Figure 5.17 Performance of various controllers for area 1 and area 2 with GDB under nominal conditions

Case iv: Parametric uncertainty with non-linearities

The robustness of the controllers has been further estimated by disturbing the different parameters by ± 50%. Figure 5.18 and Figure 5.19 show the performance of the controllers on the system having non-linearity as well as parametric uncertainty. The proposed INFOPID controller shows the much improved performance over conventional controllers.

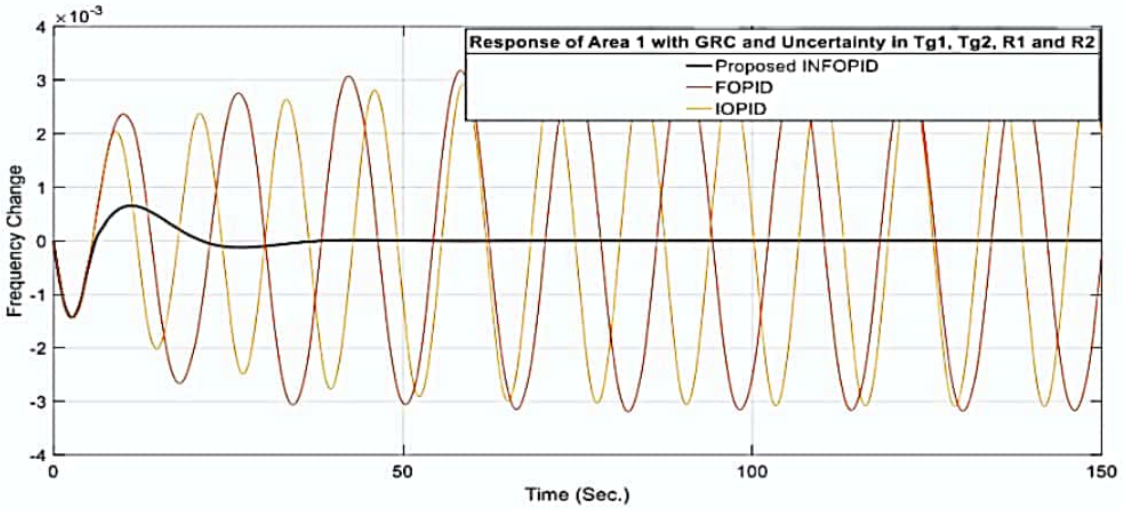

(a) Response of area 1with GRC for uncertainty in T_{g1},T_{g2}, $R_1$and R_2

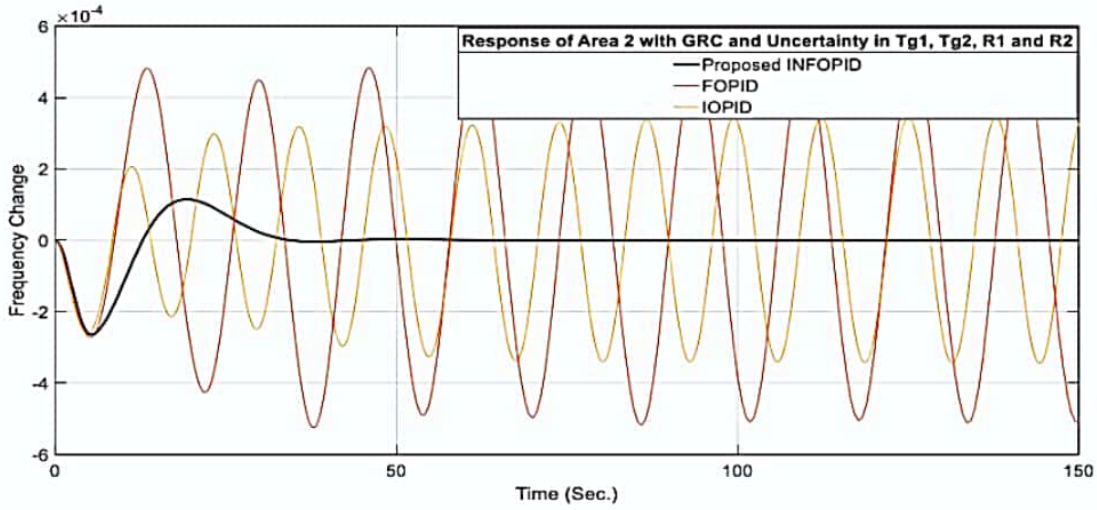

(b) Response of area 2 with GRC for uncertainty in T_{g1},T_{g2}, $R_1$and R_2

Figure 5.18 Performance of various controllers for area 1 and area 2 with GRC and parametric uncertainty

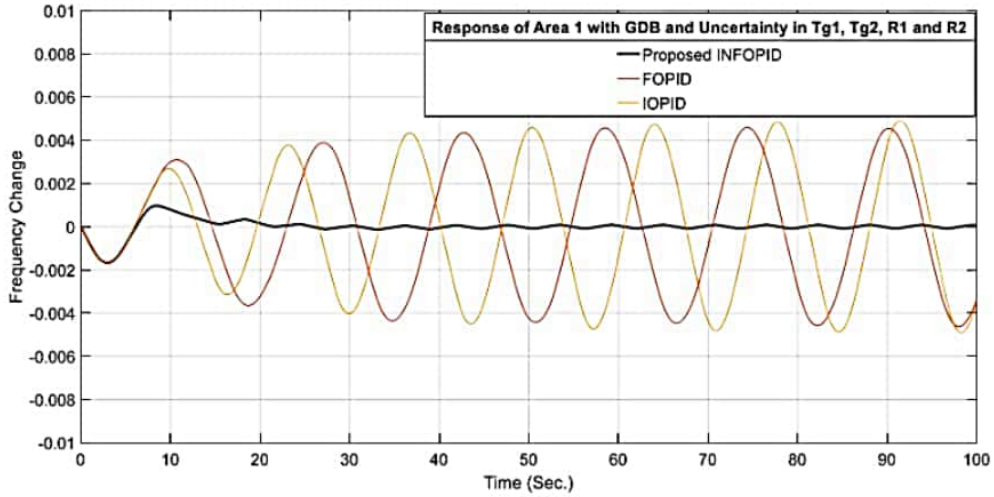

(a) Response of area 1with GDB for uncertainty in T_{g1},T_{g2},$R_1$and R_2

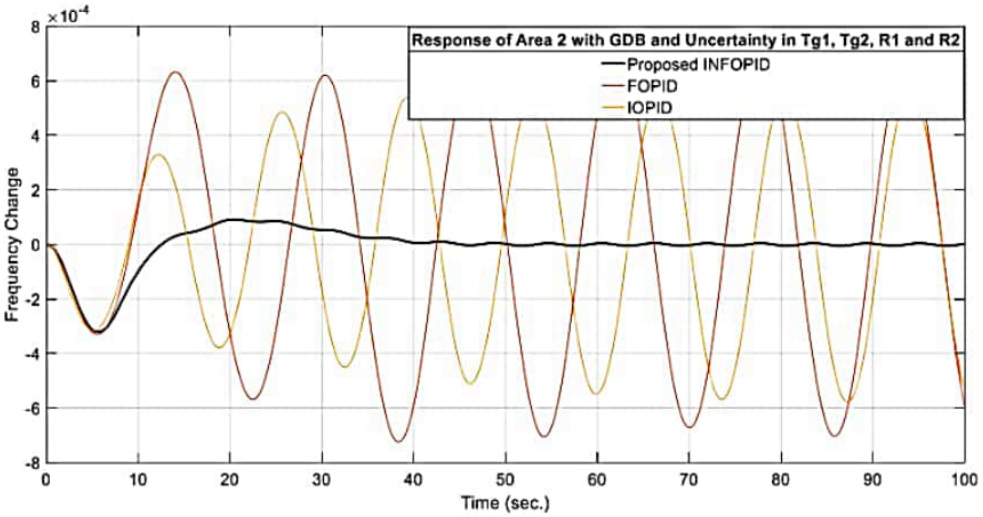

(b) Response of area 2 with GDB for uncertainty in T_{g1},T_{g2}, $R_1$and R_2

Figure 5.19 Performance of various controllers for area 1 and area 2 with GDB and parametric uncertainty

5.3.5 Performance Analysis

In this section, the performance of the various controllers has been analyzed quantitatively. The quantitative analysis of the presented INFOPID controller with the prevailing nominal controllers, i.e. the IOPID and FOPID controllers suggested by Alomoush [246], have been done by using various integral error criterion as shown in Tables 5.14-5.19.

Table 5.14 Performance analysis of various controllers under nominal conditions

	Area1			Area 2		
	ITAE	ISE	IAE	ITAE	ISE	IAE
INFOPID	0.01321	2.332×10^{-6}	0.002476	0.0268	2.013×10^{-6}	0.004063
FOPID	0.04428	1.135×10^{-5}	0.007623	0.8826	0.0003017	0.07106
IOPID	0.2368	0.0002953	0.04236	0.2358	0.0002055	0.03982

Table 5.15 Performance analysis of various controllers under different parameter changes

Parameter variation		Area1			Area 2		
		ITAE	ISE	IAE	ITAE	ISE	IAE
+50% change in Tg	INFOPID	0.01696	3.946×10^{-6}	0.003265	0.02699	2.523×10^{-6}	0.004167
	FOPID	0.1279	2.94×10^{-5}	0.01799	0.8876	0.00031	0.07193
	IOPID	0.229	0.0003289	0.04205	0.2299	0.0002342	0.03982
+50% change in Tg and -50% change in Tt	INFOPID	0.01076	1.615×10^{-6}	0.001997	0.02633	1.706×10^{-6}	0.003932
	FOPID	0.03892	8.201×10^{-6}	0.006605	0.8774	0.0002966	0.07032
	IOPID	0.2436	0.0002584	0.04231	0.2419	0.0001852	0.03983
+50% change in Tg, -50% change in Tt and -50% change in R	INFOPID	0.01319	2.72×10^{-6}	0.002551	0.02581	1.785×10^{-6}	0.003877
	FOPID	4.352	0.009303	0.3015	0.8804	0.0003139	0.07168
	IOPID	0.2318	0.0002627	0.04135	0.2411	0.0001922	0.03978

Table 5.16 Performance analysis of various controllers under nominal conditions with GRC

	Area1			Area 2		
	ITAE	ISE	IAE	ITAE	ISE	IAE
INFOPID	3.643	0.005347	0.3094	0.004428	1.983×10^{-8}	0.000505
FOPID	323.9	0.1453	4.252	1.56	3.309×10^{-6}	0.02014
IOPID	281.2	0.1133	3.702	7.83	8.623×10^{-5}	0.1011

Table 5.17 Performance analysis of various controllers with GRC under different parameter changes

Parameter variation		Area1			Area 2		
		ITAE	ISE	IAE	ITAE	ISE	IAE
+50% change in Tg, and -50% change in R	INFOPID	5.61	0.01656	0.5266	0.007779	6.557×10^{-8}	0.000907
	FOPID	961.9	1.232	12.23	4.866	3.151×10^{-5}	0.06132
	IOPID	888.9	1.028	11.05	22.99	0.00068	0.2831

Table 5.18 Performance analysis of various controllers under nominal conditions with GDB

	Area1			Area 2		
	ITAE	ISE	IAE	ITAE	ISE	IAE
INFOPID	6.581	0.007761	0.4134	0.006531	3.138×10^{-8}	0.0006483
FOPID	187.5	0.1697	3.631	0.8806	3.668×10^{-6}	0.01677
IOPID	224.1	0.2262	4.206	5.673	0.0001349	0.103

Table 5.19 Performance analysis of various controllers with GDB under different parameter changes

Parameter variation		Area1			Area 2		
		ITAE	ISE	IAE	ITAE	ISE	IAE
+50% change in Tg, and -50% change in R	INFOPID	14.33	0.0226	0.7172	0.05118	1.275×10^{-7}	0.001917
	FOPID	598.4	1.533	10.96	2.951	3.76×10^{-5}	0.05401
	IOPID	604.8	1.536	10.84	14.99	0.0009131	0.2644

The collation of different error criterion for change in different system parameters shows that the proposed INFOPID controller provides better performance under the given perturbed conditions than the nominal controllers. Moreover, the proposed controller also gives improved results in the presence of non-linearities like generation rate constraints (GRC) and governor dead band (GDB).

Summary

The INFOPID controller design has been carried out for power control in perturbed PHWR system and LFC in perturbed two area interconnected power system. The FO controllers are designed using the concepts of reduced order modelling, stability boundary locus, Edge theorem, Kharitinov and gain-phase margin tester. It was observed that the proposed controllers provide more robust performance under various real time conditions like parameter fluctuations, system non-linearities, system instability etc. in comparison to the nominal controllers. Hence, the proposed controllers are likely to be more useful when implemented to the real time PHWR and LFC system. The results obtained in this chapter can be directly used by the engineering community working in the field of load frequency control and PHWR. The detailed analysis of the system performance using various control algorithms will help the engineers working in the field in selecting an appropriate and efficient controller design method which can help in improving the system performance under real time conditions.

CHAPTER 6

CONCLUSION AND FUTURE SCOPE

In recent times, fractional order control system has established as a very robust and consummate policy in the control system theory. This type of control system has been found to be more close to real time dynamics of the large and complex systems and hence gives good control performance in most of the practical applications. Although a lot has been explored in direction of using fractional calculus in system modelling and scheming competent control strategies for fractional controller design, however, still there is scope of improvement in this field. The accessible methods in literature are mathematically complex and have restricted pertinence. Hence, the endeavor of this work was to accomplish fractional system modelling and devise facile and robust controller design schemes.

The performance analysis of any dynamic system essentially requires mathematical modelling. The fractional order modelling has been found to perfectly estimate the real time behavior for large and complicated systems. Hence, using various optimization techniques, modelling of a liquid-liquid heat exchanger system in fractional order templates has been carried out. The fractional first and second order templates with time delay have been used for its system modelling. The encouraging results obtained showed that the second order estimated models better fit the original data than the first order models for the considered application.

The mathematical complexity increases while controller design due to higher order dynamics of a system. The unstable sixth order Pressurized Heavy Water Reactor system has been reduced using Balanced Truncation technique to a lower third order system while perpetuating the predominant characteristics of the higher order original system. The states corresponding to the smaller Hankel Singular Values (HSVs) have been truncated to achieve the reduced order model.

The stability boundary locus technique with specific gain-phase margin has been used for fractional order PID controller design for the higher (sixth) order model of the PHWR using corresponding reduced (third) order model. The proposed FOPID controller works very well and gives a stable response even when applied on the original higher order PHWR system whereas the existing controllers gave unstable results. Moreover, it has also been observed that proposed FOPID

controller exhibits lesser settling time in comparison to the integer order PID controller. With the proposed controller, a reduction of almost 40% in the settling time has been achieved for all the operating conditions of PHWR.

In addition, INFOPID controllers have also been designed for perturbed PHWR and two area interconnected power system. These controllers have been designed keeping in mind possible uncertainties in the system parameters. Stability Boundary Locus technique and Edge theorem have been used for the fractional controller design for the perturbed PHWR fractional order system. The eight nuclear reactor models and eight interval conditions (±50% variations in system parameters) for each reactor model of the PHWR have been considered in the design of the controller. Different error criterion has been used as an evaluation parameter for comparing the performance of the proposed controller with the existing methods. Moreover, the proposed controller demonstrated a faster set point tracking ability and was found to be much more robust as compared to nominal controllers under different step back conditions.

Similarly, the fractional order controller design has been accomplished using Kharitonov's theorem and Stability boundary locus technique for frequency control in a perturbed two area interconnected power system. The system parameters such as governor constant, turbine time constant and step load perturbation (magnitude and location) have been changed for analyzing the performance of the devised controller. Further, the effect of nonlinearities like Generation Rate Constraint (GRC) and Governor Dead Band (GDB) have also been observed on the system's performance. The proposed controller provided improved robustness under the given perturbed conditions than the existent controllers.

Since the work carried out in this thesis is of the simulation level, the hardware implementation and testing of the fractional order controllers designed here can be considered as the future work. In future, techniques can also be developed for the design of fractional order controllers for the non-linear systems.

List of Publications

Published

[1] **Ruchika Lamba**, Sunil K. Singla, Swati Sondhi, "Fractional order PID controller for power control in perturbed pressurized heavy water reactor", Nuclear Engineering and Design, Vol.323, pp. 84-94. Elsevier. doi: 10.1016/j.nucengdes.2017.08.013 (SCIE Impact Factor- 1.620)

[2] **Ruchika Lamba**, Sunil Kumar Singla, Swati Sondhi, "Design of Fractional Order PID Controller for Load Frequency Control in Perturbed two area Interconnected System", Electric Power Components and Systems. Taylor's and Francis. doi: 10.1080/15325008.2019.1660736. (SCIE Impact Factor- 0.824)

[3] **Ruchika Lamba**, Swati Sondhi, Sunil K. Singla "Reduced Order Model Based FOPID Controller Design for Power Control in Pressurized Heavy Water Reactor with Specific Gain - Phase Margin", Progress in Nuclear Energy. Elsevier. (SCIE Impact Factor- 1.508)

Communicated

[1] **Ruchika Lamba**, Sunil K. Singla, Swati Sondhi, "Fractional System Modeling of Liquid – Liquid Heat Exchanger Using Various Optimization Techniques", Sadhana Springer. (SCIE Impact Factor- 0.849)

References

[1] J. A. V. Selvi, T. K. Radhakrishnan, and S. Sundaram, "Model based IMC controller for processes with dead time model based IMC controller for processes," *Instrum. Sci. Technol.*, vol. 34, no. 4, pp. 463–474, 2006.

[2] R. Jain, N. Sivakumaran, and T. K. Radhakrishnan, "Design of self tuning fuzzy controllers for nonlinear systems," *Expert Syst. Appl.*, vol. 38, pp. 4466–4476, 2011.

[3] J. T. Machado, V. Kiryakova, and F. Mainardi, "Recent history of fractional calculus," *Commun. Nonlinear Sci. Numer. Simul.*, vol. 16, no. 3, pp. 1140–1153, 2011.

[4] A. Carpinteri and F. Mainardi, *Fractals and Fractional Calculus in Continuum Mechanics*. USA: Springer- Verlag, 1997.

[5] R. Caponetto, G. Dongola, L. Fortuna, and I. Petras, *Fractional Systems:Modeling and Control Applications*, World Scie. Singapore: World Scientific, 2010.

[6] S. Das, *Functional Fractional Calculus*, 2nd ed. Springer Science & Business Media, 2011.

[7] D. Matignon, "Stability results for fractional differential equations with applications to control processing," *Comput. Eng. Syst. Appl.*, vol. 2, no. 1, pp. 963–968, 1996.

[8] I. Petras, Y. Chen, B. M. Vinagre, and I. Podlubny, "Stability of linear time invariant systems with interval fractional orders and interval coefficients," in *Second IEEE International Conference on Computational Cybernetics*, 2004, pp. 341–346.

[9] I. K. Hwan, S. L. Hyun, and W. B. Jong, "Robust stability analysis of commensurate fractional order interval polynomials," *2009 Second ISECS Int. Colloq. Comput. Commun. Control. Manag.*, pp. 384–387, 2009.

[10] I. Petráš, Y. Chen, and B. m. Vinagre, "A robust stability test procedure for a class of uncertain LTI fractional order systems," *Int. Carpathian Control Conf. ICCC*, pp. 247–252, 2002.

[11] N. Tan, Ö. Faruk Özgüven, and M. Mine Özyetkin, "Robust stability analysis of fractional order interval polynomials," *ISA Trans.*, vol. 48, no. 2, pp. 166–172, 2009.

[12] K. Zhou, G. Salomon, and E. Wu, "Balanced realization and model reduction for unstable systems," *Int. J. Robust Nonlinear Control*, vol. 9, no. 3, pp. 183–198, 1999.

[13] B. Maâmar and M. Rachid, "IMC-PID-fractional-order-filter controllers design for integer order systems," *ISA Trans.*, vol. 53, no. 5, pp. 1620–1628, 2014.

[14] C. Yeroglu and N. Tan, "Note on fractional-order proportional-integral-differential controller design," *IET Control Theory Appl.*, vol. 5, no. 17, pp. 1978–1989, 2011.

[15] C. Zhao, D. Xue, and Y. Q. Chen, "A fractional order PID tuning algorithm for a class of fractional order plants," *IEEE Int. Conf. Mechatronics Autom. ICMA 2005*, pp. 216–221.

[16] H. S. Ahn, V. Bhambhani, and Y. Chen, "Fractional-order integral and derivative controller for temperature profile tracking," *Sadhana - Acad. Proc. Eng. Sci.*, vol. 34, no. 5, pp. 833–850, 2009.

[17] M. Bettayeb and R. Mansouri, "Fractional IMC-PID-filter controllers design for non integer order systems," *J. Process Control*, vol. 24, no. 4, pp. 261–271, 2014.

[18] M. Tavakoli-Kakhki and M. Haeri, "Fractional order model reduction approach based on retention of the dominant dynamics: Application in IMC based tuning of FOPI and FOPID controllers," *ISA Trans.*, vol. 50, no. 3, pp. 432–442, 2011.

[19] S. E. Hamamci, "Stabilization using fractional-order PI and PID controllers," *Nonlinear Dyn.*, vol. 51, no. 1, pp. 329–343, 2007.

[20] T. Vinopraba, N. Sivakumaran, S. Narayanan, and T. K. Radhakrishnan, "Design of internal model control based fractional order PID controller," *J. Control Theory Appl.*, vol. 10, no. 3, pp. 297–302, 2012.

[21] S. Das, *Functional fractional calculus for system identification and controls*. New York: Springer Berlin Heidelberg, 2008.

[22] V. A. Vyawahare and P. S. V. Nataraj, "Fractional-order modeling of neutron transport in a nuclear reactor," *Appl. Math. Model.*, vol. 37, pp. 9747–9767, 2013.

[23] D. Matignon, "Stability properties for generalized fractional differential systems," *ESAIM Proc.*, vol. 5, pp. 145–158, 1998.

[24] I. Podlubny, "Fractional-order systems and $PI^{\lambda}D^{\mu}$ Controllers," *IEEE Trans. Automat. Contr.*, vol. 44, no. 1, pp. 208–214, 1999.

[25] A. Maddahi, N. Sepehri, and W. Kinsner, "Fractional-order control of hydraulically powered actuators: Controller Design and Experimental Validation," *IEEE/ASME Trans. Mechatronics*, vol. 24, no. 2, pp. 796–807, 2019.

[26] D. Tiwari, N. Pachauri, A. Rani, and V. Singh, "Fractional order PID (FOPID) controller based temperature control of bioreactor," in *International Conference on Electrical, Electronics, and Optimization Techniques*, 2016, pp. 2968–2973.

[27] M. Jain, A. Rani, N. Pachauri, V. Singh, and A. P. Mittal, "Design of fractional order 2-DOF PI controller for real-time control of heat flow experiment," *Eng. Sci. Technol. an Int. J.*, vol. 22, no. 1, pp. 215–228, 2019.

[28] P. Mishra, V. Kumar, and K. P. S. Rana, "A fractional order fuzzy PID controller for binary distillation column control," *Expert Syst. Appl.*, vol. 42, no. 22, pp. 8533–8549, 2015.

[29] H. Ya Li and G. Rui Kun, "Application of fractional-order model reference adaptive control on industry boiler burning system," in *IEEE International Conference on Intelligent Computation Technology and Automation*, 2010, vol. 1, pp. 750–753.

[30] Y.-S. Deng, K.-Y. Qin, and S.-Q. Shao, "Synchronization in coupled fractional order Chen-system and its application in secure communication," in *IEEE International Conference on Communications, Circuits and Systems*, 2009, pp. 839–841.

[31] Y. S. Deng and K. Y. Qin, "Fractional order Liu-system synchronization and its application multimedia security," in *IEEE International Conference on Communications, Circuits and Systems*, 2010, pp. 769–772.

[32] R. Sharma, P. Gaur, and A. P. Mittal, "Performance analysis of two-degree of freedom fractional order PID controllers for robotic manipulator with payload," *ISA Trans.*, vol. 58, pp. 279–291, 2015.

[33] M. P. Aghababa, "Optimal design of fractional-order PID controller for five bar linkage robot using a new particle swarm optimization algorithm," *Soft Comput.*, vol. 20, no. 10, pp. 4055–4067, 2016.

[34] N. Nikdel, M. Badamchizadeh, V. Azimirad, and M. A. Nazari, "Fractional-order adaptive backstepping control of robotic manipulators in the presence of model uncertainties and external disturbances," *IEEE Trans. Ind. Electron.*, vol. 63, no. 10, pp. 6249–6256, 2016.

[35] A. Kumar and V. Kumar, "A novel interval type-2 fractional order fuzzy PID controller: Design, performance evaluation, and its optimal time domain tuning," *ISA Trans.*, vol. 68, pp. 251–275, 2017.

[36] M. R. Chen, H. Wang, G. Q. Zeng, Y. X. Dai, and D. Q. Bi, "Optimal P-Q control of grid-connected inverters in a microgrid based on adaptive population extremal optimization," *Energies*, vol. 11, no. 8, pp. 1–19, 2018.

[37] NasimUllah, M. Asghar, A. Khattak, and M. M. Rafiq, "Comparison of integer and fractional order robust controllers for DC/DC converter feeding constant power load in a DC microgrid," *Sustain. Energy, Grids Networks*, vol. 12, pp. 1–9, 2017.

[38] V. Kumar, P. Gaur, and A. P. Mittal, "High performance predictive current control of a three phase VSI: An experimental assessment," *Sadhana - Acad. Proc. Eng. Sci.*, vol. 39, no. 6, pp. 1295–1310, 2014.

[39] V. Kumar, P. Gaur, and A. P. Mittal, "Predictive torque and flux control of an induction machine drive using fuzzy multi-criteria decision making," *Sadhana - Acad. Proc. Eng. Sci.*, vol. 42, no. 3, pp. 343–352, 2017.

[40] I. Pan and S. Das, "Frequency domain design of fractional order PID controller for AVR system using chaotic multi-objective optimization," *Int. J. Electr. Power Energy Syst.*, vol. 51, pp. 106–118, 2013.

[41] S. Sondhi and Y. V. Hote, "Fractional order PID controller for load frequency control," *Energy Convers. Manag.*, vol. 85, pp. 343–353, 2014.

[42] S. Jain and Y. V. Hote, "Design of fractional PID for load frequency control via internal model control and big bang big crunch optimization," *IFAC-PapersOnLine*, vol. 51, no. 4,

pp. 610–615, 2018.

[43] S. Saxena, "Load frequency control strategy via fractional-order controller and reduced-order modeling," *Int. J. Electr. Power Energy Syst.*, vol. 104, pp. 603–614, 2019.

[44] A. Zamani, S. M. Barakati, and S. Yousо, "Design of a fractional order PID controller using GBMO algorithm for load – frequency control with governor saturation consideration," *ISA Trans.*, vol. 64, pp. 56–66, 2016.

[45] I. Petras, *Fractional-Order Nonlinear Systems, Modeling, Analysis and Simulation*. Springer London, 2011.

[46] R. Mohsenipour and M. Fathi Jegarkandi, "Robust D -stability analysis of fractional order interval systems of commensurate and incommensurate orders," *IET Control Theory Appl.*, vol. 13, no. 8, pp. 1039–1050, 2019.

[47] B. Senol and C. Yeroglu, "Computation of the value set of fractional order uncertain polynomials: A 2q convex parpolygonal approach," *Proc. IEEE Int. Conf. Control Appl.*, pp. 686–691, 2012.

[48] F. Merrikh-Bayat and M. Afshar, "Extending the root-locus method to fractional-order systems," *J. Appl. Math.*, pp. 1–13, 2008.

[49] H. Ahn, Y. Chen, and I. Podlubny, "Robust stability checking of a class of linear interval fractional order system using lyapunov inequality," *IFAC Proc. Vol.*, pp. 89–94, 2006.

[50] K. Akbari Moornani and M. Haeri, "Robust stability testing function and Kharitonov-like theorem for fractional order interval systems," *IET Control Theory Appl.*, vol. 4, no. 10, pp. 2097–2108, 2010.

[51] J. Lu and G. Chen, "Robust stability and stabilization of fractional-order interval systems : An LMI Approach," *IEEE Tranctions Autom. Control*, vol. 54, no. 6, pp. 1294–1299, 2009.

[52] J. G. Lu and Y. Q. Chen, "Robust stability and stabilization of fractional-order interval systems with the fractional order : The 0<<1 Case," *IEEE Trans. Automat. Contr.*, vol. 55, no. 1, pp. 152–158, 2010.

[53] M. S. Tavazoei and M. Haeri, "A note on the stability of fractional order systems," *Math. Comput. Simul.*, vol. 79, no. 5, pp. 1566–1576, 2009.

[54] J. Sabatier, M. Moze, and C. Farges, "LMI stability conditions for fractional order systems," *Comput. Math. with Appl.*, vol. 59, no. 5, pp. 1594–1609, 2010.

[55] B. Senol, A. Ates, B. Baykant Alagoz, and C. Yeroglu, "A numerical investigation for robust stability of fractional-order uncertain systems," *ISA Trans.*, vol. 53, no. 2, pp. 189–198, 2014.

[56] B. B. Alagoz, C. Yeroglu, B. Senol, and A. Ates, "Probabilistic robust stabilization of fractional order systems with interval uncertainty," *ISA Trans.*, vol. 57, pp. 101–110, 2015.

[57] S. Zheng, "Robust stability of fractional order system with general interval uncertainties," *Syst. Control Lett.*, vol. 99, pp. 1–8, 2017.

[58] S. Gupta, R. Gupta, and S. Padhee, "Parametric system identification and robust controller design for liquid–liquid heat exchanger system," *IET Control Theory Appl.*, vol. 12, no. 10, pp. 1474–1482, 2018.

[59] Y. Zhu, *Multivariable System Identification For Process Control*, 1st ed. Elsevier Science, 2001.

[60] G. Giordano, S. Gros, and J. Sjöberg, "An improved method for Wiener–Hammerstein system identification based on the fractional approach," *Automatica*, vol. 94, pp. 349–360, 2018.

[61] S. Hadjiloucas and R. K. H. Galvão, "Fractional Order and non-linear system identification algorithms for biomedical applications," in *International Conference on Mathematical Modeling in Physical Sciences*, 2014, vol. 490, pp. 1–6.

[62] S. Ijaz, L. Yan, and M. T. Hamayun, "Fractional order modeling and control of dissimilar redundant actuating system used in large passenger aircraft," *Chinese J. Aeronaut.*, vol. 31, no. 5, pp. 1141–1152, 2018.

[63] K. M. Li, M. Sen, and A. Pacheco-Vega, "Fractional-order-based system identification for heat exchangers," in *Proceedings of the 3rd World Congress on Momentum, Heat and Mass Transfer*, 2018, pp. 1–10.

[64] M. A. Taleb, O. Béthoux, and E. Godoy, "Identification of a PEMFC fractional order model," *Int. J. Hydrogen Energy*, vol. 42, no. 2, pp. 1499–1509, 2017.

[65] S. S. Tabatabaei, H. A. Talebi, and M. Tavakoli, "A novel adaptive order/parameter identification method for variable order systems application in viscoelastic soft tissue modeling," *Chaos, Solitons and Fractals*, vol. 102, pp. 447–455, 2017.

[66] A. N. Eddine, B. Huard, J. D. Gabano, T. Poinot, A. Thomas, and S. Martemianov, "Time domain diffusion parameters identification of electrochemical impedance models using fractional order system," *IFAC-PapersOnLine*, vol. 51, no. 15, pp. 377–382, 2018.

[67] W. Yu, Y. Luo, and Y. Pi, "Fractional order modeling and control for permanent magnet synchronous motor velocity servo system," *Mechatronics*, vol. 23, no. 7, pp. 813–820, 2013.

[68] A. Nasser Eddine, B. Huard, J. D. Gabano, T. Poinot, A. Thomas, and S. Martemianov, "Frequential identification of an electrochemical cell impedance using fractional modeling," *IFAC-PapersOnLine*, vol. 51, no. 15, pp. 802–807, 2018.

[69] A. Jalloul, K. Jelassi, and J.-C. Trigeassou, "Non integer identification of rotor skin effect in induction machines," *Int. J. Electr. Comput. Eng.*, vol. 3, no. 3, 2013.

[70] D. Valério and J. Sá da Costa, "Finding a fractional model from frequency and time responses," *Commun. Nonlinear Sci. Numer. Simul.*, vol. 15, no. 4, pp. 911–921, 2010.

[71] O. Enacheanu, D. Riu, N. Retière, and P. Enciu, "Identification of fractional order models for electrical networks," in *32nd Annual Conference on IEEE Industrial Electronics*, 2006, pp. 5392–5396.

[72] S. Abrashov, R. Malti, M. Moze, X. Moreau, F. Aioun, and F. Guillemard, "Simple and robust experiment design for system identification using fractional models," *IEEE Trans. Automat. Contr.*, vol. 62, no. 6, pp. 2648–2658, 2017.

[73] R. Malti, A. Mayoufi, and S. Victor, "Experiment design for system identification using fractional models of the second kind," *IFAC-PapersOnLine*, vol. 51, no. 15, pp. 371–376, 2018.

[74] W. Li, C. Peng, and Y. Wang, "Frequency domain subspace identification of commensurate fractional order input time delay systems," *Int. J. Control. Autom. Syst.*, vol. 9, no. 2, pp. 310–316, 2011.

[75] Y. Hu, Y. Fan, Y. Wei, Y. Wang, and Q. Liang, "Subspace-based continuous-time identification of fractional order systems from non-uniformly sampled data," *Int. J. Syst. Sci.*, vol. 47, no. 1, pp. 122–134, 2016.

[76] H. Ase and T. Katayama, "A subspace-based identification of Wiener-Hammerstein benchmark model," *Control Eng. Pract.*, vol. 44, pp. 126–137, 2015.

[77] L. Vanbeylen, "A fractional approach to identify Wiener-Hammerstein systems," *Automatica*, vol. 50, no. 3, pp. 903–909, 2014.

[78] R. Malti, S. Victor, and A. Oustaloup, "Advances in system identification using fractional models," *J. Comput. Nonlinear Dyn.*, vol. 3, no. 2, pp. 021401(1–7), 2008.

[79] Y. Tang, H. Liu, W. Wang, Q. Lian, and X. Guan, "Parameter identification of fractional order systems using block pulse functions," *Signal Processing*, vol. 107, pp. 272–281, 2015.

[80] Y. Tang, N. Li, M. Liu, Y. Lu, and W. Wang, "Identification of fractional-order systems with time delays using block pulse functions," *Mech. Syst. Signal Process.*, vol. 91, pp. 382–394, 2017.

[81] Y. Li, X. Meng, B. Zheng, and Y. Ding, "Parameter identification of fractional order linear system based on Haar wavelet operational matrix," *ISA Trans.*, vol. 59, pp. 79–84, 2015.

[82] K. Kothari, U. Mehta, and J. Vanualailai, "A novel approach of fractional-order time delay system modeling based on Haar wavelet," *ISA Trans.*, vol. 80, pp. 371–380, 2018.

[83] A. Djouambi, A. Voda, and A. Charef, "Recursive prediction error identification of fractional order models," *Commun. Nonlinear Sci. Numer. Simul.*, vol. 17, no. 6, pp. 2517–2524, 2012.

[84] Y. Dai, Y. Wei, Y. Hu, and Y. Wang, "Modulating function-based identification for fractional order systems," *Neurocomputing*, vol. 173, pp. 1959–1966, 2016.

[85] N. Gehring and J. Rudolph, "An algebraic approach to the identification of linear systems with fractional derivatives," *IFAC-PapersOnLine*, vol. 50, no. 1, pp. 6214–6219, 2017.

[86] S. Abrashov, R. Malti, M. Moze, X. Moreau, and F. Guillemard, "Optimal input design for continuous-time system identification: application to fractional systems," *IFAC-PapersOnLine*, vol. 48, no. 28, pp. 1307–1312, 2015.

[87] R. Cui, Y. Wei, Y. Chen, S. Cheng, and Y. Wang, "An innovative parameter estimation for fractional-order systems in the presence of outliers," *Nonlinear Dyn.*, vol. 89, no. 1, pp. 453–463, 2017.

[88] D. Wang, X. Wang, and P. Han, "Identification of thermal process using fractional-order transfer function based on intelligent optimization," in *IEEE International Conference on Mechatronic and Embedded Systems and Applications*, 2010, pp. 498–503.

[89] A. Sahoo, T. K. Radhakrishnan, and C. S. Rao, "Modeling and control of a real time shell and tube heat exchanger," *Resour. Technol.*, vol. 3, no. 1, pp. 124–132, 2017.

[90] N. A. Khan, A. M. Khan, and M. Kamil, "Modelling of spiral coil heat exchanger: Model with Easy Simulation Using Ms-Excel," *J. Inst. Eng. Ser. E*, vol. 95, no. 1, pp. 19–25, 2014.

[91] X. Xu, X. Zhang, P. Ke, C. Wang, H. Yang, and C. Yang, "Study on the heat transfer characteristic of compact heat exchanger based on experimental data," *Procedia Eng.*, vol. 121, pp. 293–299, 2015.

[92] T. Gao, B. G. Sammakia, J. F. Geer, A. Ortega, and R. Schmidt, "Dynamic analysis of cross flow heat exchangers in data centers using transient effectiveness method," *IEEE Trans. Components, Packag. Manuf. Technol.*, vol. 4, no. 12, pp. 1925–1935, 2014.

[93] A. K. Tiwari, P. Ghosh, J. Sarkar, H. Dahiya, and J. Parekh, "Numerical investigation of heat transfer and fluid flow in plate heat exchanger using nanofluids," *Int. J. Therm. Sci.*, vol. 85, pp. 93–103, 2014.

[94] J. Zambrano, J. Sanchis, J. M. Herrero, and M. Martínez, "WH-EA: An Evolutionary Algorithm for Wiener-Hammerstein System Identification," *Complexity*, vol. 2018, pp. 1–17, 2018.

[95] M. Yousefi, R. Enayatifar, and A. N. Darus, "Optimal design of plate-fin heat exchangers by a hybrid evolutionary algorithm," *Int. Commun. Heat Mass Transf.*, vol. 39, no. 2, pp. 258–263, 2012.

[96] H. Zarea, F. Moradi Kashkooli, A. Mansuri Mehryan, M. R. Saffarian, and E. Namvar Beherghani, "Optimal design of plate-fin heat exchangers by a Bees Algorithm," *Appl. Therm. Eng.*, vol. 69, pp. 267–277, 2014.

[97] M. Yousefi, R. Enayatifar, A. N. Darus, and A. H. Abdullah, "Optimization of plate-fin heat exchangers by an improved harmony search algorithm," *Appl. Therm. Eng.*, vol. 50, no. 1, pp. 877–885, 2013.

[98] M. Yousefi, A. N. Darus, and H. Mohammadi, "An imperialist competitive algorithm for optimal design of plate-fin heat exchangers," *Int. J. Heat Mass Transf.*, vol. 55, pp. 3178–3185, 2012.

[99] G. N. Xie, B. Sunden, and Q. W. Wang, "Optimization of compact heat exchangers by a genetic algorithm," *Appl. Therm. Eng.*, vol. 28, pp. 895–906, 2008.

[100] Wang Lei and Wu Qidi, "Linear system parameters identification based on ant system algorithm," in *International Conference on Control Applications*, 2001, pp. 401–406.

[101] S. Bittanti and L. Piroddi, "Nonlinear identification and control of a heat exchanger: A Neural Network Approach," *J. Franklin Inst.*, vol. 334B, no. 1, pp. 135–153, 1997.

[102] M. Al-Dhaifallah, K. S. Nisar, P. Agarwal, and A. Elsayyad, "Modeling and identification of heat exchanger process using least squares support vector machines," *Therm. Sci.*, vol. 21, no. 6, pp. 2859–2869, 2017.

[103] X. Deng, "System identification based on particle swarm optimization algorithm," in *IEEE International Conference on Computational Intelligence and Security*, 2009, pp. 259–263.

[104] J. Lv, "Improved artificial fish swarm algorithm applied on the static model of the induction motor parameter identification," *Appl. Mech. Mater.*, vol. 220–223, pp. 753–761, 2012.

[105] H. Du and N. Zhang, "Application of evolving Takagi-Sugeno fuzzy model to nonlinear system identification," *Appl. Soft Comput. J.*, vol. 8, no. 1, pp. 676–686, 2008.

[106] J. Wang, L. Zhang, D. Xu, P. Zhang, and G. Zhang, "A simplified fractional order equivalent circuit model and adaptive online parameter identification method for lithium-ion batteries," *Math. Probl. Eng.*, vol. 2019, pp. 1–8, 2019.

[107] M. R. Sathya and M. M. T. Ansari, "Load frequency control using Bat inspired algorithm based dual mode gain scheduling of PI controllers for interconnected power system," *Electr. Power Energy Syst.*, vol. 64, pp. 365–374, 2015.

[108] A. H. Gandomi, X. S. Yang, and A. H. Alavi, "Cuckoo search algorithm: A metaheuristic approach to solve structural optimization problems," *Eng. Comput.*, vol. 29, no. 1, pp. 17–35, 2013.

[109] P. Upadhyay, R. Kar, D. Mandal, and S. P. Ghoshal, "A new design method based on firefly algorithm for IIR system identification problem," *J. King Saud Univ. - Eng. Sci.*, vol. 28, no. 2, pp. 174–198, 2016.

[110] A. Gotmare, R. Patidar, and N. V. George, "Nonlinear system identification using a cuckoo search optimized adaptive Hammerstein model," *Expert Syst. Appl.*, vol. 42, no. 5, pp. 2538–2546, 2015.

[111] P. Díaz *et al.*, "An improved crow search algorithm applied to energy problems," *Energies*, vol. 11, no. 3, pp. 1–22, 2018.

[112] X. Gao and Y. Liu, "Parameter identification based on modified simulated annealing differential evolution algorithm for giant magnetostrictive actuator," *AIP Adv.*, vol. 8, no. 1, 2018.

[113] Z. Wu, D. Shen, M. Shang, and S. Qi, "Parameter identification of single-phase inverter based on improved moth flame optimization algorithm," *Electr. Power Components Syst.*, vol. 47, no. 4–5, pp. 456–469, 2019.

[114] Y. S. N. Malleswararao and M. Chidambaram, "Non-linear controllers for a heat exchanger," *J. Process Control*, vol. 2, no. 1, pp. 17–21, 1992.

[115] X. Liu, "Optimization design on fractional order PID controller based on adaptive particle swarm optimization algorithm," *Nonlinear Dyn.*, vol. 84, no. 1, pp. 379–386, 2016.

[116] L. Chaib, A. Choucha, and S. Arif, "Optimal design and tuning of novel fractional order PID power system stabilizer using a new metaheuristic Bat algorithm," *Ain Shams Eng. J.*, vol. 8, no. 2, pp. 113–125, 2017.

[117] X. Gao and Y. Liu, "Parameter identification based on modified simulated annealing differential evolution algorithm for giant magnetostrictive actuator," *AIP Adv.*, vol. 8, no. 1, pp. 1–9, 2018.

[118] B. Mohanty, B. V. S. Acharyulu, and P. K. Hota, "Moth-flame optimization algorithm optimized dual-mode controller for multiarea hybrid sources AGC system," *Optim. Control Appl. methods*, vol. 39, no. 2, pp. 720–734, 2017.

[119] K. Gallivan, E. Grimme, and P. Van Dooren, "Pade approximation of large-scale dynamic systems with Lanczos methods," in *IEEE 33rd Conference on Decision and Control*, 1994, vol. 1, pp. 443–448.

[120] J. Pal, "An algorithmic method for the simplification of linear dynamic scalar systems," *Int. J. Control*, vol. 43, no. 1, pp. 257–269, 1986.

[121] H. Xiheng, "FF-Pade method of model reduction in frequency domain," *IEEE Trans. Automat. Contr.*, vol. 32, no. 3, pp. 243–246, 1987.

[122] T. N. Lucas, "New matrix method for multipoint Padé approximation of transfer functions," *Int. J. Syst. Sci.*, vol. 24, no. 5, pp. 809–818, 1993.

[123] T. N. Lucas, "Extension of matrix method for complete multipoint Padé approximation," *Electron. Lett.*, vol. 29, no. 20, pp. 1805–1806, 1993.

[124] M. J. Bosley, H. W. Kropholler, and F. P. Lees, "On the relation between the continued fraction expansion and moments matching methods of model reduction," *Int. J. Control*, vol. 18, no. 3, pp. 461–474, 1973.

[125] Y. Shamash, "Time moments and markov parameters of composite systems," *Electron. Lett.*, vol. 15, no. 4, pp. 131–132, 1979.

[126] R. Parthasarathy and H. Singh, "Minimal realisation of a symmetric transfer function matrix using markov parameters and moments," *Electron. Lett.*, vol. 11, no. 15, pp. 324–326, 1975.

[127] S. Biradar, Y. V. Hote, and S. Saxena, "Reduced-order modeling of linear time invariant systems using big bang big crunch optimization and time moment matching method," *Appl. Math. Model.*, vol. 40, no. 15–16, pp. 7225–7244, 2016.

[128] C. F. Chen and L. S. Shieh, "A novel approach to linear model simplification," *Int. J. Control*, vol. 8, no. 6, pp. 561–570, 1968.

[129] Y. Bistritz, "A direct Routh stability method for discrete system modelling," *Syst. Control Lett.*, vol. 2, no. 2, pp. 83–87, 1982.

[130] C. Hwang and C. S. Hsieh, "Order reduction of discrete-time system via bilinear routh approximation," *J. Dyn. Syst. Meas. Control. Trans. ASME*, vol. 112, no. 2, pp. 292–297, 1990.

[131] C. Hwang and Y. C. Lee, "A new family of routh approximants," *Circuits, Syst. Signal Process.*, vol. 16, no. 1, pp. 1–25, 1997.

[132] C. Hwang and T. Y. Guo, "Matrix Routh-approximant reduced-order modelling for multivariable systems," *Int. J. Syst. Sci.*, vol. 16, no. 6, pp. 697–712, 1985.

[133] B. Bandyopadhyay, O. Ismail, and R. Gorez, "Routh-Pade approximation for interval systems," *IEEE Trans. Automat. Contr.*, vol. 39, no. 12, pp. 2454–2456, 1994.

[134] S. F. Yang, "Comments on routh-pade model reduction of interval systems," *IEEE Trans. Automat. Contr.*, vol. 50, no. 2, pp. 273–275, 2005.

[135] A. Lepschy and U. Viaro, "A note on the model reduction problem," *IEEE Trans. Automat. Contr.*, vol. 28, no. 4, pp. 525–527, 1983.

[136] N. Habib and R. Prasasd, "An observation on the differentiation and modified cauer continued fraction expansion approaches of model reduction technique," in *XXXII National Systems Conference*, 2008, pp. 574–579.

[137] S. S. Lamba, R. Gorez, and B. Bandyopadhyay, "New reduction technique by step error minimization for multivariable systems," *Int. J. Syst. Sci.*, vol. 19, no. 6, pp. 999–1009, 1988.

[138] H. Manohar and D. K. Sambariya, "Model order reduction of MIMO system using differentiation method," in *10th International Conference on Intelligent Systems and Control*, 2016, no. 2, pp. 1–5.

[139] G. V. K. R. Sastry and G. R. Rao, "Simplified polynomial derivative technique for the reduction of large-scale interval systems," *IETE J. Res.*, vol. 49, no. 6, pp. 405–409, 2003.

[140] T. C. Chen, C. Y. Chang, and K. W. Han, "Model reduction using the stability-equation method and the Padé approximation method," *J. Franklin Inst.*, vol. 309, no. 6, pp. 473–

490, 1980.

[141] J. Pal, "Improved Padé approximants using stability equation method," *Electron. Lett.*, vol. 19, no. 11, pp. 426–427, 1983.

[142] T. C. Chen, C. Y. Chang, and K. W. Han, "Model reduction using the stability-equation method and the continued-fraction method," *Int. J. Control*, vol. 32, no. 1, pp. 81–94, 1980.

[143] G. Parmar, R. Prasad, and S. Mukherjee, "Order reduction of linear dynamic systems using stability equation method and GA," *Int. J. Electr. Robot. Electron. Commun. Eng.*, vol. 1, no. 2, pp. 243–249, 2007.

[144] S. R. Desai and R. Prasad, "A new approach to order reduction using stability equation and big bang big crunch optimization," *Syst. Sci. Control Eng.*, vol. 1, no. 1, pp. 20–27, 2013.

[145] A. Sikander and R. Prasad, "Soft computing approach for model order reduction of linear time invariant systems," *Circuits, Syst. Signal Process.*, vol. 34, no. 11, pp. 3471–3487, 2015.

[146] D. K. Sambariya and G. Arvind, "Reduced order modelling of SMIB power system using stability equation method and firefly algorithm," in *IEEE 6th International Conference on Power Systems*, 2016, pp. 1–6.

[147] A. K. Sinha and J. Pal, "Simulation based reduced order modelling using a clustering technique," *Comput. Electr. Eng.*, vol. 16, no. 3, pp. 159–169, 1990.

[148] J. Singh, K. Chattterjee, and C. B. Vishwakarma, "Two degree of freedom internal model control-PID design for LFC of power systems via logarithmic approximations," *ISA Trans.*, vol. 72, pp. 185–196, 2018.

[149] O. Alsmadi, Z. Abo-Hammour, D. Abu-Al-Nadi, and S. Saraireh, "Soft computing techniques for reduced order modelling: Review and Application," *Intell. Autom. Soft Comput.*, vol. 22, no. 1, pp. 125–142, 2016.

[150] C. B. Vishwakarma and R. Prasad, "MIMO system reduction using modified pole clustering and genetic algorithm," *Model. Simul. Eng.*, vol. 2009, 2009.

[151] H. N. Soloklo, O. Nail, and M. M. Farsangi, "Model reduction by hermite polynomials and genetic algorithm," *J. Math. Comput. Sci.*, vol. 09, no. 03, pp. 188–202, 2014.

[152] H. N. Soloklo and M. M. Farsangi, "Model order reduction by using legendre expansion and harmony search algorithm," *Majlesi J. Electr. Eng.*, vol. 9, no. 1, pp. 25–35, 2015.

[153] A. B. H. Adamou-Mitiche and L. Mitiche, "Multivariable systems model reduction based on the dominant modes and genetic algorithm," *IEEE Trans. Ind. Electron.*, vol. 64, no. 2, pp. 1617–1619, 2017.

[154] E. J. Davison, "A method for simplifying linear dynamic systems," *IEEE Trans. Automat. Contr.*, vol. 11, no. 1, pp. 93–101, 1966.

[155] H. Inooka and G. Obinata, "Mixed method of aggregation and I.S.E. criterion approaches for system reduction," *Electron. Lett.*, vol. 1, no. 3, pp. 88–90, 1977.

[156] O. M. K. Alsmadi, Z. S. Abo-Hammour, and A. M. Al-Smadi, "Artificial neural network for discrete model order reduction with substructure preservation," *Appl. Math. Model.*, vol. 35, no. 9, pp. 4620–4629, 2011.

[157] D. I. Abu-Al-Nadi, O. M. K. Alsmadi, Z. S. Abo-Hammour, M. F. Hawa, and J. S. Rahhal, "Invasive weed optimization for model order reduction of linear MIMO systems," *Appl. Math. Model.*, vol. 37, no. 6, pp. 4570–4577, 2013.

[158] K. Mustaqim, A. Didik Khusnul, A. Erna, and A. Dieky, "Model reduction of unstable systems using balanced truncation method and its application to shallow water equations," *IOP Conf. Ser. J. Phys.*, vol. 855, pp. 1–7, 2017.

[159] B. C. Moore, "Principal component analysis in linear systems: controllability, observability, and model reduction," *IEEE Trans. Automat. Contr.*, vol. 26, no. 1, pp. 17–32, 1981.

[160] D. K. Arif, Widodo, Salmah, and E. Apriliani, "Implementation of the algorithm kalman filter on reduction model," in *International Conference on Mathematics, Statistics and its Applications*, 2012, pp. 23–31.

[161] S. Ghosh and N. Senroy, "Balanced truncation based reduced order modeling of wind farm," *Int. J. Electr. Power Energy Syst.*, vol. 53, no. 1, pp. 649–655, 2013.

[162] G. Wang, V. Sreeram, and W. Q. Liu, "A new frequency-weighted balanced truncation method and an error bound," *IEEE Tranctions Autom. Control*, vol. 44, no. 9, pp. 1734–1737, 1999.

[163] D. Kumar and S. K. Nagar, "Model reduction by extended minimal degree optimal Hankel norm approximation," *Appl. Math. Model.*, vol. 38, pp. 2922–2933, 2014.

[164] S. E. Hamamci, "An algorithm for stabilization of fractional-order time delay systems using fractional-order PID controllers," *IEEE Trans. Automat. Contr.*, vol. 52, no. 10, pp. 1964–1969, 2007.

[165] B. N. Datta, *Numerical Methods for Linear Control Systems*, 1st ed. Elsevier, 2005.

[166] W. M. Stacey, *Nuclear Reactor Physics.*, 2nd ed. Wiley, 2007.

[167] S. Saha *et al.*, "Design of a fractional order phase shaper for iso-damped control of a PHWR under step-back condition," *IEEE Trans. Nucl. Sci.*, vol. 57, no. 3, pp. 1602–1612, 2010.

[168] S. Das and A. Gupta, "Fractional order modeling of a PHWR under step-back condition and control of its global power with a robust $PI^{\lambda}D^{\mu}$ controller," *IEEE Trans. Nucl. Sci.*, vol. 58, no. 5, pp. 2431–2441, 2011.

[169] D. B. Talange, B. Bandyopadhyay, and A. P. Tiwari, "Spatial control of a large PHWR by decentralized periodic output feedback and model reduction techniques," *IEEE Trans. Nucl.*

Sci., vol. 53, no. 4, pp. 2308–2317, 2006.

[170] S. S. Bhase and B. M. Patre, "Robust FOPI controller design for power control of PHWR under step-back condition," *Nucl. Eng. Des.*, vol. 274, pp. 20–29, 2014.

[171] S. Saha *et al.*, "Design of a fractional order phase shaper for iso-damped control of a PHWR under step-back condition," *IEEE Trans. Nucl. Sci.*, vol. 57, no. 3, pp. 1602–1612, 2010.

[172] S. Das, I. Pan, S. Das, and A. Gupta, "Improved model reduction and tuning of fractional-order $PI^{\lambda}D^{\mu}$ controllers for analytical rule extraction with genetic programming," *ISA Transactions*, vol. 51, no. 2. pp. 237–261, 2012.

[173] V. D. Hajare and B. M. Patre, "Design of PID controller based on reduced order model and Characteristic Ratio Assignment method," in *IEEE International Conference on Control Applications*, 2013, pp. 1270–1274.

[174] S. Das, S. Saha, S. Das, and A. Gupta, "On the selection of tuning methodology of FOPID controllers for the control of higher order processes," *ISA Trans.*, vol. 50, no. 3, pp. 376–388, 2011.

[175] M. R. Bongulwar and B. M. Patre, "Design of $PI^{\lambda}D^{\mu}$ controller for global power control of Pressurized Heavy Water Reactor," *ISA Trans.*, vol. 69, pp. 234–241, 2017.

[176] B. M. Vinagre, C. A. Monje, A. J. Calderon, and J. I. Suarez, "Fractional PID controllers for industry application. A Brief Introduction," *J. Vib. Control*, vol. 13, no. 9–10, pp. 1419–1429, 2007.

[177] C. A. Monje, B. M. Vinagre, V. Feliu, and Y. Chen, "Tuning and auto-tuning of fractional order controllers for industry applications," *Control Eng. Pract.*, vol. 16, no. 7, pp. 798–812, 2008.

[178] S. E. Hamamci and M. Koksal, "Calculation of all stabilizing fractional-order PD controllers for integrating time delay systems," *Comput. Math. with Appl.*, vol. 59, no. 5, pp. 1621–1629, 2010.

[179] F. Padula and A. Visioli, "On the fragility of fractional-order PID controllers for FOPDT processes," *ISA Trans.*, vol. 60, pp. 228–243, 2016.

[180] M. Li, P. Zhou, Z. Zhao, and J. Zhang, "Two-degree-of-freedom fractional order-PID controllers design for fractional order processes with dead-time," *ISA Trans.*, vol. 61, pp. 147–154, 2016.

[181] X. Liu, D. Jiang, and K. Y. Lee, "Decentralized fuzzy MPC on spatial power control of a large PHWR," *IEEE Trans. Nucl. Sci.*, vol. 63, no. 4, pp. 2343–2351, 2016.

[182] S. Sagar, S. Kaur, and S. Sondhi, "Fractional order IMC-PID controller design for the pressurized heavy water reactor," in *3rd International Conference on Electrical, Electronics, Engineering Trends, Communication, Optimization and Sciences (EEECOS)-2016*, 2016, pp. 72–77.

[183] L. Dazi, L. Liu, Q. Jin, and K. Hirasawa, "Maximum sensitivity based fractional IMC-PID controller design for non-integer order system with time delay," *J. Process Control*, vol. 31, pp. 17–29, 2015.

[184] S. Sondhi and Y. V Hote, "Fractional IMC design for fractional order gas turbine model," in *9th International Conference on Industrial and Information Systems*, 2014, pp. 1–5.

[185] D. Li, X. He, T. Song, and Q. Jin, "Fractional order IMC controller design for two-input-two-output fractional order system," *Int. J. Control. Autom. Syst.*, vol. 17, no. 4, pp. 936–947, 2019.

[186] S. Sondhi and Y. V Hote, "Stability testing and IMC based fractional order PID controller design for heating furnace system," in *Annual IEEE India Conference (INDICON)*, 2014, pp. 1–5.

[187] W. Zheng and Y. Pi, "Study of the fractional order proportional integral controller for the permanent magnet synchronous motor based on the differential evolution algorithm," *ISA Trans.*, vol. 63, pp. 387–393, 2016.

[188] A. A. Zamani, S. Tavakoli, and S. Etedali, "Fractional order PID control design for semi-active control of smart base-isolated structures: A multi-objective cuckoo search approach," *ISA Trans.*, vol. 67, pp. 222–232, 2017.

[189] R. Sharma, K. P. S. Rana, and V. Kumar, "Performance analysis of fractional order fuzzy PID controllers applied to a robotic manipulator," *Expert Syst. Appl.*, vol. 41, no. 9, pp. 4274–4289, 2014.

[190] K. Naidu, H. Mokhlis, and A. H. A. Bakar, "Multiobjective optimization using weighted sum Artificial Bee Colony algorithm for Load Frequency Control," *Electr. Power Energy Syst.*, vol. 55, pp. 657–667, 2014.

[191] S. Hanwate, Y. V. Hote, and S. Saxena, "Adaptive policy for load frequency control," *IEEE Trans. Power Syst.*, vol. 33, no. 1, pp. 1142–1144, 2018.

[192] A. Ateş and C. Yeroglu, "Optimal fractional order PID design via Tabu Search based algorithm," *ISA Trans.*, vol. 60, pp. 109–118, 2016.

[193] W. M. Baig, Z. Hou, and S. Ijaz, "Fractional order controller design for a semi-active suspension system using Nelder-Mead optimization," in *IEEE 29th Chinese Control And Decision Conference (CCDC)*, 2017, pp. 2808–2813.

[194] V. Kumar, K. P. S. Rana, J. Kumar, P. Mishra, and S. S. Nair, "A robust fractional order fuzzy P + fuzzy I + fuzzy D controller for nonlinear and uncertain system," *Int. J. Autom. Comput.*, vol. 14, no. 4, pp. 474–488, 2017.

[195] C. Li, N. Zhang, X. Lai, J. Zhou, and Y. Xu, "Design of a fractional-order PID controller for a pumped storage unit using a gravitational search algorithm based on the Cauchy and Gaussian mutation," *Inf. Sci. (Ny).*, vol. 396, pp. 162–181, 2017.

[196] G. Q. Zeng, J. Chen, Y. X. Dai, L. M. Li, C. W. Zheng, and M. R. Chen, "Design of fractional order PID controller for automatic regulator voltage system based on multi-objective extremal optimization," *Neurocomputing*, vol. 160, pp. 173–184, 2015.

[197] Z. Gao, "Analytical criterion on stabilization of fractional-order plants with interval uncertainties using fractional-order PD$^{\mu}$ controllers with a filter," *ISA Trans.*, vol. 83, pp. 25–34, 2018.

[198] Z. Gao, "Robust stability criterion for fractional-order systems with interval uncertain coefficients and a time-delay," *ISA Trans.*, vol. 58, pp. 76–84, 2015.

[199] J. Bondia, A. Kieffer, E. Walter, J. Monreal, and J. Pico, "Guaranteed tuning of PID controllers for parametric uncertain systems," in *43rd IEEE Conference on Decision and Control*, 2004, pp. 2948–2953.

[200] Y. W. Tu and M. T. Ho, "Robust second-order controller synthesis for model matching of interval plants and its application to servo motor control," *IEEE Trans. Control Syst. Technol.*, vol. 20, no. 2, pp. 530–537, 2012.

[201] S. Sondhi and Y. V. Hote, "Fractional-order PI controller with specific gain–phase margin for MABP control," *IETE J. Res.*, vol. 61, no. 2, pp. 142–153, 2015.

[202] Z. Gao, "Robust stabilization of interval fractional-order plants with one time-delay by fractional-order controllers," *J. Franklin Inst.*, vol. 354, no. 2, pp. 767–786, 2017.

[203] T. Liang, J. Chen, and C. Lei, "Algorithm of robust stability region for interval plant with time delay using fractional order PI$^{\lambda}$D$^{\mu}$ controller," *Commun. Nonlinear Sci. Numer. Simul.*, vol. 17, no. 2, pp. 979–991, 2012.

[204] S. Zheng, X. Tang, and B. Song, "A graphical tuning method of fractional order proportional integral derivative controllers for interval fractional order plant," *J. Process Control*, vol. 24, no. 11, pp. 1691–1709, 2014.

[205] Z. Gao, "Robust stabilization criterion of fractional-order controllers for interval fractional-order plants," *Automatica*, vol. 61, pp. 9–17, 2015.

[206] S. Sondhi and Y. V. Hote, "Fractional order PID controller for perturbed load frequency control using Kharitonov's theorem," *Int. J. Electr. Power Energy Syst.*, vol. 78, pp. 884–896, 2016.

[207] T. Liang, J. Chen, and H. Zhao, "Robust stability region of fractional order PI$^{\lambda}$controller for fractional order interval plant," *Int. J. Syst. Sci.*, vol. 44, no. 9, pp. 1762–1773, 2013.

[208] H. Purohit and P. S. V Nataraj, "Optimized and automated synthesis of robust PID controller with quantitative feedback theory," in *IEEE International Conference on Industrial Instrumentation and Control (ICIC)*, 2015, pp. 105–110.

[209] S. Bhattacharya, L. H. Keel, and S. P. Bhattacharyya, "Robust stabilizer synthesis for interval plants using H-infinity methods," in *Decision and Control, Proceedings of the 32nd*

IEEE Conference, 1993, pp. 3003–3008.

[210] S. Saxena and Y. V. Hote, "Decentralized PID load frequency control for perturbed multi-area power systems," *Int. J. Electr. Power Energy Syst.*, vol. 81, pp. 405–415, 2016.

[211] S. Saxena, Y. V Hote, and S. Sondhi, "Fractional-order PI control of DC servo system using the stability boundary locus approach," in *IEEE 10th International Conference on Industrial and Information Systems*, 2015, pp. 182–186.

[212] M. Toulabi, S. Bahrami, and A. M. Ranjbar, "Application of Edge theorem for robust stability analysis of a power system with participating wind power plants in automatic generation control task," *IET Renew. Power Gener.*, vol. 11, no. 7, pp. 1049–1057, 2017.

[213] P. Chen and Y. Z. Lu, "Automatic design of robust optimal controller for interval plants using genetic programming and Kharitonov theorem," *Int. J. Comput. Intell. Syst.*, vol. 4, no. 5, pp. 826–836, 2011.

[214] Y. J. Lee and M. G. Na, "Modelling of nuclear reactor and power control by extended frequency method," in *IECON 2006 - 32nd Annual Conference on IEEE Industrial Electronics*, 2006, pp. 61–66.

[215] C. Liu, J. F. Peng, F. Y. Zhao, and C. Li, "Design and optimization of fuzzy-PID controller for the nuclear reactor power control," *Nucl. Eng. Des.*, vol. 239, no. 11, pp. 2311–2316, 2009.

[216] Y. J. Lee and M. G. Na, "Robust controller design for the nuclear reactor power by extended frequency response method," *Nucl. Eng. Technol.*, vol. 38, no. 6, pp. 551–560, 2006.

[217] S. R. Shimjith, A. P. Tiwari, M. Naskar, and B. Bandyopadhyay, "Space-time kinetics modeling of advanced heavy water reactor for control studies," *Ann. Nucl. Energy*, vol. 37, no. 3, pp. 310–324, 2010.

[218] M. Das *et al.*, "Network control system applied to a large pressurized heavy water reactor," *IEEE Trans. Nucl. Sci.*, vol. 53, no. 5, pp. 2948–2956, 2006.

[219] S. Das, S. Mukherjee, S. Das, I. Pan, and A. Gupta, "Continuous order identification of PHWR models under step-back for the design of hyper-damped power tracking controller with enhanced reactor safety," *Nucl. Eng. Des.*, vol. 257, pp. 109–127, 2013.

[220] S. Sardar, T., Saha Ray, S., Bera, R.K., Biswas, B.B. and Das, "The solution of coupled fractional neutron diffusion equations with delayed neutrons," *Journal, Int. Sci. Nucl. Energy*, vol. 5, no. 2, pp. 105–113, 2010.

[221] B. B. Das, S. and Biswas, "Fractional divergence for neutron flux profile in nuclear reactor," *Int. J. Nucl. Energy Sci. Technol.*, vol. 3, no. 2, pp. 139–159, 2007.

[222] G. Espinosa Paredes, M. A. Polo Labarrios, E. G. Espinosa Martínez, and E. del Valle Gallegos, "Fractional neutron point kinetics equations for nuclear reactor dynamics," *Ann. Nucl. Energy*, vol. 38, pp. 307–330, 2011.

[223] M. R. Toulabi, M. Shiroei, and A. M. Ranjbar, "Robust analysis and design of power system load frequency control using the Kharitonov 's theorem," *Electr. Power Energy Syst.*, vol. 55, pp. 51–58, 2014.

[224] D. Gobinda and S. Majhi, "A new control scheme for PID load frequency controller of single-area and multi-area power systems," *ISA Trans.*, vol. 52, pp. 242–251, 2013.

[225] A. Delassi, S. Arif, and L. Mokrani, "Frequency stability enhancement in power system using high-order sliding mode control," in *IEEE 4th International Conference on Electrical Engineering (ICEE)*, 2015, pp. 1–4.

[226] B. Mohanty, S. Panda, and P. K. Hota, "Controller parameters tuning of differential evolution algorithm and its application to load frequency control of multi-source power system," *Electr. Power Energy Syst.*, vol. 54, pp. 77–85, 2014.

[227] Y. Mi, Y. Fu, C. Wang, S. Member, P. Wang, and S. Member, "Decentralized Sliding Mode Load Frequency Control for Multi-Area Power Systems," *IEEE Trans. Power Syst.*, vol. 28, no. 4, pp. 4301–4309, 2013.

[228] W. Tan, "Decentralized load frequency controller analysis and tuning for multi-area power systems," *Energy Convers. Manag.*, vol. 52, pp. 2015–2023, 2011.

[229] W. Tan and H. Zhou, "Robust analysis of decentralized load frequency control for multi-area power systems," *Electr. Power Energy Syst.*, vol. 43, pp. 996–1005, 2012.

[230] Y. Zhang, L. Dong, and Z. Gao, "Load frequency control for multiple-area power systems," in *American Control Conference*, 2009, pp. 2773–2778.

[231] S. Debbarma and S. Lalit Chandra, "Automatic generation control of multi-area system using non-integer order I^{λ} D^{μ} controller," in *IEEE 1st International Conference on Power and Energy in NERIST (ICPEN)*, 2012, pp. 1–6.

[232] K. Jagatheesan, B. Anand, N. Dey, A. S. Ashour, C. Barna, and V. E. Balas, "Automatic generation control of an interconnected multi-area reheat thermal power systems with conventional proportional- integral controller considering various performance indices," in *11th IEEE International Symposium on Applied Computational Intelligence and Informatics*, 2016, pp. 289–294.

[233] R. Kumar Sahu, S. Panda, A. Biswal, and G. T. Chandra Sekhar, "Design and analysis of tilt integral derivative controller with filter for load frequency control of multi-area interconnected power systems," *ISA Trans.*, vol. 61, pp. 251–264, 2016.

[234] M. T. Alrifai, M. F. Hassan, and M. Zribi, "Decentralized load frequency controller for a multi-area interconnected power system," *Electr. Power Energy Syst.*, vol. 33, pp. 198–209, 2011.

[235] M. Rahmani and N. Sadati, "Two-level optimal load – frequency control for multi-area power systems," *Electr. Power Energy Syst.*, vol. 53, pp. 540–547, 2013.

[236] M. Ma, H. Chen, X. Liu, and F. Allgöwer, "Distributed model predictive load frequency control of multi-area interconnected power system," *Int. J. Electr. Power Energy Syst.*, vol. 62, pp. 289–298, 2014.

[237] Y. Sun, N. Li, X. Zhao, Z. Wei, G. Sun, and C. Huang, "Robust H_∞ load frequency control of delayed multi-area power system with stochastic disturbances," *Neurocomputing*, vol. 193, pp. 58–67, 2016.

[238] M. Rahmani and N. Sadati, "Hierarchical optimal robust load-frequency control for power systems," *IET Gener. Transm. Distrib.*, vol. 6, no. 4, pp. 303–312, 2012.

[239] A. Khodabakhshian and M. Edrisi, "A new robust PID load frequency controller," *Control Eng. Pract.*, vol. 16, pp. 1069–1080, 2008.

[240] H. Bevrani, Y. Mitani, and K. Tsuji, "Robust decentralised load-frequency control using an iterative linear matrix inequalities algorithm," *IEE Proceedings-Generation, Transm. Distrib.*, vol. 151, no. 3, pp. 347–354, 2004.

[241] D. Rerkpreedapong, A. Hasanovic, and A. Feliachi, "Robust load frequency control using genetic algorithms and linear matrix inequalities," *IEEE Trans. Nucl. Sci.*, vol. 18, no. 2, pp. 855–861, 2003.

[242] A. Khodabakhshian, "Enhancement of power system performance by LFC analysis of hydro power plants using QFT," *Euro. Trans. Electr. Power*, pp. 323–338, 2008.

[243] W. Tan, "Tuning of PID load frequency controller for power systems," *Energy Convers. Manag.*, vol. 50, no. 6, pp. 1465–1472, 2009.

[244] W. Tan, "Unified tuning of PID load frequency controller for power systems via IMC," *IEEE Trans. Power Syst.*, vol. 25, no. 1, pp. 341–350, 2010.

[245] S. Saxena and Y. V Hote, "Load frequency control in power systems via internal model control scheme and model order reduction," *IEEE Trans. Nucl. Sci.*, vol. 28, no. 3, pp. 2749–2757, 2013.

[246] M. I. Alomoush, "Load frequency control and automatic generation control using fractional-order controllers," *Electr. Eng.*, vol. 91, pp. 357–368, 2010.

[247] S. Prakash and S. K. Sinha, "Simulation based neuro-fuzzy hybrid intelligent PI control approach in four-area load frequency control of interconnected power system," *Appl. Soft Comput.*, vol. 23, pp. 152–164, 2014.

[248] B. Kumar, T. Kumar, J. Ranjan, S. Panda, and S. Kumar, "A novel hybrid LUS – TLBO optimized fuzzy-PID controller for load frequency control of multi-source power system," *Electr. Power Energy Syst.*, vol. 74, pp. 58–69, 2016.

[249] H. A. Yousef, K. Al-kharusi, and M. H. Albadi, "Load frequency control of a multi-area power system : An Adaptive Fuzzy Logic Approach," *IEEE Trans. Power Syst.*, vol. 29, no. 4, pp. 1822–1830, 2014.

[250] T. Kumar Pati, J. Ranjan Nayak, B. Kumar Sahu, and B. Gantayat, "Load frequency control of an interconnected three-area thermal power system using conventional PID & fuzzy-logic controller," in *IEEE International Conference on Energy, Power and Environment: Towards Sustainable Growth (ICEPE)*, 2015, pp. 1–6.

[251] S. Prakash and S. K. Sinha, "Application of artificial intelligence in load frequency control of interconnected power system," *Int. J. Eng. Sci. Technol.*, vol. 3, no. 4, pp. 264–275, 2011.

[252] E. Nikmanesh, O. Hariri, H. Shams, and M. Fasihozaman, "Pareto design of load frequency control for interconnected power systems based on multi-objective uniform diversity genetic algorithm," *Electr. Power Energy Syst.*, vol. 80, pp. 333–346, 2016.

[253] U. K. Rout, R. K. Sahu, and S. Panda, "Design and analysis of differential evolution algorithm based automatic generation control for interconnected power system," *Ain Shams Eng. J.*, vol. 4, pp. 409–421, 2013.

[254] W. Tan, S. Chang, and R. Zhou, "Electric power components and systems load frequency control of power systems with load frequency control of power systems with governor deadband (GDB) non-linearity," *Electr. Power Components Syst.*, vol. 45, no. 12, pp. 1305–1314, 2017.

[255] W. Tan, S. Chang, and R. Zhou, "Load frequency control of power systems with non-linearities," *IET Gener. Transm. Distrib.*, vol. 11, no. 17, pp. 4307–4313, 2017.

[256] S. C. Tripathy, R. Balasubramanian, and P. S. C. Nair, "Effect of superconducting magnetic energy storage on automatic generation control," *IEEE Trans. Power Syst.*, vol. 7, no. 3, pp. 1266–1273.